8-1978

Compensation requirements for an automatic tensioning device used in winding superconducting coils/

Gary Melvin Henderson
University of Tennessee

Follow this and additional works at: https://trace.tennessee.edu/utk_gradthes

To the Graduate Council:

I am submitting herewith a thesis written by Gary Melvin Henderson entitled "Compensation requirements for an automatic tensioning device used in winding superconducting coils/." I have examined the final electronic copy of this thesis for form and content and recommend that it be accepted in partial fulfillment of the requirements for the degree of Master of Science, with a major in Electrical Engineering.

<div align="right">J. M. Googe, Major Professor</div>

We have read this thesis and recommend its acceptance:

<div align="right">Accepted for the Council:</div>
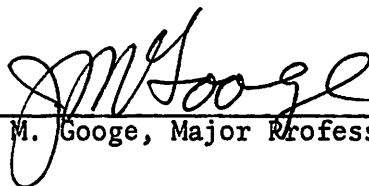
<div align="right">Carolyn R. Hodges</div>

<div align="right">Vice Provost and Dean of the Graduate School</div>

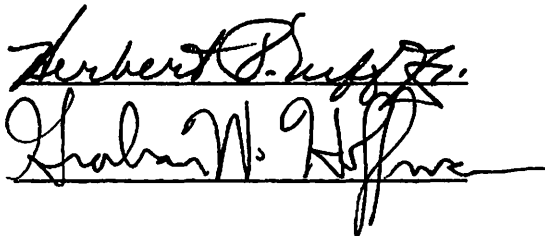(Original signatures are on file with official student records.)

To the Graduate Council:

I am submitting herewith a thesis written by Gary Melvin Henderson entitled "Compensation Requirements for an Automatic Tensioning Device Used in Winding Superconducting Coils." I recommend that it be accepted in partial fulfillment of the requirements for the degree of Master of Science, with a major in Electrical Engineering.

J. M. Googe, Major Professor
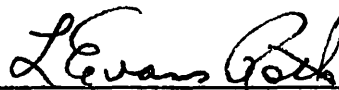
We have read this thesis and
recommend its acceptance:

Accepted for the Council:

Vice Chancellor
Graduate Studies and Research

COMPENSATION REQUIREMENTS FOR AN AUTOMATIC

TENSIONING DEVICE USED IN WINDING

SUPERCONDUCTING COILS

A Thesis

Presented for the

Master of Science

Degree

The University of Tennessee, Knoxville

Gary Melvin Henderson

August 1978

ACKNOWLEDGMENTS

ABSTRACT

This thesis investigates the applicability of a commercial controller for stabilizing an automatic tensioning device used in winding operations for large superconducting coils. Unsuccessful results with the commercial unit leads to the design of a compensation network. Root locus techniques are utilized in arriving at a suitable compensation network to stabilize the tension machine control system. Simulated tests of the system's response to a step input and to a pulse disturbance are performed using IBM's Continuous System Modeling Program.

TABLE OF CONTENTS

LIST OF TABLES

LIST OF FIGURES

CHAPTER I

INTRODUCTION

At the turn of the century scientists and engineers, engaged in controlled nuclear fusion research, plan to demonstrate steam power plants that will generate electricity from the energy produced by nuclear fusion.

Nuclear fusion, the same reaction powering the sun and stars, occurs when the nuclei of two light atoms—namely deuterium and tritium, two hydrogen isotopes—fuse together. The fused atoms form the nucleus of a heavier element and release an enormous amount of energy.

Fusion of two atoms only occurs at extremely high temperatures in the order of 60 to 100 million degrees Kelvin. At these high temperatures, matter cannot exist in any of the common states—solid, liquid, or gas—but exists only as a plasma. In plasma, the electrons are separated from the atomic nuclei. Hence plasma is ionized gas. Confinement of this plasma is one of the major problem areas of fusion reactor development.

In experimental fusion machines the plasma is confined by three magnetic fields. These fields, called poloidal, vertical and toroidal, hold the plasma in the shape of a torus, or doughnut as shown in Figure 1.1.

The poloidal field, B_p, is produced by a large current flowing in the plasma. The vertical field, B_V, is produced by toroidal windings in the direction of the plasma, and the toroidal magnetic field, B_T, is
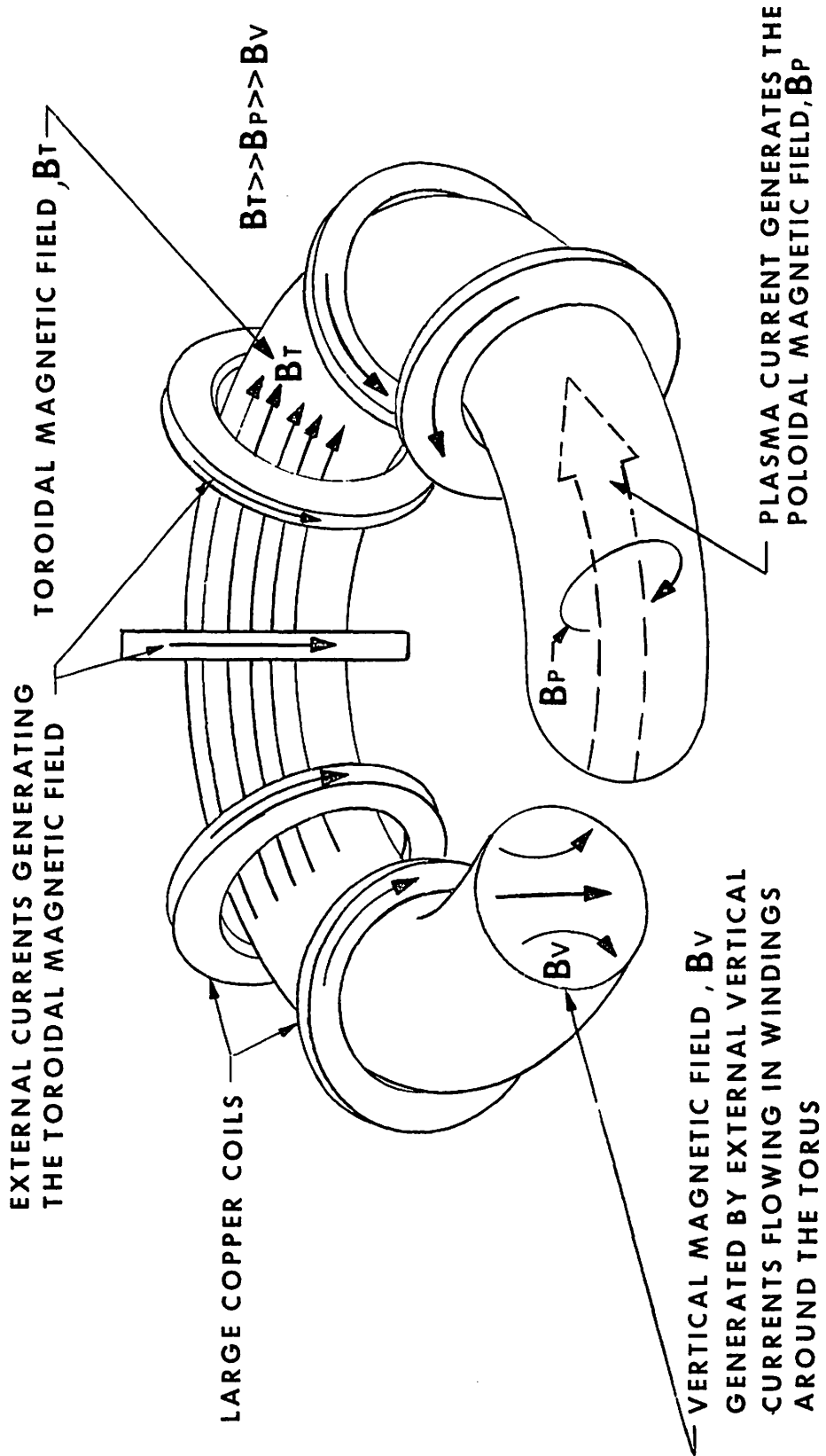
Figure 1.1. An Example of the Plasma Confinement by Use of Magnetic Fields.

Source: Steiner, Don, "Nuclear Fusion: Focus on Tokomak," IEEE Spectrum, July, 1977, p. 35.

obtained using large copper coils placed around the perimeter of the reactor with the plasma passing through the coils' centers.[1,2,3]

Plasma confinement is largely dependent upon the toroidal field coils. These large copper coils are cooled by water and sometimes liquid nitrogen. If the fusion reactor is to prove an economical source of electricity, plasma confinement must be accomplished by more efficient coils than used to date.

One consideration for more efficient coils is the use of superconducting coils to generate the toroidal magnetic field. The term superconductivity refers to the property of certain metals having zero resistance at temperatures within a few degrees of absolute zero.[4] The coils required to confine the plasma to the appropriate density will have an inside diameter of 5 to 7 meters and will produce a magnetic field strength of 8 teslas[2](1 tesla = 10^4 gauss, where 1 gauss is approximately equal to the earth's magnetic field strength). Cooled by liquid helium, the superconducting coils circulate large amounts of current with very little energy lost in the form of heat, and consequently will produce a stronger magnetic field than the equivalent energy input to water or nitrogen cooled copper coils. The size and field strength requirements of large superconducting coils present an enormous challenge to industry to fabricate such coils. Reliable fabrication equipment and techniques must be developed to manufacture large superconducting coils.

A comprehensive program to design and construct large superconducting coils for the toroidal fields in Controlled Thermonuclear Research

machines is presently being undertaken by industrial participants and the Fusion Energy Division of the Oak Ridge National Laboratory.* An important part of this program is directed toward analyzing the stresses that the superconducting coils undergo in a fusion machine.

Theoretical calculations to predict the behavior of the superconductor subjected to the tremendous magnetic fields, thermal stresses, and various other forces existing in a fusion machine are being made in an effort to study coil strengths and weaknesses. Winding the superconducting coils in constant tension allows the theoretical calculations to be more predictable.[5]

A 3-meter coil-winding facility has been built to test wind superconducting coils in constant tension. Larger coils will be fabricated later after winding equipment and techniques have been developed.

Conventional winding techniques for controlling tension in conductor wire or thread being wrapped onto a bobbin employ a dancer or follower arm to regulate braking action of a torque motor resisting the winding operation. This is generally accomplished by passing the conductor around a weighted roller connected to a pivot arm thereby allowing the roller to move up and down freely. Displacement of the pivot arm from the desired position produces an error signal which increases or decreases the braking action of the torque motor. Unfortunately this technique cannot be utilized when wrapping a

superconductor because it must not be bent on a short radius. A specially designed tension machine to minimize scarring, bending and burning of the superconductor during winding operations for superconducting coils is employed in the control system analyzed in this thesis.

A description of the tension machine is given in Chapter II and includes a block diagram identifying system components. In Chapter III the analytical model of the control system is developed.

The components of the actual system are designed around commercially available units, and therefore the controller purchased for stability compensation is a commercial controller. Stability analysis is discussed in Chapter IV and indicates that the commercial controller is insufficient by itself for satisfactorily stabilizing the system. Additional compensation networks for the tension machine are discussed in Chapter V. A summary of the overall thesis and some comments by the author are given in Chapter VI.

A discussion of the type of commercial controller used in the thesis and the computer programs used are given in the appendices.

CHAPTER II

SYSTEM DESCRIPTION

The tension machine, shown in Figure 2.1, is an experimental device
for use in a practice winding facility developed to test wind super-
conducting coils. The machine's function is to control tension in the
superconductor during coil winding operations. It consists of a
conductor straightener, a two belt system, a gear reducer, a three-phase
torque motor, and a support frame and platform. Roller bearings are
mounted on the bottom surface of the machine to minimize frictional
forces between the platform and the floor. A tension load cell
connected between the frame and a stationary object restrains movement
of the tension machine.

In Figure 2.2 a sketch of the coil winding operation is shown.
During winding operations the payout reel containing the superconductor
feeds wire to the tension machine. The payout reel is designed to
uncoil the conductor without pulling against the tension machine. The
conductor passes through the tension machine's straightener, the two
belt system and finally is wound onto the bobbin of the winding machine.

The passage of the conductor through the tension machine forces the
two belts to rotate in opposite directions. A normal force applied to
the belt system by a pressure nut and spring assures minimum or no
slippage of the conductor with respect to the two belts. Connected to
one of four pulleys in the belt system is the gear reducer and torque
motor. During normal operation of the winding sequence the torque
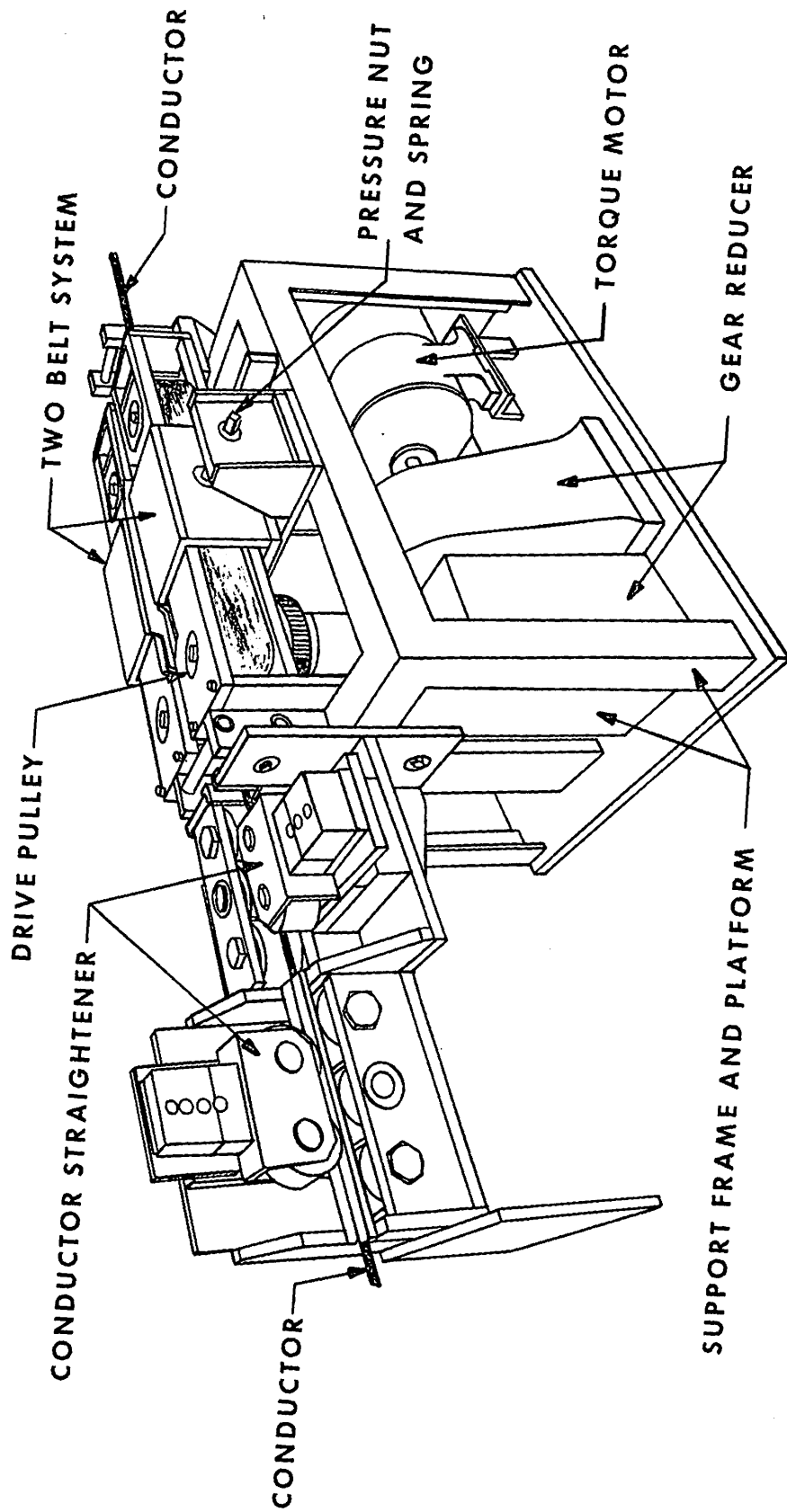
Figure 2.1. Tension Machine.
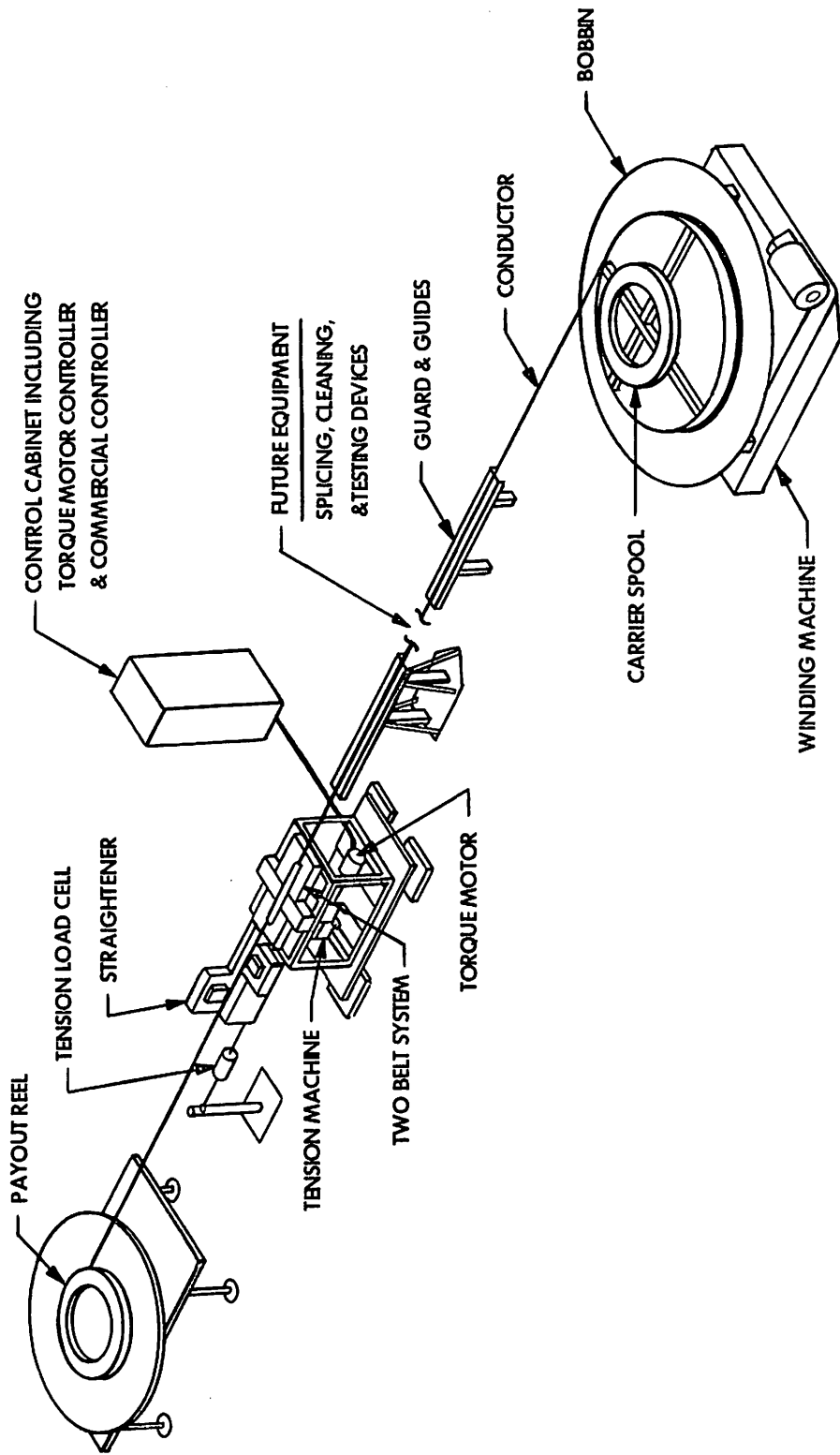
Figure 2.2. Coil Winding Operation.

motor's shaft is driven backward by the action of the conductor passing through the belts of the tension machine. The negative rotation of the torque motor causes a braking action. It is this braking action that produces a tension in the conductor as it is wrapped onto the coil.

By Newton's third law, the force exerted by the tension machine on the superconductor is met with an equal and opposite force exerted on the tension machine by the superconductor. Since the tension load cell inhibits the movement of the tension machine, it measures the force (tension) exerted on the conductor.

The force exerted on the load cell is converted to an electrical signal which is measured by a recorder containing a control slidewire and mechanical set point. The set point actually controls a dc voltage level scaled to represent pounds force and is the reference input for desired tension. The control slidewire, which is a wirewound resistor with a wiper contact, is part of a bridge network inside the recorder. Repositioning of the slidewire's wiper occurs each time the feedback signal from the load cell system changes. This action unbalances the recorder's bridge network and produces an error voltage proportional to the difference between the desired and actual tension.

A commercially manufactured controller with proportional, integral and derivative control actions—also called a PID Controller—provides limited system compensation requirements (a discussion of a PID Controller is given in Appendix A). The controller accepts the error voltage from the recorder and produces an actuating signal for the torque motor's control unit.

The torque motor's controller is a three-phase device for controlling stator voltages to the torque motor. Motor output torque is controlled by varying the firing angle of silicon controlled rectifiers (SCRs) in each phase of the motor stator windings. Varying the firing angle of the SCRs changes the voltage and current supplied to the motor, and hence changes the torque output. Since the torque developed on the driven belt system pulley by the torque motor acting through the gear reducer resists the winding operation, altering the torque output changes the conductor tension. A descriptive block diagram of the control system is shown in Figure 2.3.

In Figure 2.3, F_W represents the force in the conductor and T represents the force measured by the load cell. These forces are equivalent neglecting the frictional forces between the platform of the tension machine and the floor.

System model development is presented in the following chapter. Each system block shown in the descriptive diagram of Figure 2.3 is discussed in detail to arrive at a mathematical representation of the control system for stability analysis and compensation in Chapters IV and V.
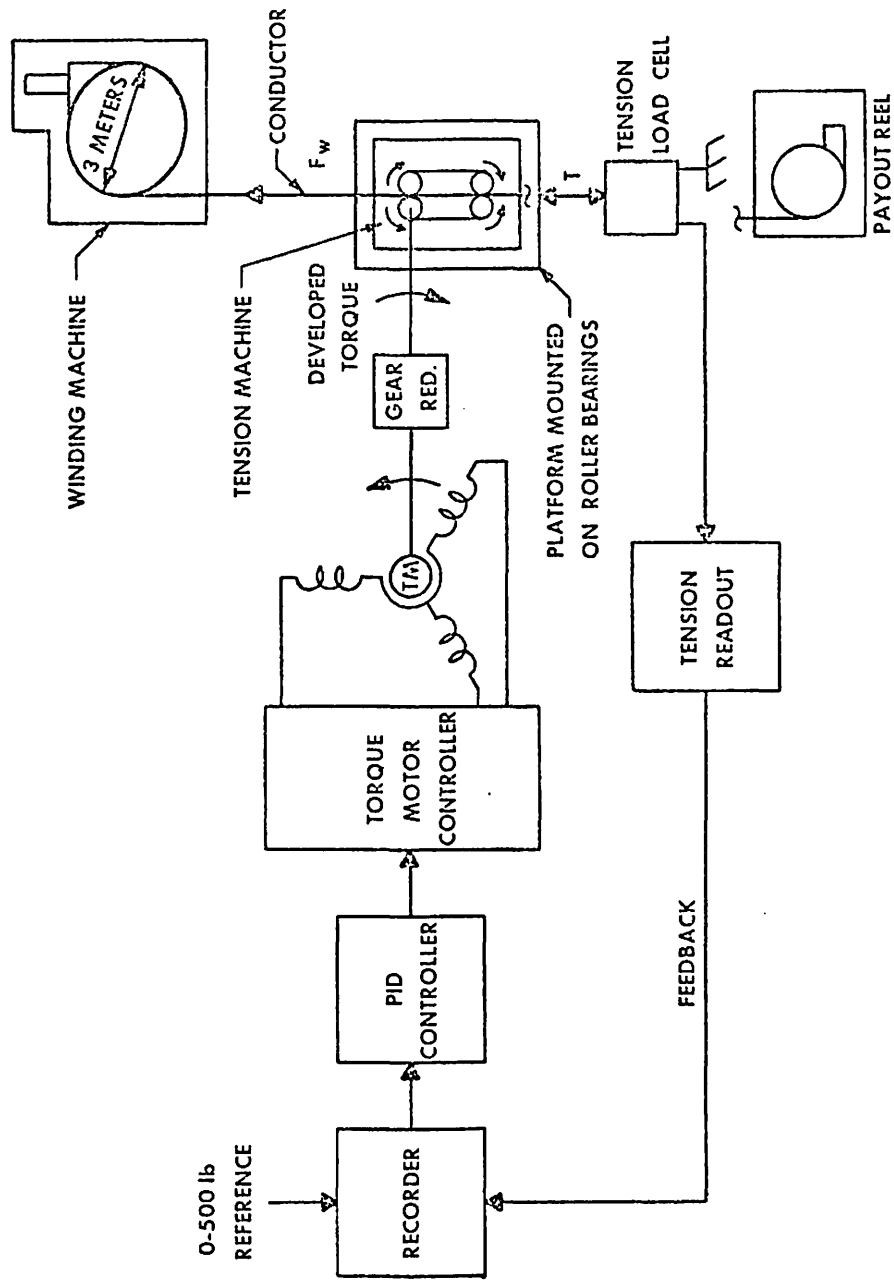
Figure 2.3. Descriptive System Block Diagram.

CHAPTER III

SYSTEM MODEL DEVELOPMENT

In developing the mathematical model from which the stability
analysis can be obtained, each system component must be analyzed
separately to arrive at a relation between input and output. Knowing
the individual relationships of the components and assuming these
relationships to be linear, an overall transfer function of the system
model can be obtained. Figure 3.1 represents the block diagram of the
system to be modeled. Modeling of each block diagram component begins
with the load cell system.

Load Cell System

The controlled variable is force in the conductor wire and is
proportional to tension measured by the load cell. The force in the
conductor causes the entire skid system, on which the tension machine is
mounted, to be displaced some distance. This displacement is sensed by
the tension load cell which transfers deflection of its sensing member
to the load cell amplifier network which produces a 0 to 10 millivolt
signal corresponding to the instrument's full range of 0 to 500 pounds.
Total deflection of the sensing element in the cell is 0.003 inch,
thereby giving a gain constant for the load cell system of

$$K_{CG} = \frac{10 \text{ mV}}{0.003 \text{ inch}} = 3.33 \frac{\text{Volts}}{\text{inch}} \quad . \tag{3-1}$$

Figure 3.1. System Block Diagram.

The load cell system response to a unit step input is approximately 10 milliseconds, which corresponds to a time constant of 6 to 7 milliseconds. Since the bandwidth of the tension machine, recorder and commercial controller is much lower than that of the load cell system, this time constant can be neglected during system stability analysis. Relating input to output for the load cell system gives a simple order lag transfer function which is represented by

$$\frac{\text{output}}{\text{input}} = \frac{K_{CG}}{1 + \tau_{LC}s} \qquad (3\text{-}2)$$

where K_{CG} is the load cell gain, τ_{LC} is the time constant, and s is the Laplace transform variable.

Motor Controller and Torque Motor

Before the transfer function for the torque motor and the motor controller is developed, a brief description of the motor and controller is in order.

The motor is a special induction machine designed to operate backwards against normal rotation. It is used as a torque motor brake to regulate tension by resisting the passage of the conductor through the belt system. The controller varies the firing angle of silicon controlled rectifiers (SCRs) in each phase leg of the motor. The firing angle is varied in response to a remote 0 to 10 volt dc signal supplied by the commercial PID (proportional, integral, and derivative) controller. Figure 3.2 shows the SCRs connected in series with the stator windings of the motor.
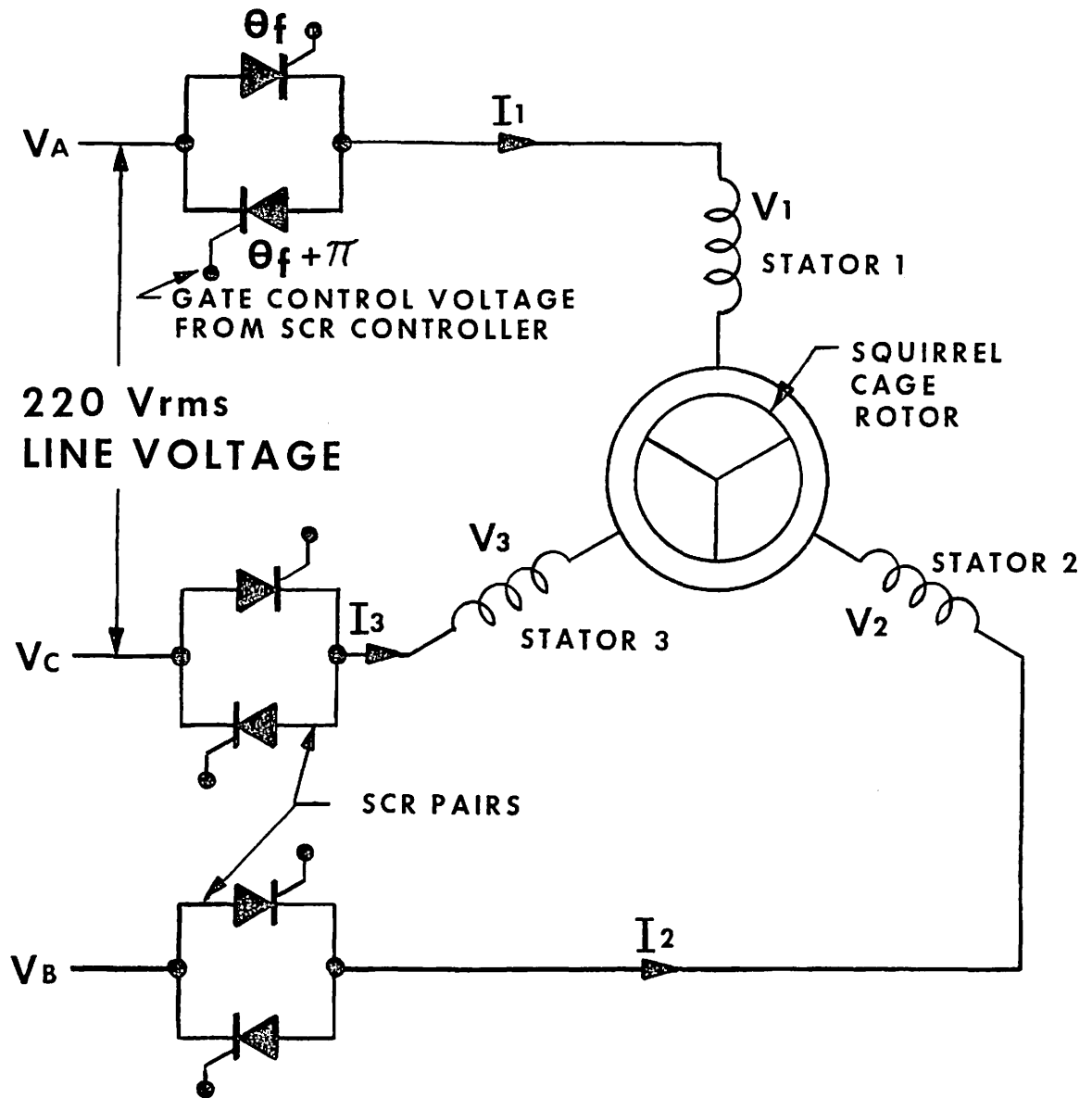
Figure 3.2. Induction Motor with SCR Phase Control of Stator Voltages.

Line phase voltages in Figure 3.2 are represented by V_A, V_B, and V_C, and stator voltages are represented by V_1, V_2 and V_3. θ_f and $\theta_f + \pi$ represent the firing angle of the SCR pair in phase leg 1 for both the positive and negative half cycles of the incoming voltage sine wave.

Several approximations were made in developing the analytical model and transfer function for the SCR controller and induction motor. Rigorous solutions to the complex voltage and current waveforms resulting from thyristor firing of induction motors have been done in the literature,[6,7] although numerical results can only be obtained by digital computer. A rigorous solution for the voltage and currents for any time t will not be pursued in this thesis. Instead an approximate solution for currents and voltages in the motor will be developed based on the equivalent circuit of an induction motor.

Since the equivalent circuit will give a reasonable representation of the induction motor, a relationship between the voltage applied to the stator windings and the output torque developed by the motor can be derived.

The torque motor and SCR pair for each phase can be represented by the equivalent circuit shown in Figure 3.3.[8]

The parameters in Figure 3.3 are defined as follows:

$\vec{V}_{1rms}$ represents the rms line voltage,

$\vec{V}_1$ is the stator phase voltage, $(\vec{V}_{1rms}/\sqrt{3})$,

$\vec{I}_1$ is the stator current,

$\vec{I}_2/a$ is the rotor current referred to the stator,

ω_1 is the line angular frequency in radians/second,
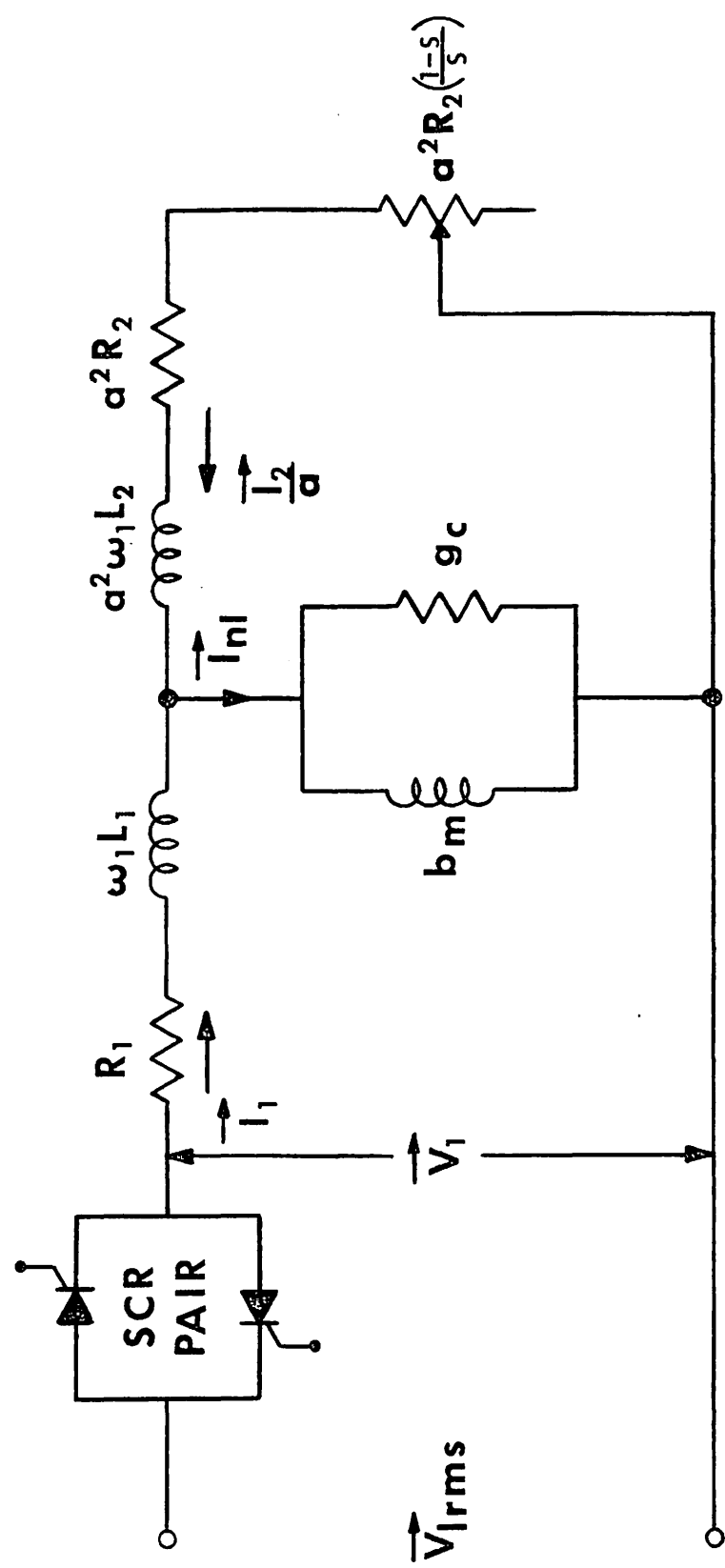
Figure 3.3. An Equivalent Circuit of the 3-Phase Induction Motor with All Quantities Referred to the Stator.

a   is the transformation ratio between the stator and

            rotor,

$a^2 R_2$ is the resistance of the rotor winding referred to the

            stator,

b_m is the susceptance of the air gap,

g_c is the core loss component,

$\vec{I}_{nl}$ is the no load current,

$a^2 R_2 (\frac{1-S}{S})$ is the mechanical shaft load of the motor, and

S   is the slip of the motor.

The thyristors shown in the equivalent circuit will be treated as ideal switching elements. That is, the forward voltage drop during conduction (which for the devices used in the controller is 1.5 volts), the leakage current during blockage, and the turn on and turn off times are negligible.

Neglecting the SCR voltage drop and moving the magnetizing branch of the induction machine to the input terminals of the stator winding results in a simplified equivalent circuit which is shown in Figure 3.4. This simplified circuit is made with the assumption that voltage per phase, $\vec{V}_1$, into the stator is approximately equal to the voltage across the magnetizing branch. In Figure 3.4 $X_1 = \omega_1 L_1$ and $X_2 = \omega_1 L_2$.

Mechanical power can be derived from the equivalent circuit with the following equation:

$$P_{mech} = T\omega_m \qquad\qquad\qquad (3-3)$$

where T represents torque per phase and ω_m is the angular velocity of the rotor.[8]
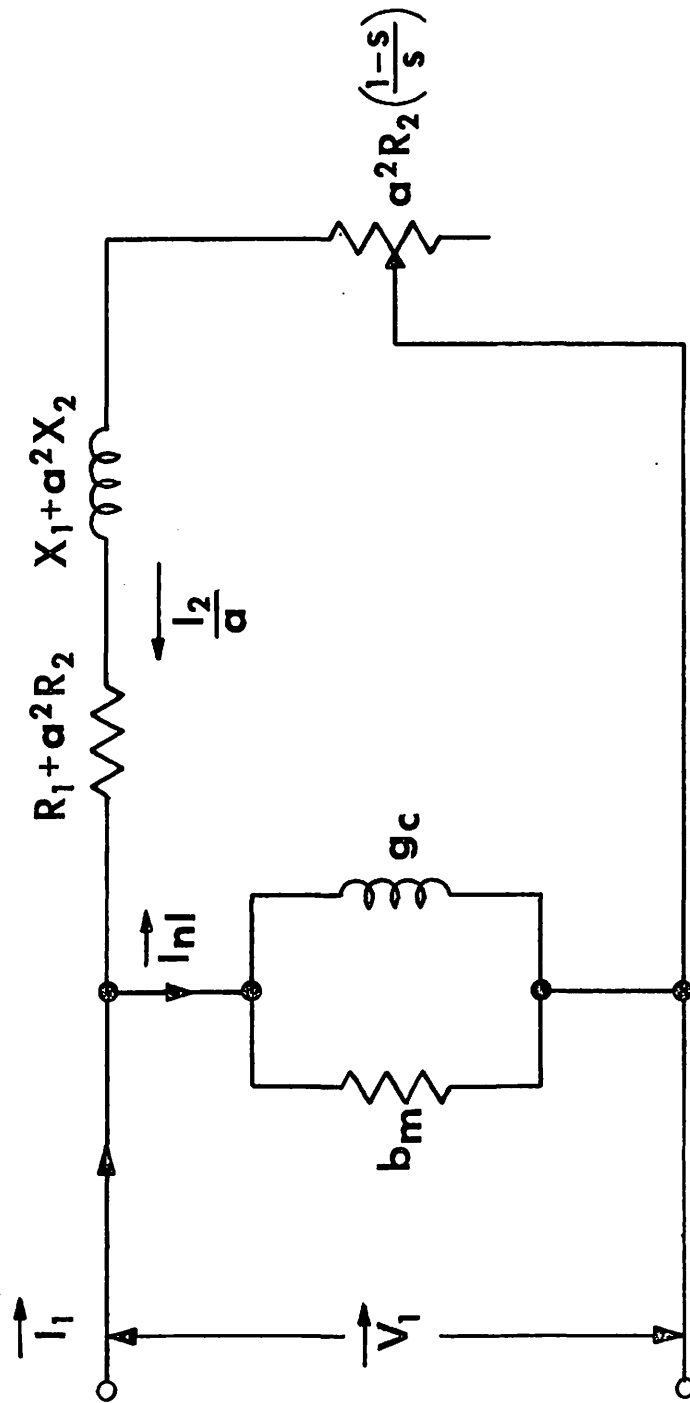
Figure 3.4. Simplification of the Induction Motor's Equivalent Circuit.

Since power $P = I^2R$, the power delivered to the load is

$$P_{mech} = \left|\frac{\vec{I}_2}{a}\right|^2 a^2 R_2 (\frac{1-S}{S}) \quad . \tag{3-4}$$

From equation (3-3),

$$P_{mech} = T\omega_m \quad ,$$

it follows that

$$T_{mech} = \frac{P_{mech}}{\omega_m} \quad , \tag{3-5}$$

and substitution for P_{mech} from equation (3-4) yields

$$T_{mech} = \frac{\left|\frac{\vec{I}_2}{a}\right|^2 a^2 R_2 (\frac{1-S}{S})}{\omega_m} \quad . \tag{3-6}$$

From the equivalent circuit (Figure 3.4), Kirchoff's voltage equation results in the following expression for $|\vec{I}_2/a|$:

$$\left|\vec{V}_1\right| = \left|\frac{\vec{I}_2}{a}\right| Z \tag{3-7}$$

where

$$Z = \left[[R_1 + a^2R_2 + a^2R_2(\frac{1-S}{S})]^2 + [X_1 + a^2X_2]^2 \right]^{1/2} \quad .$$

$$\left|\frac{\vec{I}_2}{a}\right| = \frac{\left|\vec{V}_1\right|}{Z} \quad , \text{ or}$$

$$\left|\frac{\vec{I}_2}{a}\right| = \frac{\left|\vec{V}_1\right|}{\left[[R_1 + a^2R_2 + a^2R_2(\frac{1-S}{S})]^2 + [X_1 + a^2X_2]^2 \right]^{1/2}} \quad . \quad (3-8)$$

Substituting the expression for $\left|\vec{I}_2/a\right|$ into the equation for T_{mech} yields

$$T_{mech} = \frac{\left|\vec{V}_1\right|^2 a^2R_2(\frac{1-S}{S})}{\left[[R_1 + a^2R_2 + a^2R_2(\frac{1-S}{S})]^2 + [X_1 + a^2X_2]^2 \right] \omega_m} \quad . \quad (3-9)$$

Since $\omega_m = \omega_s(1-S)$, where ω_s is the angular velocity of the rotating magnetic field, and s is the slip, equation (3-9) simplifies to

$$T_{mech} = \frac{\left|\vec{V}_1\right|^2 \frac{a^2R_2}{S}(1-S)}{\left[\left(R_1 + \frac{a^2R_2}{S}\right)^2 + (X_1 + a^2X_2)^2 \right] \omega_s(1-S)} \quad , \text{ or}$$

$$T_{mech} = \frac{\left|\vec{V}_1\right|^2 \frac{a^2R_2}{S}}{\omega_s \left[\frac{(R_1S + a^2R_2)^2}{S^2} + \frac{S^2(X_1 + a^2X_2)^2}{S^2} \right]} \quad , \text{ or}$$

$$T_{mech} = \frac{\left|\vec{V}_1\right|^2 a^2R_2S}{\omega_s \left[(R_1S + a^2R_2)^2 + S^2(X_1 + a^2X_2)^2 \right]} \quad . \quad (3-10)$$

This last expression for mechanical torque is on a per phase basis, and the total torque for all three phases can be obtained by simply multiplying by 3. Hence total torque is

$$T_{mech} = \frac{3\left|\vec{V}_1\right|^2 a^2 R_2 S}{\omega_s \left[(R_1 S + a^2 R_2)^2 + S^2 (X_1 + a^2 X_2)^2 \right]} \qquad . \qquad (3\text{-}11)$$

Holding slip (motor speed) constant in the above expression allows a plot of the torque versus rms voltage into the motor to be made. A family of curves representing torque versus rms voltage for different values of slip is shown in Figure 3.5. These curves were obtained using the following calculations. Substitution of the equivalent circuit parameters into the torque equation in (3-11) (equivalent circuit parameters are given in Appendix B) yields

$$T_{mech} = \frac{3\left|\vec{V}_1\right|^2 12.32 S}{20\pi \left[[2.23 S + 12.32]^2 + S^2 (11.2)^2 \right]} \left(\frac{volts^2 \cdot ohms}{rad/sec \cdot ohms^2}\right) \quad ,$$

$$(3\text{-}12)$$

where ω_s = 20π radians per second. Units of torque in equation (3-12) are in newton-metres. Converting the units to inch-pounds (conversion of units shown in Appendix C) and simplifying reduces equation (3-12) to

$$T_{mech} = \frac{5.2\left|\vec{V}_1\right|^2 S}{(2.23 S + 12.32)^2 + 125.44 S^2} \text{ in-lb} \qquad . \qquad (3\text{-}13)$$

By setting slip, S, constant at values ranging from S = 1 (motor stall) to S = 2 (motor shaft rotating at $-\omega_s$ against the magnetomotive force (MMF) produced by the stator voltages) equation (3-13) is used to plot torque T versus rms voltage per phase into the stator windings. As the motor is driven backwards against its torque, the slip becomes greater
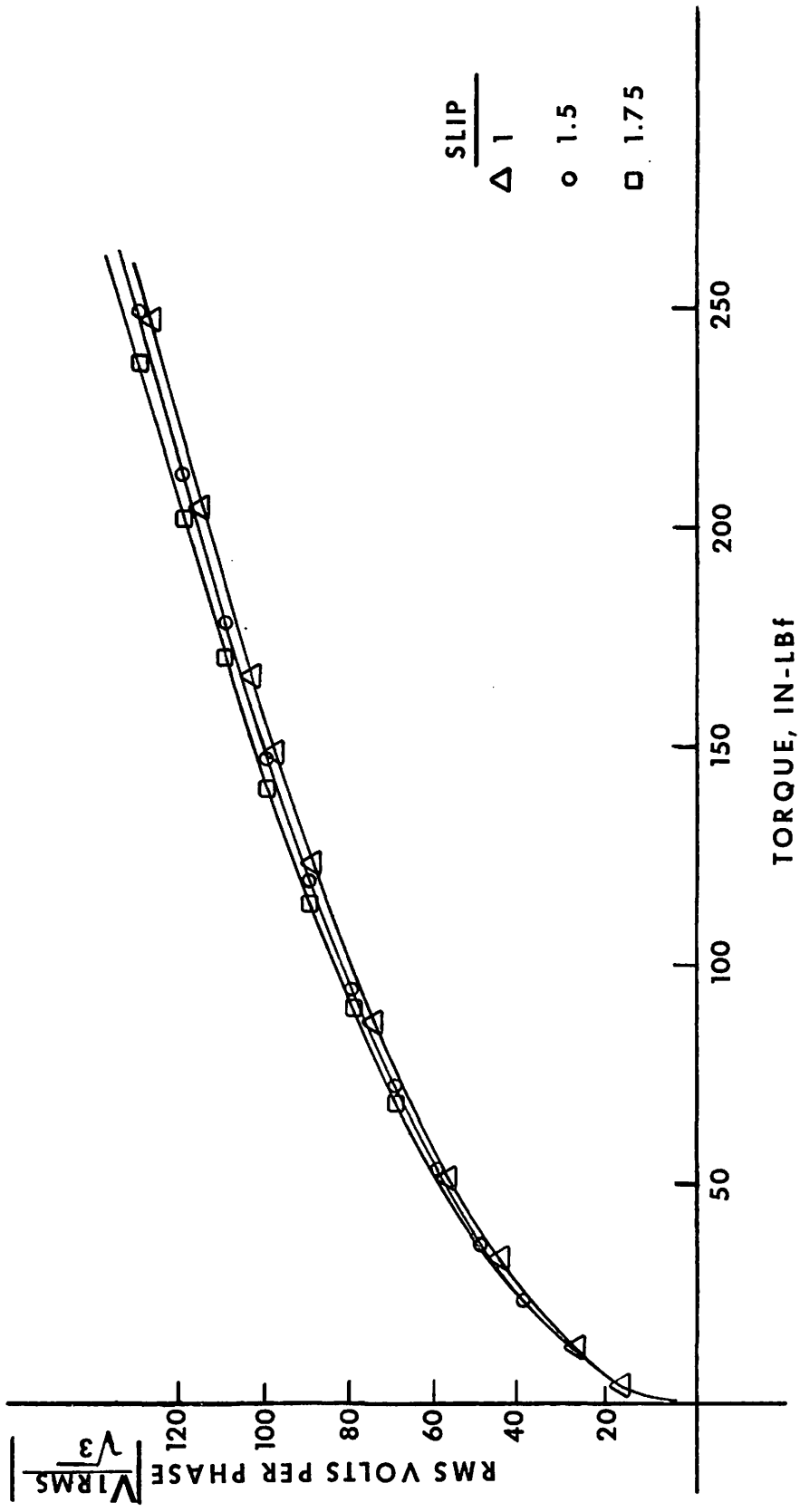
Figure 3.5. Torque versus RMS Voltage per Phase for Different Values of Slip.

than 1, and the electrical input to the rotor and the shaft input are consumed in secondary copper losses.[9]

From the curves in Figure 3.5 it is seen that torque does not vary appreciably with slip from stalled rotor conditions to negative rotor speeds up to $-3\omega_s$. This result agrees very well with the motor manufacturer's speed versus torque curves (Figure 3.6) for a typical torque motor brake.

Now that a relationship between V_{1rms} per phase and T has been plotted, a similar relationship between V_{1rms} per phase and θ_f, firing angle of the SCRs will be shown. The curve representing firing angle versus the rms stator voltage per phase will be used to make a composite curve relating firing angle and torque, thereby giving a relationship between input firing angle and output torque.

Figure 3.7 shows the waveform of the input voltage to the stator windings for any phase.[10,12] The load current waveform is also shown in this figure. θ_f and $\pi + \theta_f$ represent the SCR pair firing angles, γ represents the SCR conduction period, and α and β represent the extinction angles of the negative and positive half cycles of the load current respectively.

The waveforms shown in Figure 3.7 are the theoretical waveforms produced with a series connected RL load, representing the induction motor, controlled by a back-to-back SCR pair as shown in Figure 3.8.[10] In Figure 3.8 Req and Xeq are the equivalent impedances of the induction motor based on the equivalent circuit model presented in Figure 3.4, page 19.
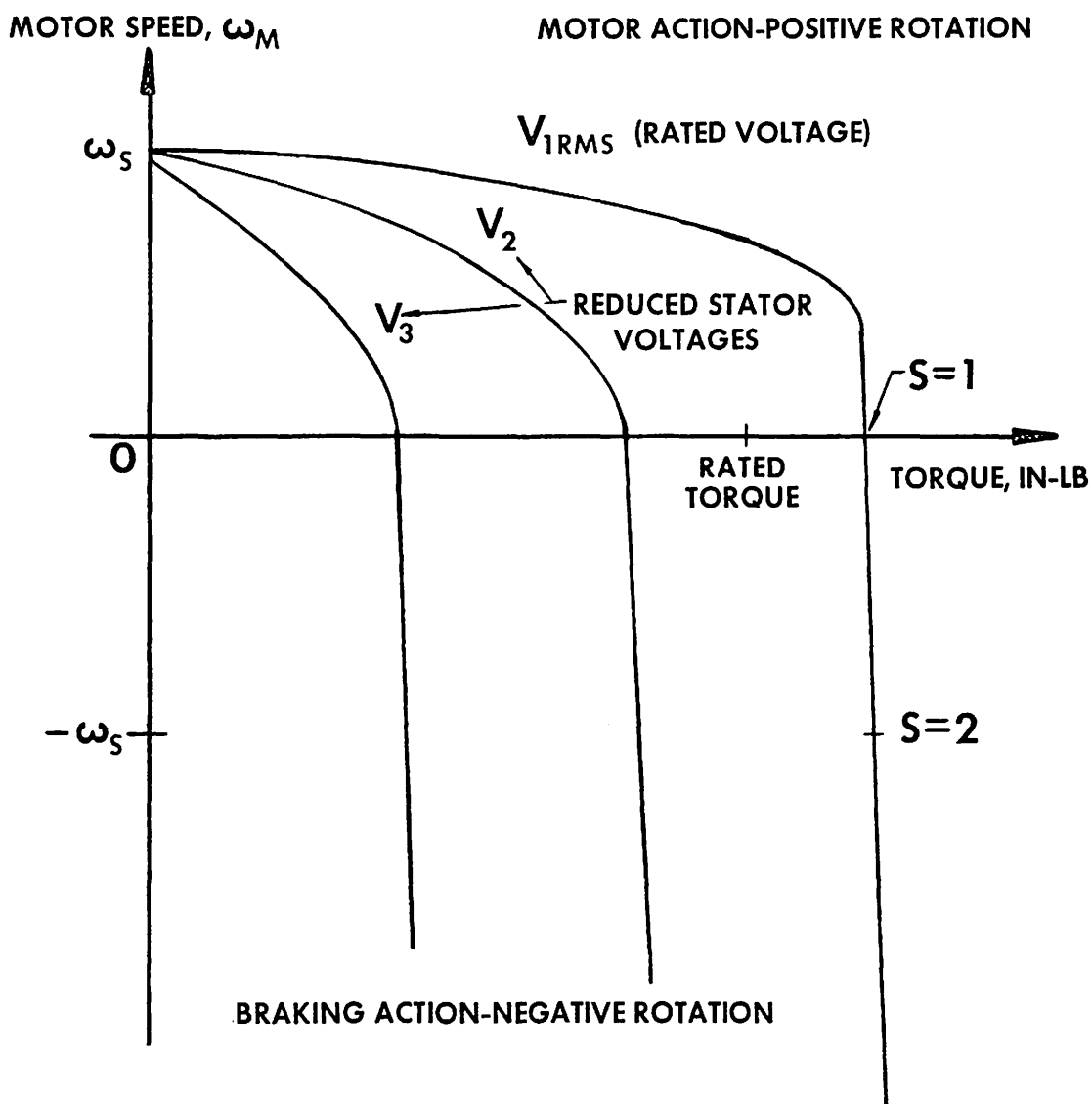
Figure 3.6. Typical Manufacturer's Speed versus Torque Curve for a Torque Motor Brake.
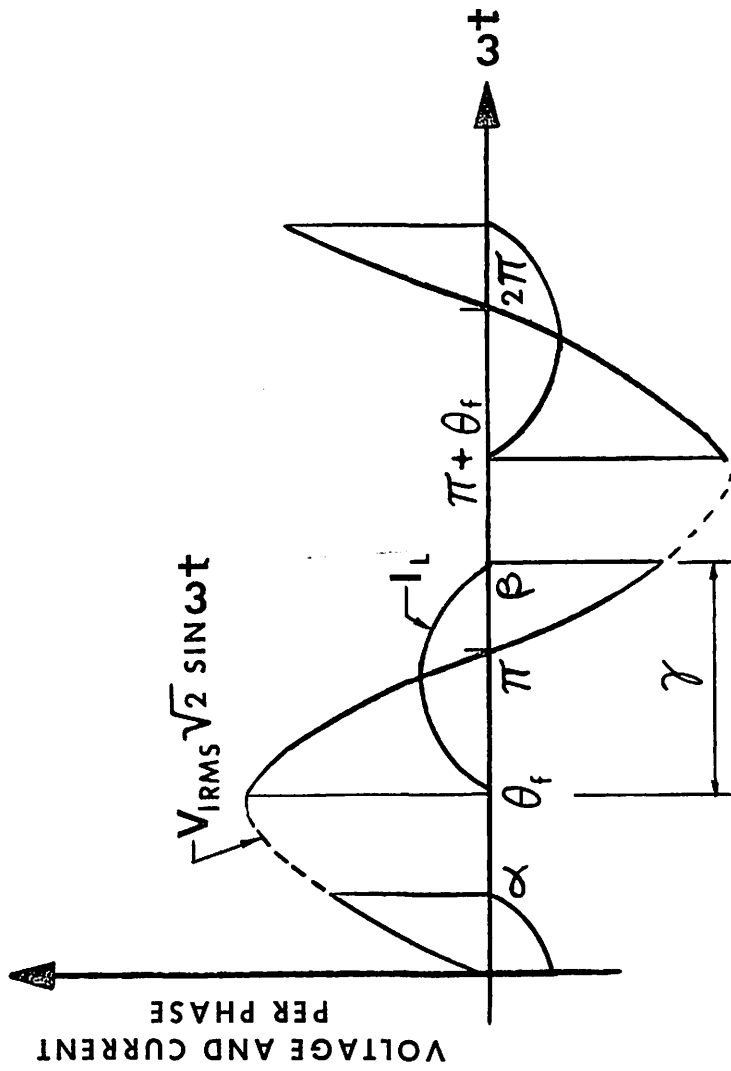
Figure 3.7. Theoretical Waveforms of the Input Voltage and Current to the Stator Winding per Phase.

Source: Shepherd, William, "Steady-State Analysis of the Series Resistance-Inductance Circuit Controlled by Silicon Controlled Rectifiers," *IEEE Trans. on Industry and General Applications*, vol. IGA-1, p. 260, July/August, 1965.
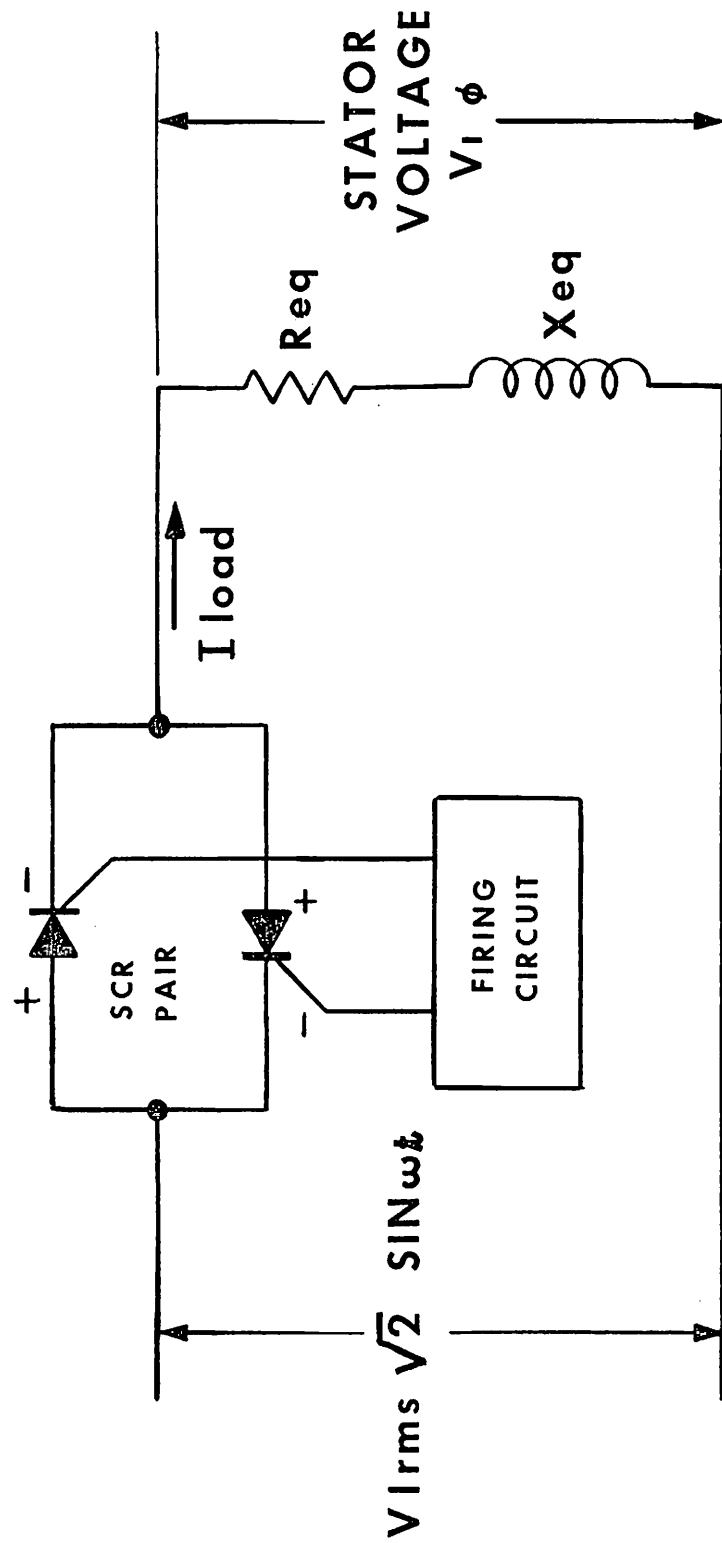
Figure 3.8. A Series Connected RL Load Controlled by a Back-to-Back SCR Pair.

It must be pointed out that the theoretical waveforms of Figure 3.7 are for a stationary single phase RL circuit. The waveforms produced by rotating RL circuits, as in an induction motor with several phases, produce harmonic components of current that alter the waveforms considerably. Figure 3.9 gives a typical waveform for line to neutral voltage of a stator winding in a 4-wire, wye-connected induction motor with an SCR firing angle of 60°.[11]

By referring the zero of time in Figure 3.7 to the start of the conduction of the SCR, the voltage per phase into the motor is given by

$$V_1/\text{phase} = \frac{V_{1rms}\sqrt{2}}{\sqrt{3}} \sin(\omega t + \theta_f) \quad .[6] \tag{3-14}$$

The rms voltage per phase as a function of the firing angle, θ_f can be determined as follows:

$$V_{1rms}/\text{phase} = \left[\frac{1}{\pi} \int_0^\gamma \left(V_{1rms}\sqrt{\frac{2}{3}}\right)^2 \sin^2(\omega t + \theta_f) d(\omega t) \right]^{1/2} \quad . \tag{3-15}$$

Making a change of variable and simplifying results in the following expression for V_{1rms}/phase:

$$V_{1rms}/\text{phase} = \left[\frac{1}{\pi} \int_{\theta_f}^{\gamma+\theta_f} \frac{2}{3}(V_{1rms}^2 \sin^2 u) du \right]^{1/2} \tag{3-16}$$

which reduces to
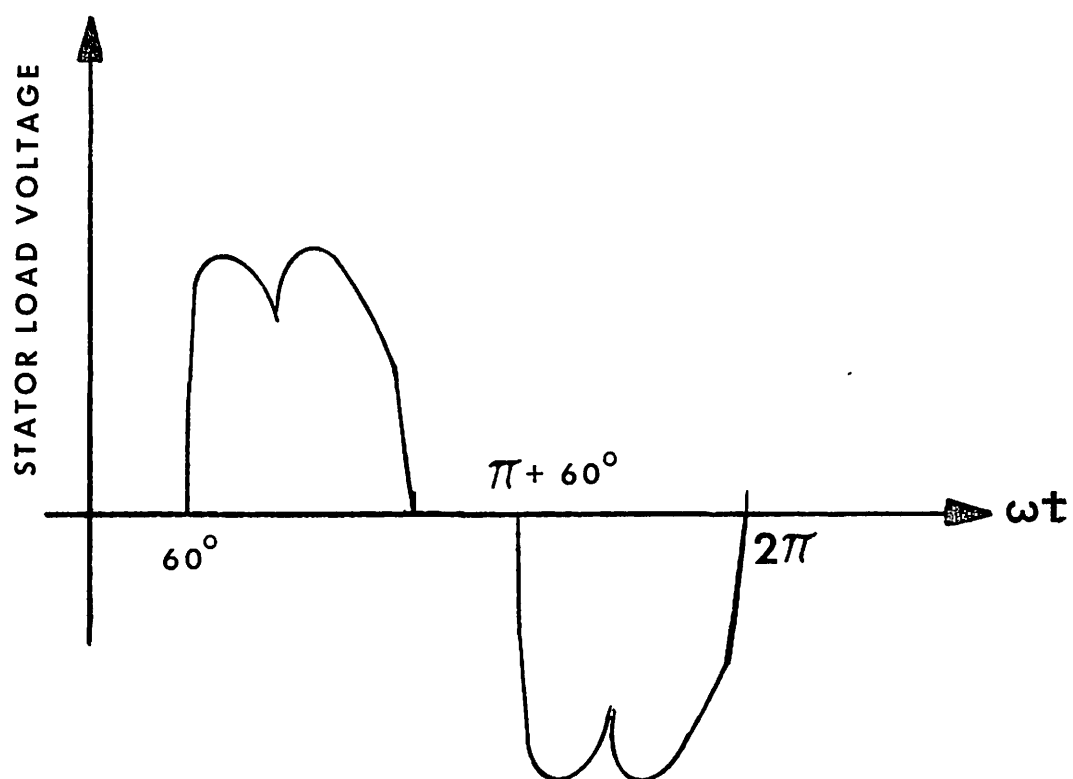
Figure 3.9. Load Voltage Waveform for a 3-Phase Induction Motor with an SCR Firing Angle of 60°.

$$V_{1rms}/\text{phase} = V_{1rms}\left[\frac{\gamma + \frac{1}{2}\sin 2\theta_f - \frac{1}{2}\sin 2(\gamma + \theta_f)}{3\pi}\right]^{1/2} .$$

(3-17)

In order to utilize equation (3-17) for plotting V_{1rms}/phase versus firing angle, θ_f, the conduction angle, γ must be known. The conduction angle, γ will be $180°$ for SCR firing angles less than or equal to the phase angle between the stator current and voltage.[12] Figure 3.10[12] shows a family of curves relating conduction angle γ and firing angle θ_f as a function of the phase angle, ϕ, where

$$\phi = \tan^{-1}\frac{Xeq}{Req} .$$

(3-18)

Req and Xeq are the equivalent impedances of the induction motor. Once the phase angle is known, the rms voltage per phase into the stator can be calculated for any pair of values of θ_f and γ using Figure 3.10 and equation (3-17). From the equivalent circuit of the induction motor given earlier in Figure 3.3, page 17, the equivalent impedances Req and Xeq can be determined. The total equivalent impedance of the equivalent circuit is

$$Zeq = R_1 + j\omega_1 L_1 + \frac{jX_m\left(\frac{a^2 R_2}{S} + ja^2\omega_1 L_2\right)}{\frac{a^2 R_2}{S} + j(X_m + a^2\omega_1 L_2)}$$

(3-19)

where X_m is the magnetizing branch impedance. Simplifying equation (3-19) reduces to
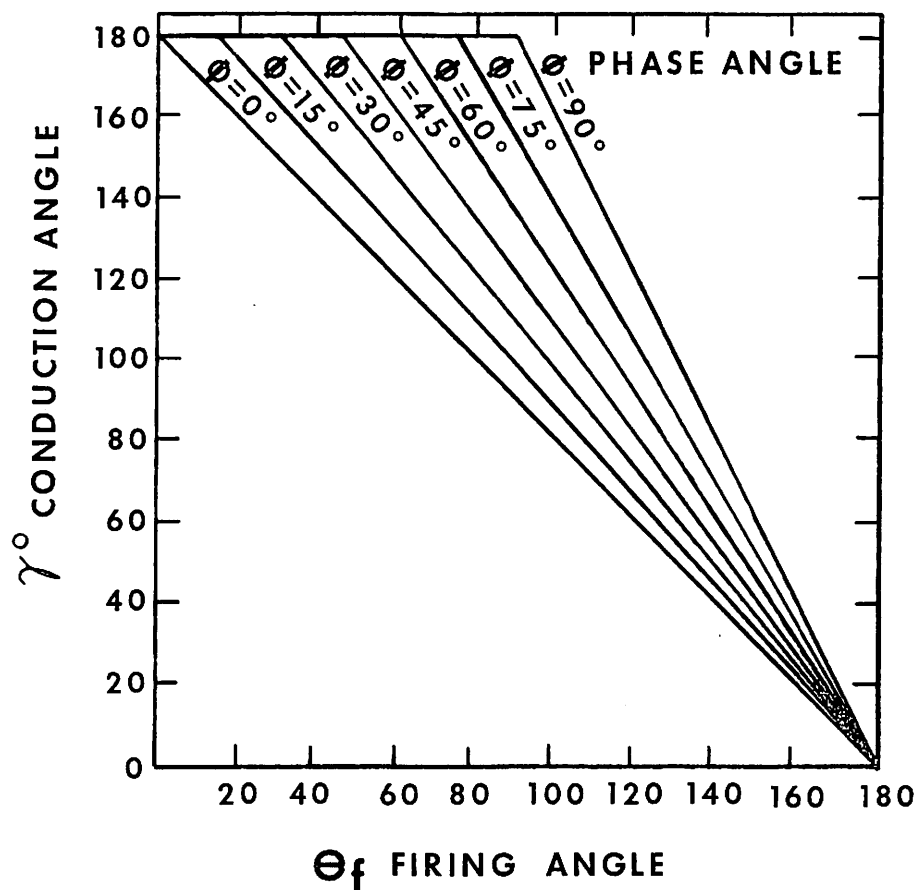
Figure 3.10. γ versus θ_f for Different Phase Angles, ϕ.

Source: Dewar, S. B. and A. Straughen, Power Semiconductor Circuits, John Wiley & Sons, New York, 1975, p. 162.

$$Z_{eq} = R_1 + jX_1 + \frac{jX_m\left(\dfrac{R_2'}{S} + jX_2\right)}{\dfrac{R_2'}{S} + j(X_m + X_2)} \quad , \text{ or}$$

$$Z_{eq} = R_1 + \frac{X_m^2\,\dfrac{R_2'}{S}}{\left[\dfrac{R_2'}{S}\right]^2 + (X_2 + X_m)^2} + j\left[X_1 + \frac{\left(\dfrac{R_2'}{S}\right)^2 + X_2(X_m + X_2)}{\left[\dfrac{R_2'}{S}\right]^2 + (X_2 + X_m)^2}\,X_m\right]$$

$$(3\text{-}20)$$

where $R_2' = a^2 R_2$, $X_1 = \omega_1 L_1$, and $X_2 = a^2\omega_1 L_2$. From equation (3-20) the equivalent impedances are

$$R_{eq} = R_1 + \frac{X_m^2\,\dfrac{R_2'}{S}}{\left[\dfrac{R_2'}{S}\right]^2 + (X_2 + X_m)^2} \quad , \text{ and} \qquad (3\text{-}21)$$

$$X_{eq} = X_1 + \frac{\left(\dfrac{R_2'}{S}\right)^2 + X_2(X_2 + X_m)}{\left[\dfrac{R_2'}{S}\right]^2 + (X_2 + X_m)^2} \cdot X_m \quad . \qquad (3\text{-}22)$$

Substituting (3-21) and (3-22) into equation (3-18) gives the expression for the phase angle as a function of slip, S

$$\phi = \tan^{-1}\frac{X_1 + \dfrac{\left(\dfrac{R_2'}{S}\right)^2 + X_2(X_2 + X_m)}{\left[\dfrac{R_2'}{S}\right]^2 + (X_2 + X_m)^2} \cdot X_m}{R_1 + \dfrac{X_m^2}{\left[\dfrac{R_2'}{S}\right]^2 + (X_2 + X_m)^2} \cdot \dfrac{R_2'}{S}} \quad . \qquad (3\text{-}23)$$

The phase angle given in equation (3-23) will vary depending on the speed of the torque motor. During a coil winding operation the maximum winding speed corresponds to a 2.4 inches per second (in/sec) linear velocity of the superconductor. Figure 3.11 shows how the velocity of the superconductor affects the torque motor shaft's speed.

In Figure 3.11 the conductor is shown passing over one of the four belt pulleys of the tension machine. This pulley is connected to the torque motor through a 57.66:1 gear reducer. The 2.4 in/sec velocity of the conductor causes the 6 inch drive pulley to turn at a speed of 7.64 revolutions per minute (rpm) which corresponds to -440.5 rpm of the torque motor.

Since slip of the rotor is defined as

$$S = \frac{\omega_s - \omega_m}{\omega_s} \quad , \text{ or}$$

$$S = \frac{N_s - N_m}{N_s} \qquad\qquad (3\text{-}24)$$

where N_s is the synchronous speed of the motor in rpm and N_m is the actual motor speed, the slip can be determined for any given conductor speed. The torque motor used in the tension machine has a synchronous speed of 600 rpm. Therefore, the slip at -440.5 rpm is determined from equation (3-24) as follows:

$$S = \frac{N_s - N_m}{N_s} = \frac{600 - (-440.5)}{600} = 1.73 \quad . \qquad (3\text{-}25)$$
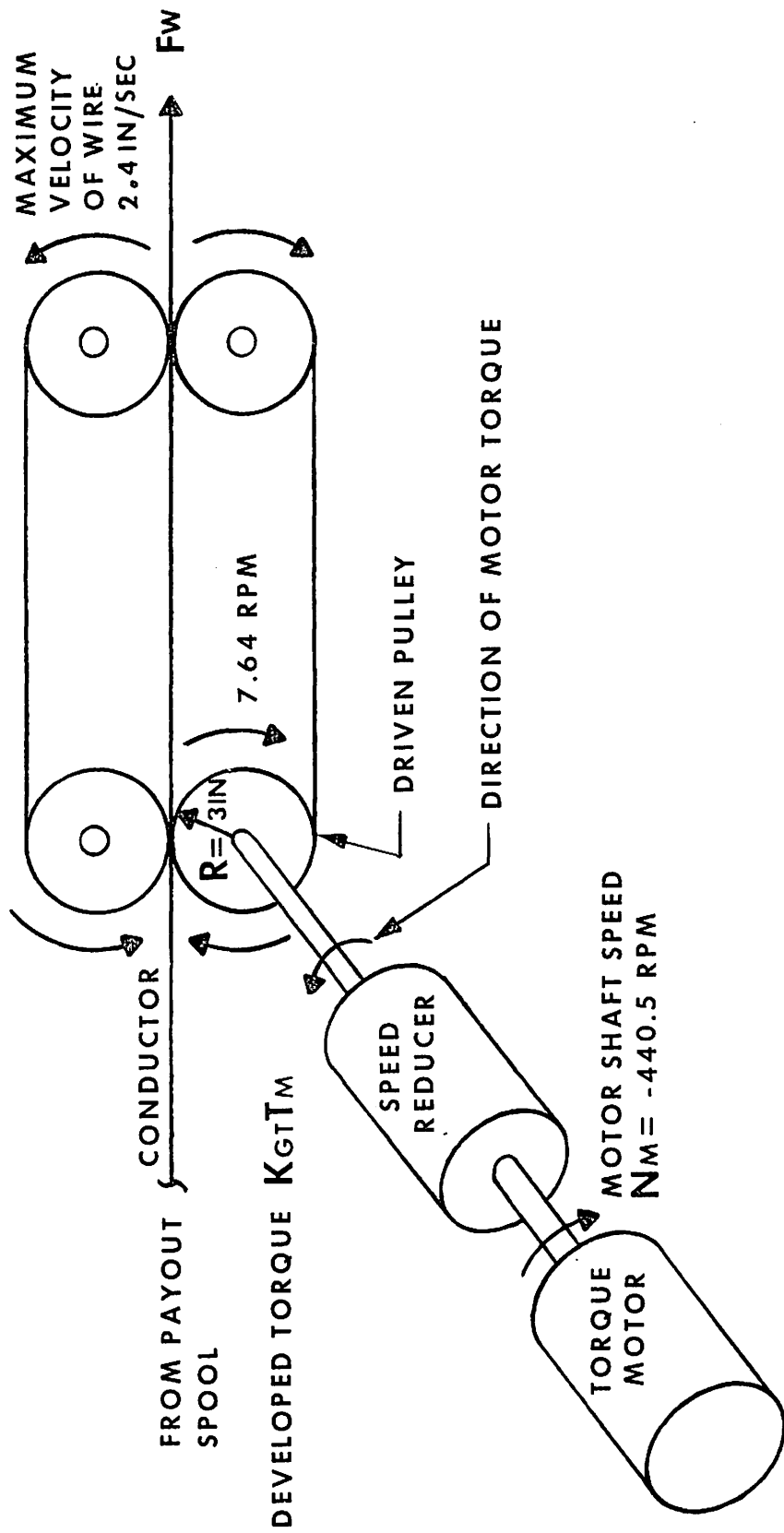
Figure 3.11. Relationship between Conductor Speed and Torque Motor Shaft Speed.

From the motor manufacturer's locked rotor and running light tests, the equivalent circuit parameters are

$$
\left.\begin{array}{l}
R_1 = 2.23\Omega \\[4pt]
X_m \simeq 50.8\Omega \\[4pt]
R_2' = 12.32\Omega \\[4pt]
X_1 = 5.6\Omega \\[4pt]
X_1 = X_2' \text{ by assumption.}
\end{array}\right\} \qquad (3\text{-}26)
$$

Now that all of the parameters in equation (3-23) are known, the phase angle, ϕ, can be determined. Substituting equations (3-25) and (3-26) into (3-23) yields

$$
\phi = \tan^{-1} \frac{11.36}{7.92} = 55° \quad . \qquad (3\text{-}27)
$$

Equation (3-27) gives the phase angle between the motor current and voltage for maximum winding speed. The phase angle for motor stall can be calculated using equation (3-23) again with slip = 1. With S = 1, the phase angle becomes

$$
\phi = \tan^{-1} \frac{12.73}{11.77} = 47° \quad . \qquad (3\text{-}28)
$$

With the phase angle known, the conduction angle γ for any SCR firing angle can be determined using Figure 3.10, page 31. Table 3.1 gives the firing angle and conduction angle for the two values of phase angle determined in equations (3-27) and (3-28).

TABLE 3.1

CONDUCTION ANGLE VERSUS FIRING ANGLE
FOR PHASE ANGLES OF 47° AND 55°[a]

θ_f	$\gamma(\phi = 47°)$	$\gamma(\phi = 55°)$
0	180	180
20	180	180
40	180	180
45	180	180
50	180	180
60	165	172
80	145	150
100	120	123
120	95	97
140	65	66
160	35	35
170	20	20
180	0	0

[a]All values in degrees.

The values of firing angle and conduction angle in Table 3.1 are used in equation (3-17) to calculate V_{1rms} per phase, the results of which are given in Table 3.2.

In Figure 3.12 the calculated fundamental load voltage per phase is shown as functions of the firing angle for the two phase angles of 47° and 55°. This figure indicates that the fundamental load voltage does not vary significantly with the phase angle for motor slips between 1 and 2. It should be pointed out that the equivalent circuit of an induction motor is based on the fundamental component of current and voltage.[6] For delayed firing angles of the SCRs, considerable harmonics begin to alter the value for voltage calculated using equation (3-17). Actual measurements of load voltages versus SCR firing angles for a typical 3-phase, wye-connected induction motor show that voltage disappears at a firing angle of 120° instead of the 180° theoretically calculated using the equivalent circuit model.[11]

In an attempt to obtain a more realistic representation for stator voltage versus firing angle for the 3-phase induction motor, results taken from actual measurements on a typical motor will be utilized. In Figure 3.13 is shown a curve representing the measured ratio of fundamental load voltage to total load voltage as firing angle increases.[11] Figure 3.14 shows the measured harmonic components of the load voltage for this motor. These two curves were obtained using a commercial electronic wave analyzer.[11] Since the harmonic components shown in Figures 3.13 and 3.14 are on a per unit basis, it is assumed that these components are typical for a 3-phase, wye-connected induction

TABLE 3.2

STATOR RMS VOLTAGE PER PHASE VERSUS FIRING ANGLE
FOR PHASE ANGLES 47° AND 55°

θ_f in Degrees	V_{1rms}/Phase in Volts (ϕ = 47°)	V_{1rms}/Phase in Volts (ϕ = 55°)
0	127	127
20	127	127
40	127	127
50	125	127
60	120	123
80	106	109
100	86	87
120	62	63
140	36	37
160	14	14
170	6	6
180	0	0
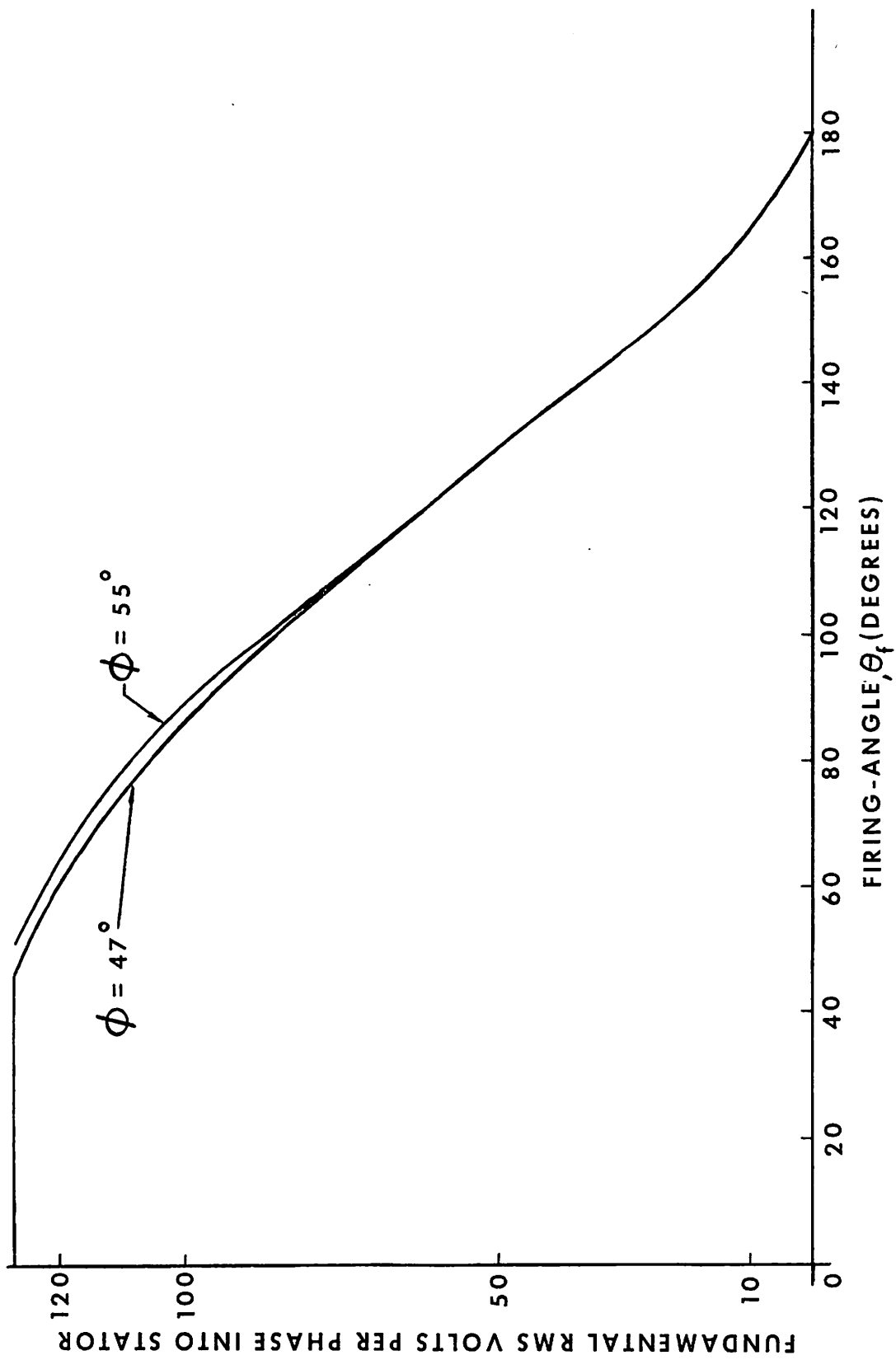
Figure 3.12. Calculated Fundamental Load Voltage into the Stator Windings versus SCR Firing Angle.

$$\frac{V_1}{\sqrt{\sum V_h^2}}$$

FIRING ANGLE, θ_f (DEGREES)
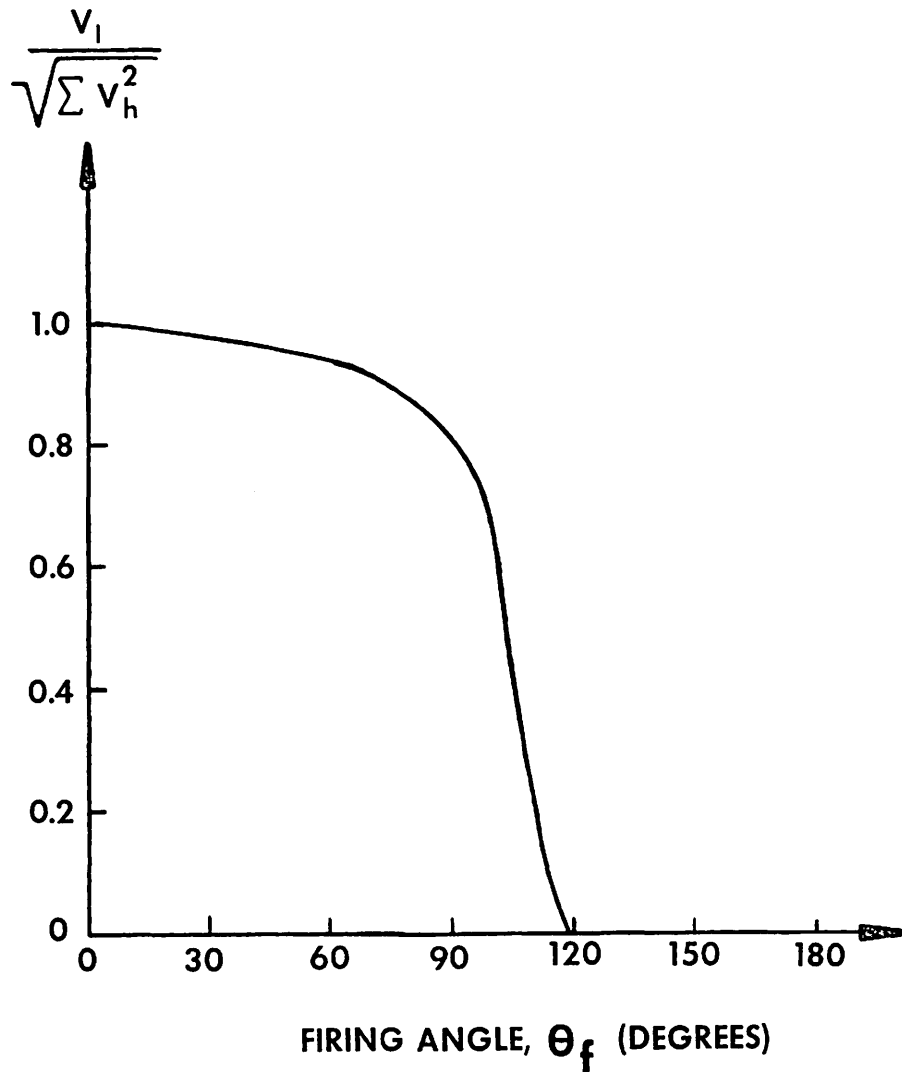
Figure 3.13. Measured Ratio of Fundamental Load Voltage, V_1, to the
Total Voltage for Each Harmonic Voltage Waveform, V_h.

Source: Shepherd, William and Jack Stanway, "The Polyphase Induction
Motor Controlled by Firing Angle Adjustment of Silicon
Controlled Rectifiers," 1964 IEEE International Convention
Record, vol. 12, pt. 4, p. 143, March 1964.
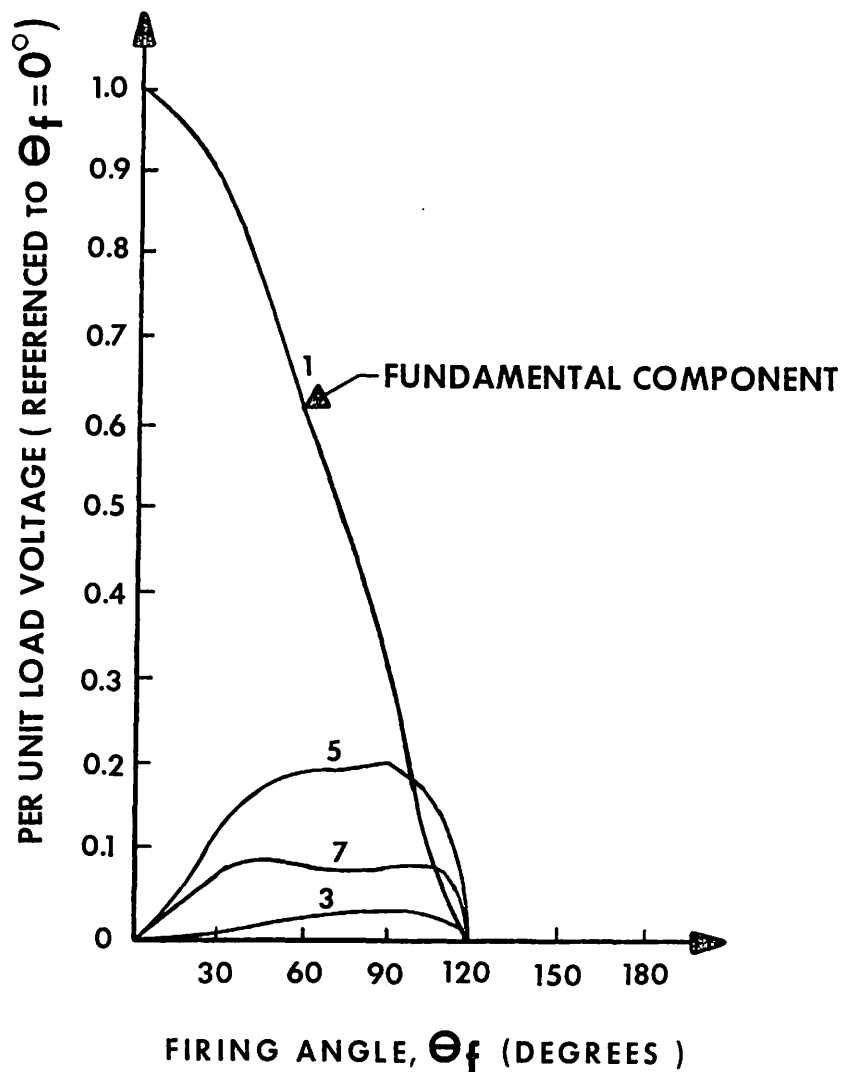
Figure 3.14. Measured Harmonic Components of the Load Voltage
Waveforms for a Typical 3-Wire, Wye-Connected Induction
Motor.

Source: Shepherd, William and Jack Stanway, "The Polyphase Induction
Motor Controlled by Firing Angle Adjustment of Silicon
Controlled Rectifiers," 1964 IEEE International Convention
Record, vol. 12, pt. 4, p. 143, March 1964.

motor. The values for the stator voltage taken from Figures 3.13 and 3.14 are shown plotted against increasing firing angles in Figure 3.15.

From Figures 3.5, page 23, and 3.15 a composite curve representing torque versus SCR firing angle is made. Since variations in rotor speed between motor stall and negative shaft speeds has little effect on the voltage versus torque curves shown in Figure 3.5, an average value for voltage was used in determining the corresponding torque value for the composite curve shown in Figure 3.16.

The range of tensions desired in manufacturing the superconducting coils is between the values of 200 and 1500 pounds. These limits correspond to approximately 10 inch-pounds (in-lb) of motor torque for 200 pounds tension and 80 in-lb for 1500 pounds tension. A straight line approximation to the curve in Figure 3.16 between torque values of 0 and 100 in-lbs corresponds to a gain constant of roughly

$$K_{\theta_f T} = - \frac{100 - 0}{90 - 50} \frac{\text{in-lbs}}{\text{degrees}} \quad , \text{ or}$$

$$K_{\theta_f T} = - 2.5 \frac{\text{in-lbs}}{\text{degree}} \quad , \tag{3-29}$$

where $K_{\theta_f T}$ represents the gain constant between SCR firing angle and output torque developed by the motor.

Thus far the model development for the SCR controller and torque motor has resulted in a relationship between input firing angle and output torque. In block diagram form the system relationship based on this development is given in Figure 3.17.[13]
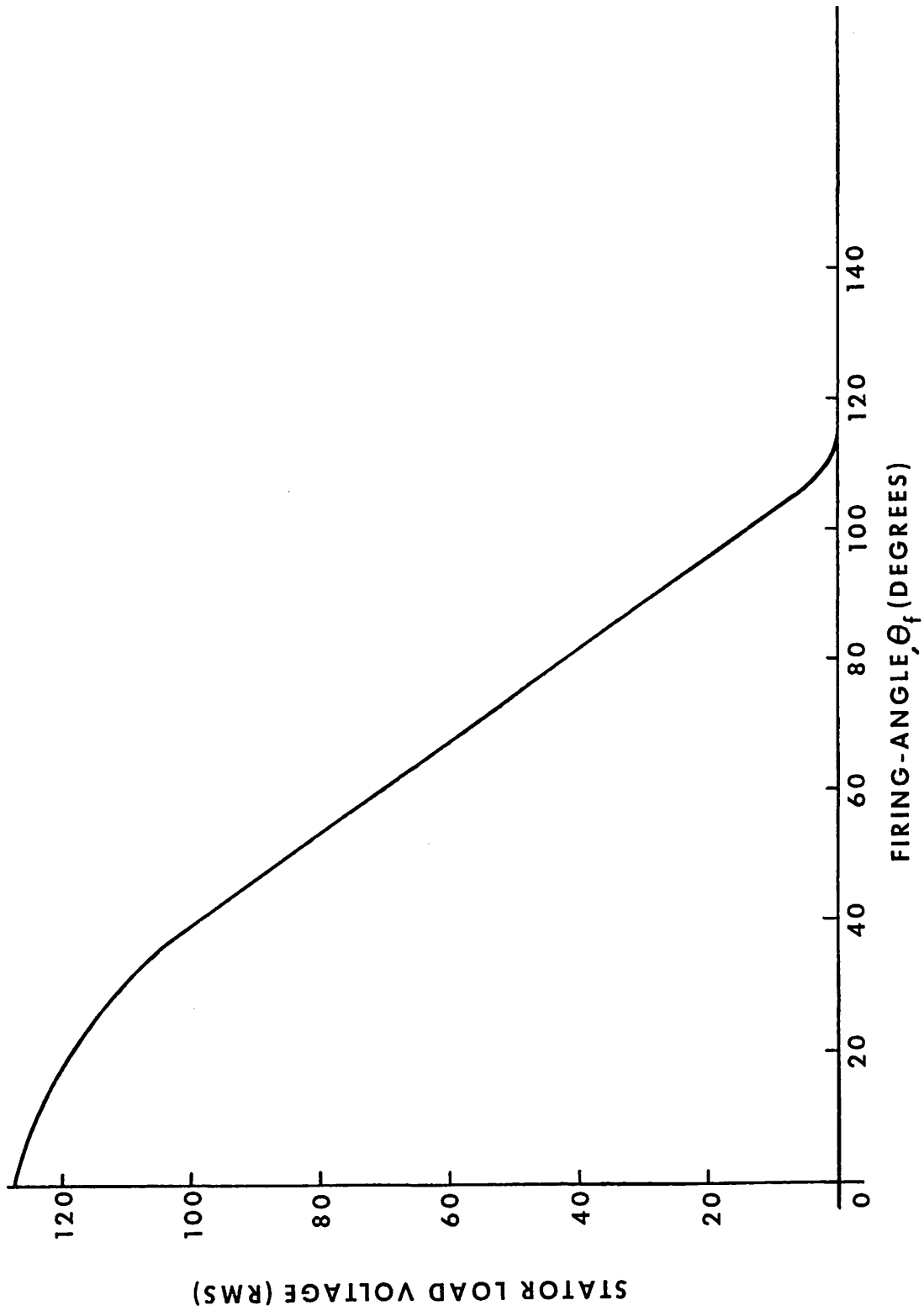
Figure 3.15. Typical Measured Stator Load Voltage versus SCR Firing Angle.
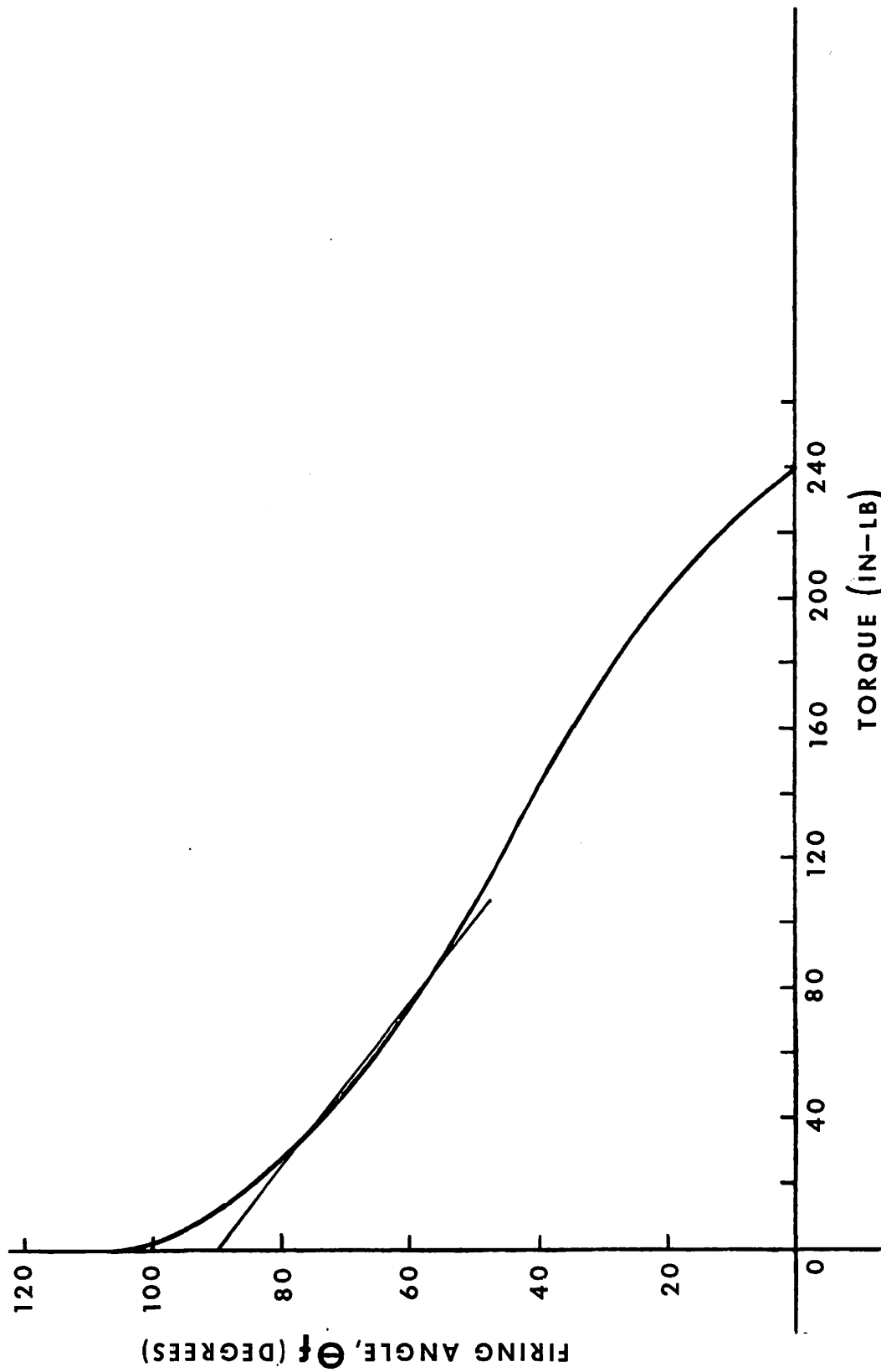
Figure 3.16. Torque versus Firing Angle.
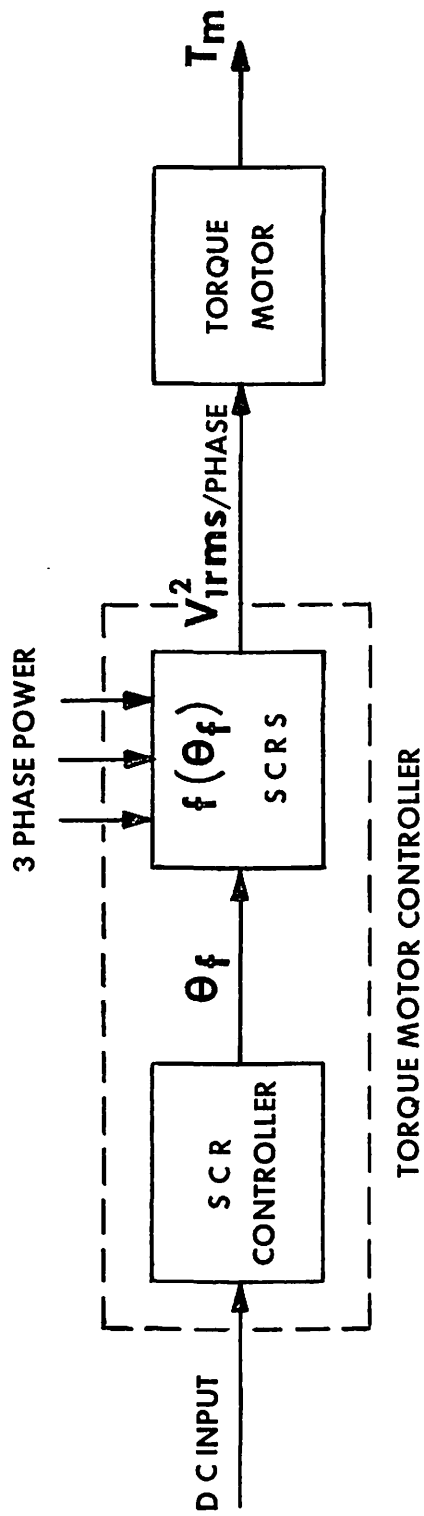
Figure 3.17.   Block Diagram of Torque Motor and Controller.

The trigger circuits varying the SCR firing angles are controlled by a 0 to 10 volt dc input signal. A 10 volt signal corresponds to a firing angle of 0 degrees, or maximum torque from the motor. Since a torque demand of approximately 80 in-lb is required for a maximum tension of 1500 pounds, only a portion (5 volts) of the input signal is used. The relation between input voltage to the controller and firing angle can be represented by

$$\frac{\text{Degrees}}{\text{dc input}} = - \frac{90° - 50°}{5 \text{ volts}} = -8 \frac{\text{degrees}}{\text{volt}} \quad . \tag{3-30}$$

Combining equations (3-29) and (3-30) yields a gain constant for the SCR controller and torque motor of

$$K_T = 20 \frac{\text{in-lbs}}{\text{volt}} \quad , \tag{3-31}$$

where K_T represents the gain constant.

Typical electrical time constants of induction motors range between 5 and 10 milliseconds. The motor electrical time constant, combined with the electrical time constant associated with the SCR controller, and equation (3-31) yield a transfer function[13]

$$\frac{T_m(s)}{E_{dc}(s)} = \frac{K_T}{1 + \tau_e s} \quad , \tag{3-32}$$

where

$T_m(s)$ represents torque output of the motor,

$E_{dc}(s)$ represents the dc voltage input to the SCR controller,

τ_e is the combined electrical time constant, and

s   is the Laplace transform variable.

Speed or Gear Reducer

The output shaft of the torque motor is connected to a 57.66:1 gear reducer. Connected to the low speed shaft of the gear reducer is the 6 inch drive pulley of the belt system described in Chapter II. Assuming 95 percent efficiency of the speed reducer in transferring the torque of the motor to the 6 inch pulley results in a gain constant for the reducer of

$$K_{GT} \simeq 55 \quad . \tag{3-33}$$

The shaft lengths of the speed reducer and the torque motor are short enough to consider stiffness in the shafts to be infinite.[14] The polar moment of inertia of the speed reducer referred to the low speed shaft is quite high (13,000 to 14,000 lb-in^2), and most of the coulomb friction torque of the belt system and gear reducer is due to the speed reducer. This friction torque is represented by T_F in the system block diagram shown on page 56.

Since the speed reducer's low speed shaft is driven by the force pulling the superconductor through the belt system, and not by the torque motor, the controlled variable on the drive pulley is torque, rather than speed as in most motor applications.

Mechanical System of Tension Machine

The constant tension device, skid, and tension load cell shown in Figures 2.1 and 2.2 on pages 7 and 8 are equivalent mechanically to

Figure 3.18. Since no slippage was assumed between the superconductor

and the two belt system, a force F_W in the conductor wire will cause the

skid to deflect some distance x. The force, F_{ps} exerted by the payout

spool on the tension machine is essentially zero. Figure 3.18 reduces

to a simple spring-mass-damper mechanical system where K is the spring

constant of the tension cell, f is the friction between the skid and

floor, and M is the mass of the skid and tension machine (wire mass is

negligible).[15]

Newton's second law of motion describes the mechanical system's

motion as follows:

$$M \frac{d^2x(t)}{dt^2} + f \frac{dx(t)}{dt} + Kx(t) = F_W(t) \quad .^{15} \tag{3-34}$$

Applying the Laplace transform to the last expression yields

$$Ms^2X(s) + fsX(s) + KX(s) = F_W(s) \quad , \tag{3-35}$$

for zero initial conditions.

The transfer function relating skid (tension cell) deflection to

applied force becomes

$$\frac{X(s)}{F_W(s)} = \frac{1}{M(s^2 + \frac{f}{M}s + \frac{K}{M})} \quad . \tag{3-36}$$
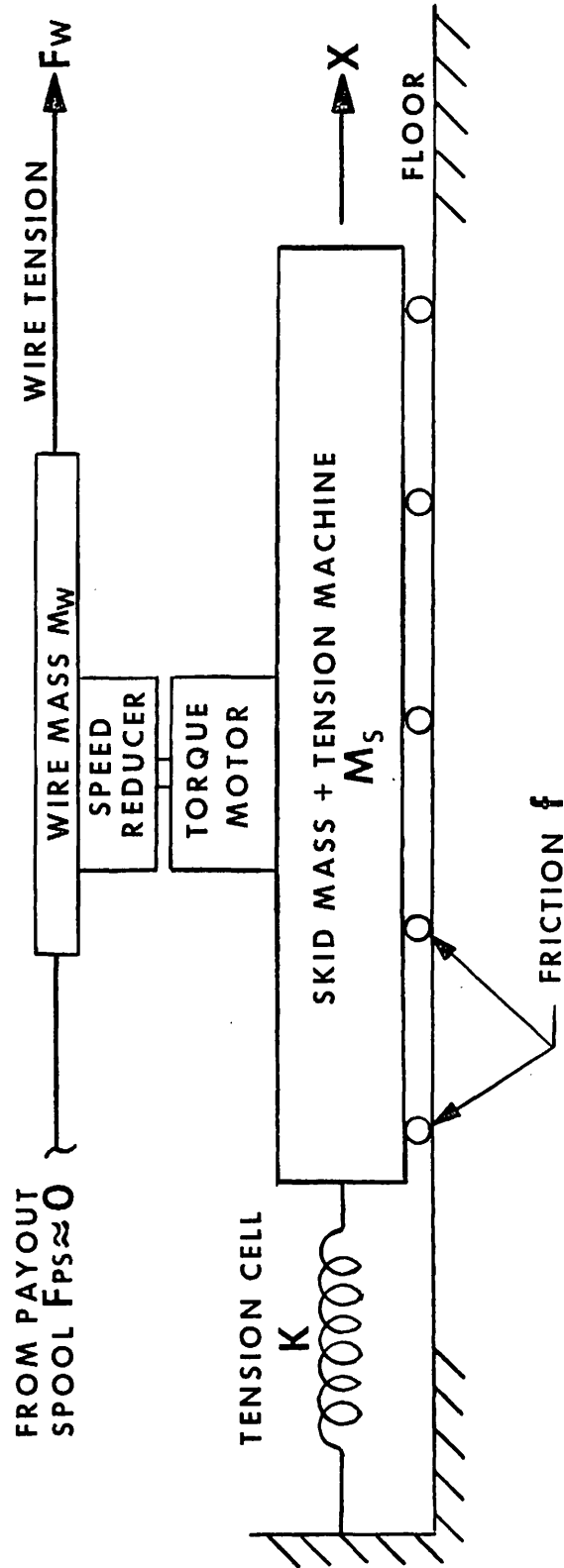
Figure 3.18. Equivalent Mechanical System.

Relationship between $F_W(s)$ and $T_m(s)$

In the previous pages expressions for $T_m(s)$ and $F_W(s)$ have been presented. An expression relating these two variables is given in the following paragraphs.

Writing torque equations for the 6 inch drive pulley of the belt system results in the following expression:

$$T_1(t) = Jeq \frac{d^2\theta_1}{dt^2} + Beq \frac{d\theta_1}{dt} + T_m(t) \frac{N_1}{N_2} \quad , \tag{3-37}$$

where

$T_1(t)$	represents the load torque developed on the drive pulley by the winding motor,
Jeq and Beq	are the equivalent polar moment of inertia and friction, respectively, for the combined torque motor rotor, speed reducer, drive pulley, and belt system,
θ_1	is the drive pulley's angular displacement,
$T_m(t)$	is the torque produced by the torque motor, and
N_1/N_2	is the turns ratio of the speed reducer.

Figure 3.19 shows the relationship of the parameters in (3-37).

Load torque $T_1(t)$ is also represented by

$$T_1(t) = R \times F_W(t) \tag{3-38}$$

where R is the moment arm of the pulley. Substituting (3-38) into (3-37) and simplifying results in the following expression for wire tension:
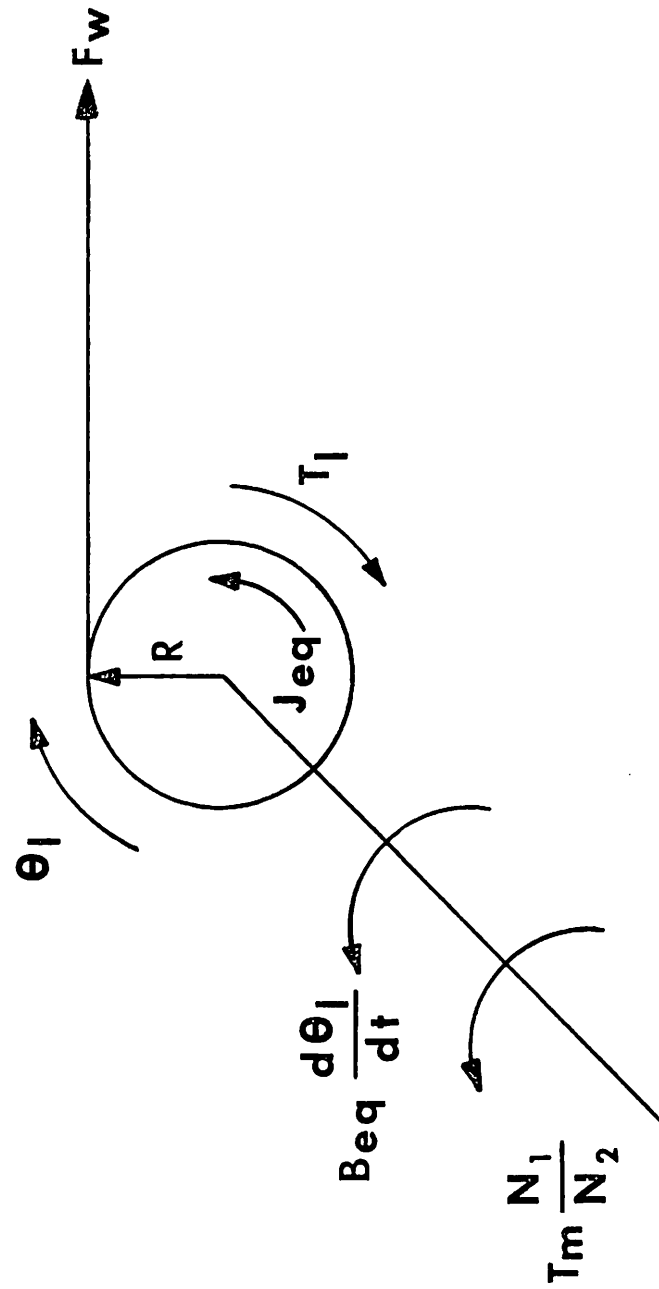
Figure 3.19. Torque Relations for Drive Pulley.

$$F_W(t) = \frac{1}{R} \left[Jeq \frac{d\omega_1(t)}{dt} + Beq\omega_1(t) + T_m(t) \frac{N_1}{N_2} \right] \quad, \qquad (3-39)$$

where $d\theta_1/dt = \omega_1$. Taking the Laplace transform of (3-39) yields

$$F_W(s) = \frac{1}{R} \left[Jeq \; s\Omega_1(s) + Beq\Omega_1(s) + T_m(s) \frac{N_1}{N_2} \right] \quad . \qquad (3-40)$$

Replacing $(Jeq \; s + Beq)\Omega_1(s)$ with $T_d(s)$, which represents a torque disturbance, and N_1/N_2 with K_{GT}, equation (3-33), reduces (3-40) to

$$F_W(s) = \frac{1}{R} \left[T_d(s) + K_{GT}T_m(s) \right] \quad . \qquad (3-41)$$

This result will be used in deriving the overall system transfer function.

Commercial Controller and Recorder

A commercial controller with proportional, integral and derivative (PID) actions was purchased for compensation requirements of the automatic tensioning device. The controller produces a milliampere current proportional to the error signal between the reference and load cell system inputs. Measuring the load cell system's signal is a strip chart recorder containing a retransmitting control slidewire. The recorder compares the measured load cell signal with the set point and "retransmits" the difference as an error signal to be processed by the PID controller.

The transfer function of the PID controller is represented by

$$\frac{M(s)}{E(s)} = K_c(1 + \frac{1}{\tau_i s} + \tau_d s) \quad ,[16] \qquad (3-42)$$

where M(s)   represents the PID output,

   E(s)   is the error input,

   K_c is the proportional gain constant,

   τ_i is the integral time constant,

   τ_d is the derivative time constant, and

   s   is the Laplace transform variable.

The gain constant and time constants associated with equation (3-42) are variable and depend on the desired control and root locations of the automatic system.

The recorder has a simple order lag transfer function with a frequency response of approximately 2.5 radians per second. In equation form the transfer function becomes

$$\frac{\text{Output}}{\text{Input}} = \frac{1}{1 + \tau_r s} \quad , \tag{3-43}$$

where τ_r is the recorder time constant.

A fixed gain constant, K_R, exists between the recorder input and controller output. This gain constant converts recorder input voltage and controller output current into the dc input voltage for the torque motor controller.

Combined Transfer Function

Combining equations (3-2), (3-32), (3-36), (3-42), (3-43) and the gain constants K_{GT}, K_R, and 1/R gives an overall open-loop transfer function for reference input to tension output of

$$GH(s) = \frac{K_c K_{GT} K_R K_{CG} K_T (1 + \frac{1}{\tau_i s} + \tau_d s)}{(1 + \tau_r s)(1 + \tau_e s)(1 + \tau_{LC} s)(s^2 + \frac{f}{M}s + \frac{K}{M})MR} \qquad (3\text{-}44)$$

The numerical values of the fixed constants in equation (3-44) are

given in Table 3.3. Substitution of these values into equation (3-44)

and neglecting the load cell, motor controller and motor electrical time

constants results in the following expression for the open-loop transfer

function:

$$GH(s) = \frac{101906 \ G_c(s)}{(1 + 0.4s)(s^2 + 1.67s + 27820)} \qquad (3\text{-}45)$$

where $G_c(s) = K_c(1 + 1/\tau_i s + \tau_d s)$.

A block diagram of the control system is given in Figure 3.20. In

Chapter IV the stability analysis of the control system is discussed.

TABLE 3.3

FIXED SYSTEM CONSTANTS

Constant	Description	Value	Units
K_{GT}	Speed reducer gear ratio	55	—
K_R	Fixed controller gain	500	$\dfrac{volts}{volt}$
K_{CG}	Load cell gain constant	3.33	$\dfrac{volts}{inch}$
K_T	SCR controller and torque motor gain constant	20	$\dfrac{in\text{-}lb_f}{volt}$
τ_r	Recorder time constant	0.4	seconds
τ_{LC}	Load cell system time constant	0.006 to 0.007	seconds
τ_e	SCR controller and motor electrical time constant	0.005 to 0.010	seconds
M	Mass of skid and tension machine	71.89	$\dfrac{lb_f\text{-}sec^2}{ft}$
f	Friction between skid and floor	10	$\dfrac{lbs\text{-}sec}{inch}$
K	Spring constant of load cell	166666.67	$\dfrac{lb_f}{inch}$
R	Radius of drive pulley	3	inches
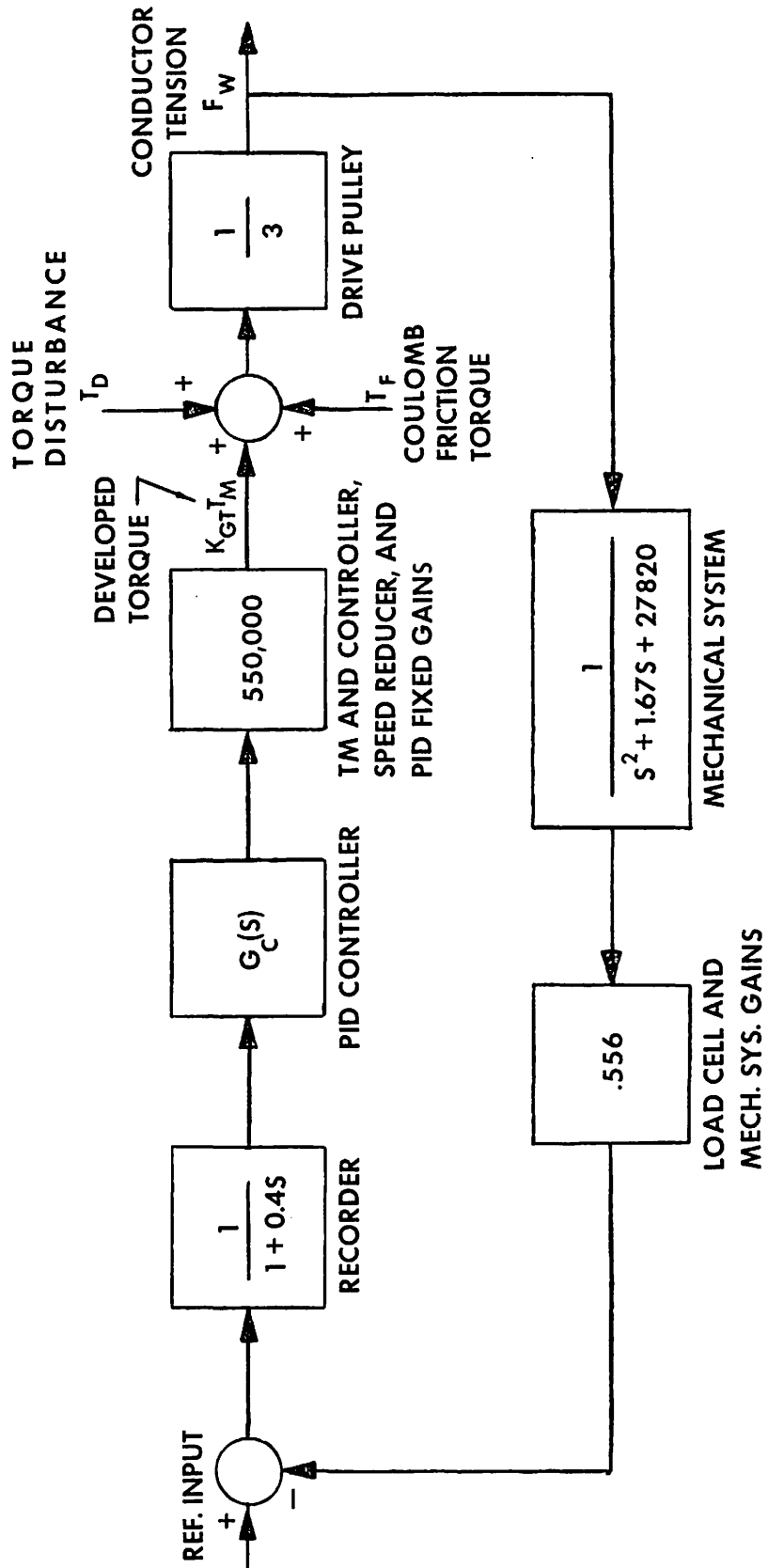
Figure 3.20. Control System Block Diagram for the Tension Machine.

CHAPTER IV

STABILITY ANALYSIS

The primary design requirement of the tension machine was to control tension within ±10 percent of the demand input. Sudden demand changes such as a step input were not expected of the system. Prior to any investigation of the system stability, compensation requirements were to be provided by the commercial PID controller with retransmitting slidewire recorder.

The stability analysis that follows is based on the application of the PID controller algorithm for system stability.

In Chapter III the open-loop transfer function for the system was developed and is repeated here for convenience:

$$GH(s) = \frac{101906 \ G_c(s)}{(1 + 0.4s)(s^2 + 1.67s + 27820)}$$

where $G_c(s)$ represents the PID controller transfer function.

Neglecting $G_c(s)$ for the moment reduces $GH(s)$ to

$$GH(s) = \frac{101906}{(1 + 0.4s)(s^2 + 1.67s + 27820)} \ . \tag{4-1}$$

A Bode diagram for the open-loop transfer function of the uncompensated system given in equation (4-1) is shown plotted in Figure 4.1. On a Bode diagram, which plots frequency ω in radians per second against system gain in decibels (dB), it is generally desired to
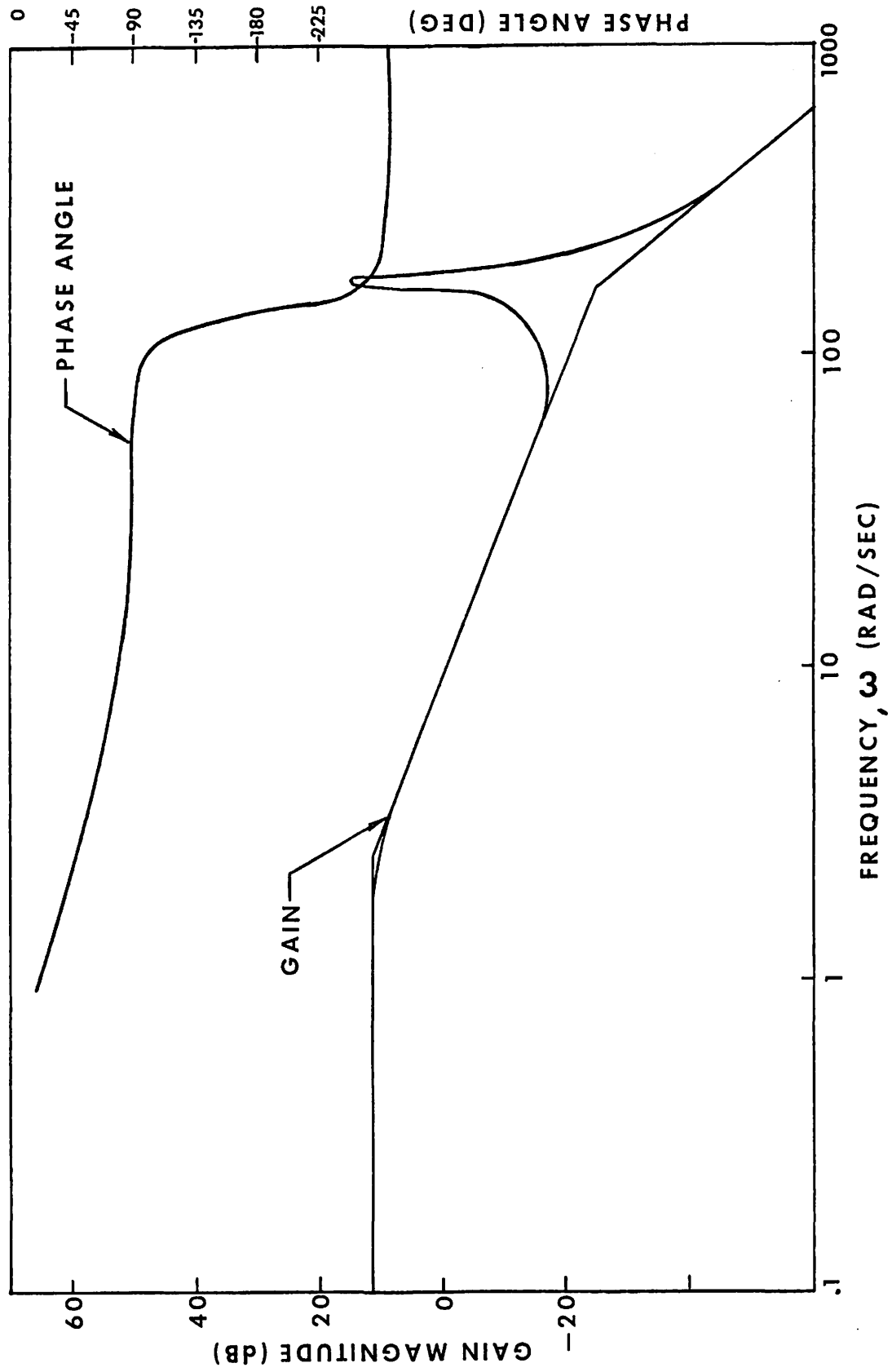
Figure 4.1. Bode Diagram for Uncompensated System (Open-Loop).

have the slope of the gain curve cross the zero dB line at -20 dB per decade with a phase margin (ϕM) between 30° and 60°. In Figure 4.1 the gain curve crosses the zero dB line at -20 dB per decade and the phase angle at crossover is approximately -75° (ϕM = 105°), but the system is very undesirable. Any attempt at meeting the desired ±10 percent of demand input would raise the gain curve and cause it to approach a roll off of -60 dB per decade at the zero dB crossover with a phase margin of 0°.

Raising the gain of the system will definitely cause instability, unless the open-loop response can be reshaped at the high frequency end to give a suitable phase margin and a desired -20 dB slope at the zero dB gain crossover. To reshape the high frequency portion of the system ($\omega \geq 166$) would require the addition of zeroes in the open-loop transfer function either in lead-lag networks or with differentiators. Either technique would widen the bandwidth of the system and add undesirable high frequency noise.[17] The undamped natural frequency of the mechanical skid system would create a problem if the bandwidth were increased by the addition of lead networks.

In an attempt to avoid the high frequency oscillation of the mechanical system, the control system's bandwidth was narrowed. The retransmitting slidewire recorder already acts as a filter to the high frequency components of the mechanical system, thereby narrowing system bandwidth. This characteristic of the recorder was combined with the PID controller in trying to stabilize the system.

From equation (3-41) the PID transfer function is

$$G_c(s) = K_c(1 + \frac{1}{\tau_i s} + \tau_d s) \quad ,$$

which can be rearranged to

$$G_c(s) = K_c \frac{(\tau_1 s + 1)(\tau_2 s + 1)}{s} \quad . \tag{4-2}$$

The integrator portion of the PID controller changes the uncompensated system from a type 0 to a type 1 system. The steady state error becomes zero for step input demands. This result satisfies the ±10 percent of demand input, but can the PID controller be adjusted for a stable system?

Using only the PID controller's integration and proportional gain functions introduces, in addition to a pole at the origin, a zero in the transfer function. Varying the controller's proportional gain and the integrator time constant interacts with this zero and causes its frequency break point to shift. A root locus diagram for the control system, including the pole at the origin introduced by the integrator, is used to judicially locate this zero.

From the root locus, Figure 4.2, it is seen that the zero must be placed to the left of the characteristic pole of the recorder. Placing the root to the right of the pole at s = -2.5 would produce loci on the negative real axis between the zero and the origin and between -2.5 and -∞. An increase in gain would cause the complex conjugate poles of the
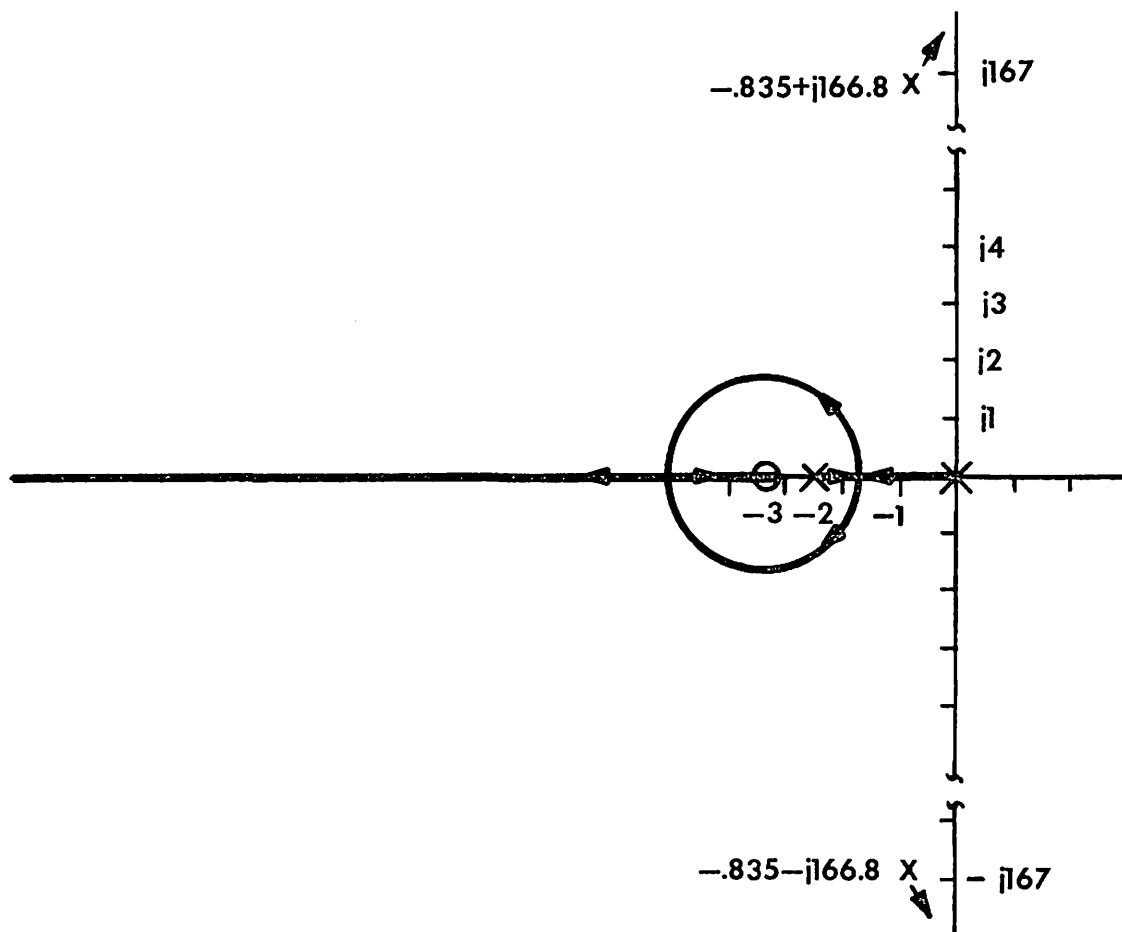
Figure 4.2. Sketch of the Approximate Root Locus of the System with the PID Controller.

mechanical skid system to migrate to the right half plane causing the system to become unstable.

Locating the zero to the left of the pole at s = -2.5 produces a stable system for low frequencies in the order of one cycle per second or less. The derivative action of the PID controller has been set to zero since it adds another zero in the overall transfer function and tends to increase bandwidth.

Although a stable system is realized by narrowing the system bandwidth, the overall performance of the system suffers because it cannot react to changing tensions greater than one cycle per second. Since the complex pole pair of the skid system is located in the vicinity of 167 radians per second (approximately 26.5 cycles per second), the skid deflection, and hence load cell movement, can be changing at a frequency too fast for the recorder and PID controller to compensate. Simulation of the system's response to a step input using the Continuous System Modeling Program (CSMP) developed by IBM is shown in Figure 4.3 (the program for the simulation is given in Appendix D).[18] The error signal (difference between demand input and the feedback signal) is also plotted in Figure 4.3. From this figure it is seen that the system has an acceptable response to a step input. However, in Figure 4.4 the effects of a pulse disturbance, simulating a momentary loss in tension from conductor slippage between the belts, on the tension output show an oscillatory error signal of approximately 7 cycles per second after the tension has settled. In actuality, this is an unreal situation, for the tension in the conductor would oscillate
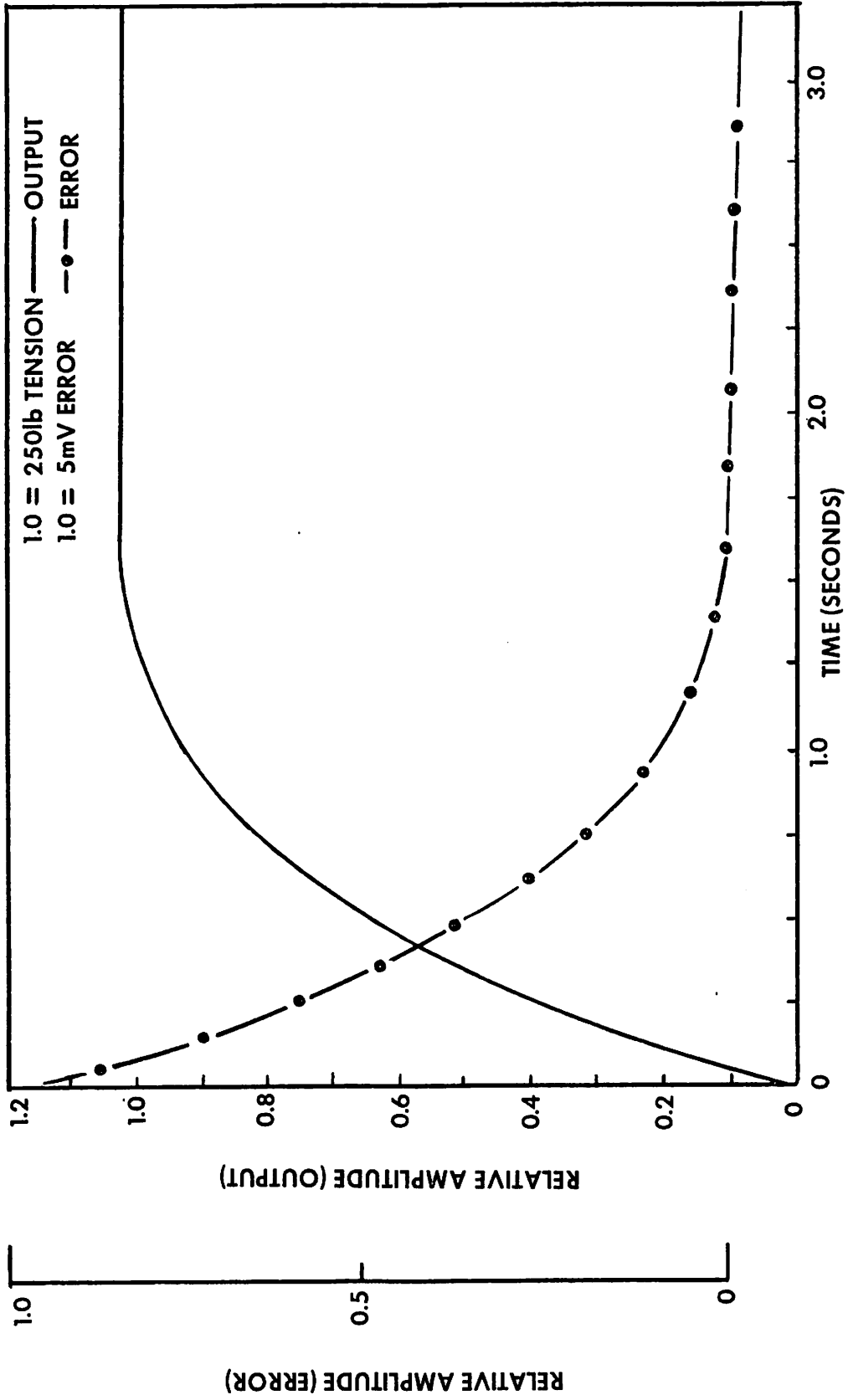
Figure 4.3. Simulated System Response and Error Signal for a Step Input.
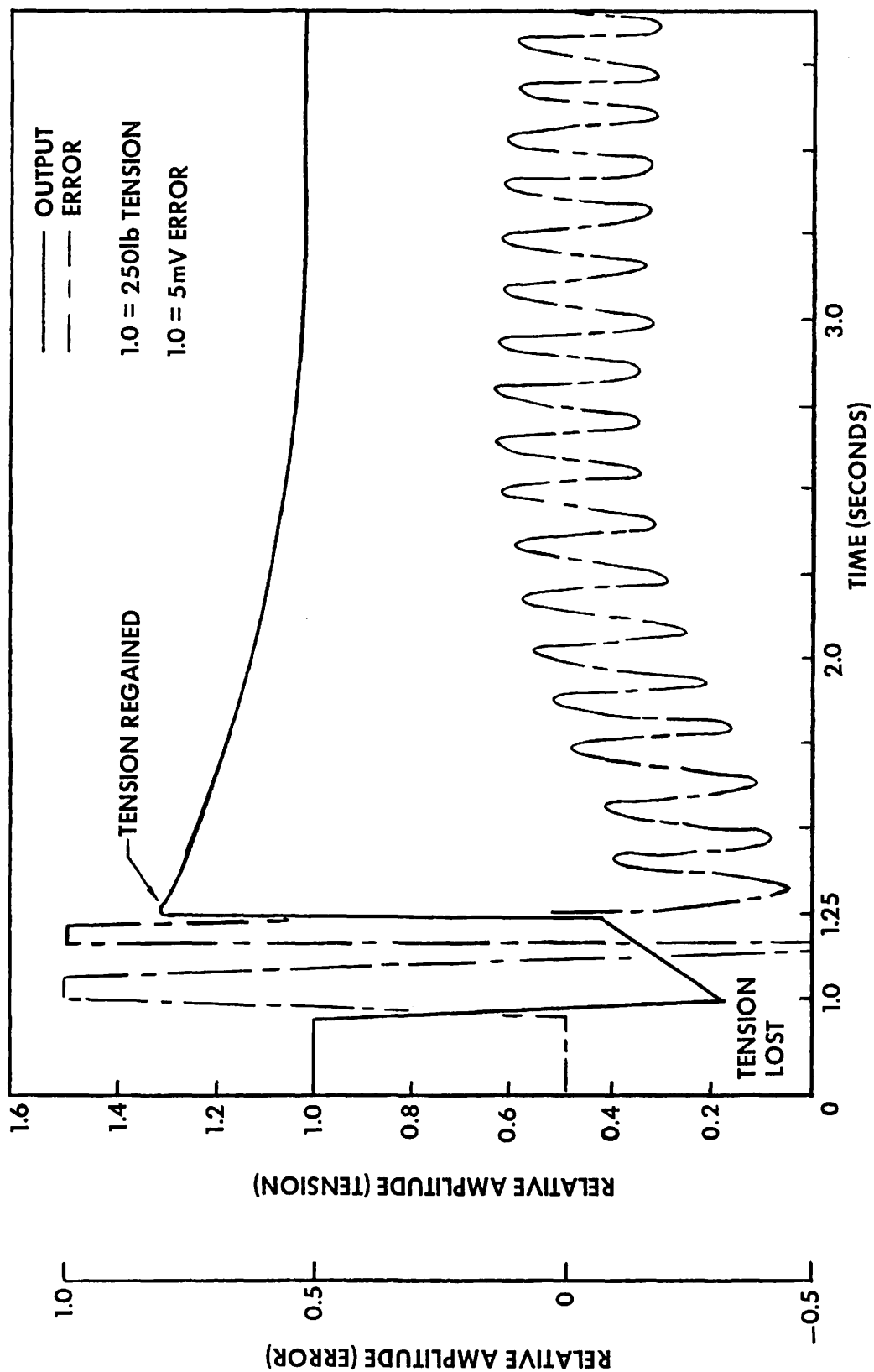
Figure 4.4. Simulated System Response and Error Signal for a Pulse Disturbance.

also. Hence the linear model of the system which assumes that there is no interaction between system blocks is in error. However, the model is sufficient for analysis, and the results just mentioned emphasize the need for a faster controller or a redesigned tension machine.

Since limited funds were available, neither of the alternatives mentioned are favorable. Instead a modification to the mechanical system to slow down its frequency of oscillation is recommended. The design analysis based on the modified mechanical system is discussed in Chapter V.

CHAPTER V

SYSTEM COMPENSATION

From Chapter IV it was shown that the mechanical system could change much faster than the recorder and PID controller could respond. Since it is desired to utilize the existing commercial controller for compensation purposes, the frequency of oscillation of the skid system must be lowered. This can be accomplished utilizing a spring and dashpot in conjunction with the tension load cell. Figure 5.1 shows the proposed arrangement.

Ideally the spring and dashpot should be chosen to correspond to the compensation network frequencies of the PID controller. This restriction would require an unrealistic damper and spring combination since the maximum integration time constant of the controller is 100 radians per minute or 1.67 radians per second, 100 times slower than the mechanical system. Commercial dashpots with damping coefficients between 20 and 30 lb-sec/inch are not unreasonable, but to alter the mechanical system's bandwidth by a factor of 100 would require an oversized damper or a very flexible spring.

A dashpot with a damping coefficient of 25 lb-sec/inch and a spring with a linear spring constant of 400 lb/inch are proposed for damping the mechanical system vibrations.

Combining the roller bearing friction of 10 lb-sec/inch given in Chapter III with the damping coefficient of the dashpot results in a total damping coefficient for the mechanical system of 35 lb-sec/inch.
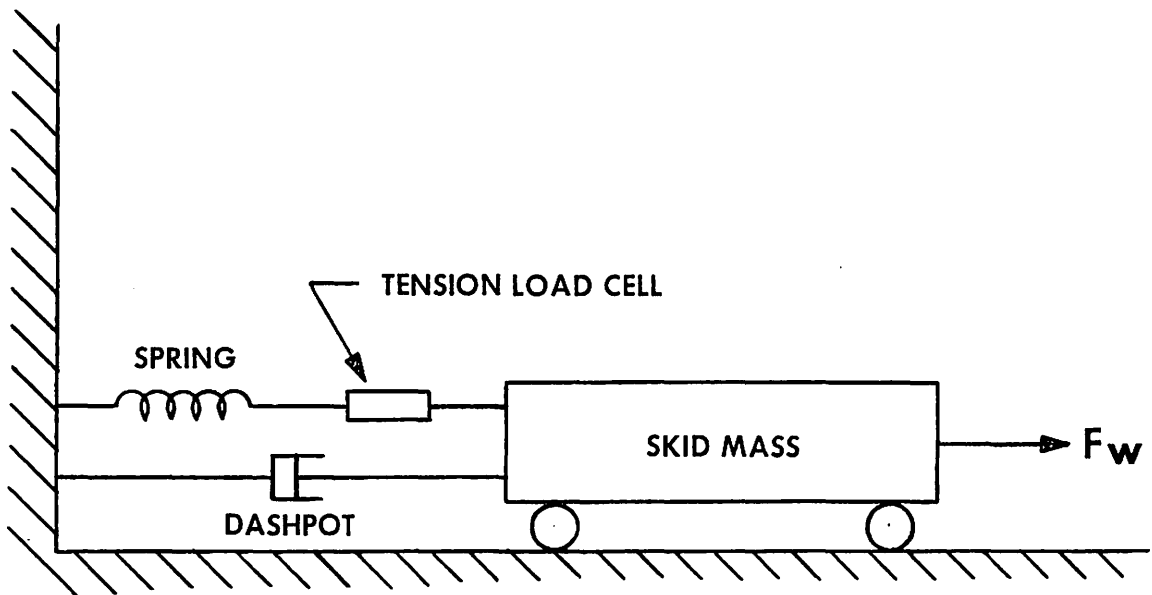
Figure 5.1. Proposed Modification to the Mechanical System.

The tension load cell can now be treated as a rigid member in series with the spring since it only moves a total of 3 mils for full range.

In Chapter III the transfer function relating skid deflection to applied force was given. This expression, repeated here for convenience, is

$$\frac{X(s)}{F_W(s)} = \frac{1}{M(s^2 + \frac{f}{M}s + \frac{K}{M})} \quad . \tag{5-1}$$

Substitution of the value for M and the new values for f and K in equation (5-1) yields for the denominator

$$71.89 \ (s^2 + 5.84s + 66.8) \ \frac{lb\text{-}sec^2}{ft} \tag{5-2}$$

which corresponds to resonant poles at

$$s_1, \ s_2 = -2.92 \pm j7.63 \quad .$$

X(s) in equation (5-1) represents the skid (spring) deflection instead of the load cell movement. The force measured by the load cell is Kx and is related to force F_W in the wire through the movement of the skid.

Since the spring constant is 400 lb/in and the output voltage of the load cell system is 10 mV/500 lb, the overall gain between skid deflection and the load cell system feedback voltage is

$$K_{fb} = (400 \ \frac{lb}{in}) (\frac{10 \ mV}{500 \ lb}) \quad , \ or$$

$$K_{fb} = 8 \frac{mV}{in} \qquad (5-3)$$

where K_{fb} represents feedback gain. The constant K_{fb} replaces K_{CG} determined in Chapter III where load cell displacement was used as skid deflection.

A modified open-loop transfer function incorporating K_{fb} and the new second order system of the spring, mass and dashpot combination given in equation (5-2) is represented by

$$GH(s) = \frac{K_{GT}K_R K_{fb} K_T G_c(s)}{(1 + \tau_r s)(s^2 + \frac{f}{M}s + \frac{K}{M})MR} \quad , \text{ or}$$

$$GH(s) = \frac{244.8 G_c(s)}{(0.4s + 1)(s^2 + 5.84s + 66.8)} \qquad (5-4)$$

where K_{GT}, K_R, K_T, $G_c(s)$, τ_r and R are defined in Table 3.3, page 55.

Substitution of the PID controller's generalized transfer function, $G_c(s)$ from equation (4-2), into (5-4) yields

$$GH(s) = \frac{244.8K(\tau_1 s + 1)(\tau_2 s + 1)}{s(0.4s + 1)(s^2 + 5.84s + 66.8)} \qquad (5-5)$$

where K, τ_1 and τ_2 are gain and time constant parameters of the controller.

Since specifications for the performance of the tension machine, other than ±10 percent control of the conductor tension, were not given, the set of specifications in Table 5.1 are proposed.

TABLE 5.1

SPECIFICATIONS

Steady-state error for a step input	$e_{ss} = 0$ ($K_p = \infty$)
Underdamped to overdamped response	$.5 \leq \xi \leq .9$
Settling time	$T_s < 2.5$ sec.

The characteristic equation of the system including the generalized PID controller transfer function is

$$1 + GH(s) = 1 + \frac{244.8K(\tau_1 s + 1)(\tau_2 s + 1)}{s(0.4s + 1)(s^2 + 5.84s + 66.8)} \quad , \text{ or}$$

$$s(0.4s + 1)(s^2 + 5.84s + 66.8) + 244.8K(\tau_1 s + 1)(\tau_2 s + 1) = 0 \quad .$$

$$(5-6)$$

In Figure 5.2 the open-loop poles for $K = 0$ in equation (5-6) are shown in the s-plane along with the region of the desired system dominant root location. The problem now becomes one of locating the zeroes of the controller network to cause the root locus to pass through the shaded region shown in Figure 5.2.

Location of the controller's zeroes in the s-plane to form an overall root locus indicative of satisfactory system performance was attempted, but no realizable solution was determined using only the PID controller because of its limited control action and frequency response. These facts can best be understood by investigating the effect of the PID controller on the root locus of equation (5-6) for different
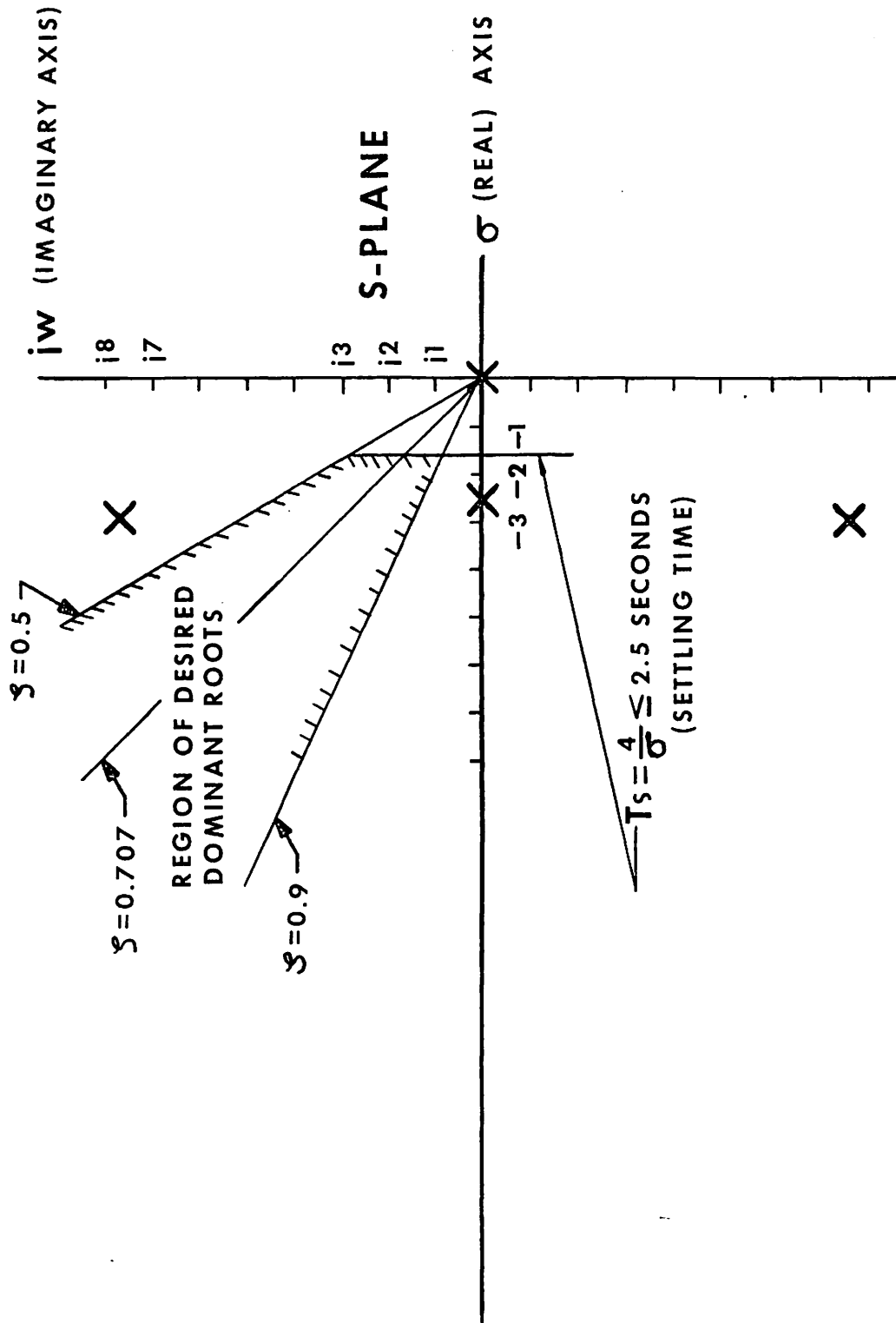
Figure 5.2. Open-Loop Poles for K = 0 in Equation (5-6).

controller settings (i.e., different proportional gains, K, and different time constants τ_1 and τ_2).

From Figure 5.2 it is seen that zeroes of the controller, for minimum phase, can both lie on the negative real axis between s = -2.5 and s = 0, or one between s = -2.5 and s = 0 and one to the left of or equal to s = -2.5, or the two zeroes can be complex. Another possibility is to set the controller's derivative action to zero thus eliminating one of the controller's zeroes. The remaining zero will lie somewhere on the negative real axis. This last possibility has been discussed in Chapter IV and will not be repeated here.

If the controller's zeroes are located on the negative real axis between s = -2.5 and s = 0, it is evident that no loci will pass through the region of acceptance in Figure 5.2. Likewise, if the zeroes are located to the right and left of s = -2.5, no loci will pass through the region of acceptability. The only possibility for the controller to cause the system's dominant roots to lie within the bounded region of Figure 5.2 is to adjust the gain, derivative and integral actions to produce complex zeroes. The idea with complex zeroes is to cancel the complex pole pair produced by the spring-mass system and to allow the remaining roots to become the dominant ones. Unfortunately the limited frequency response of the controller prevents generation of complex zeroes in the neighborhood of the complex pole pair. For example, a complex zero pair in the vicinity of s_1 = -3 + j7 and s_2 = -3 - j7 would require a PID controller setting dictated by

$$K_d s^2 + K_p s + K_i = (s + 3 + j7)(s + 3 - j7) \qquad (5-7)$$

where K_d represents the PID controller's derivative constant, K_p represents the proportional band gain, and K_i represents the integral constant.

Equating coefficients in equation (5-7) results in the following values for the controller's settings:

K_p = 6 for a proportional band of 16.67 percent,

K_d = 1 second, and

K_i = 58 repeats/second.

The controller can provide a proportional band of 16.67 percent and a rate time (derivative action) of 1 second, but the maximum reset (integral action) is 100 repeats/minute or 1.67 repeats/second. This limitation in control action indicates the need for additional or altogether different compensation networks.

In addition to the limited control action of the controller, the strip chart recorder with retransmitting slidewire has its limitations, too. The recorder's response time is too slow to follow the feedback signal produced by the tension load cell system. This fact was discussed in Chapter IV where narrowing the control system's bandwidth was investigated.

The strip chart recorder is desirable from an operational standpoint, but a much faster network for summing the feedback and reference input signals must replace the summing action of the recorder. Removing the recorder from the control loop causes the real pole at s = -2.5 to disappear. Replacement of the recorder network with linear operational amplifiers having frequency break points well beyond the control

system's bandwidth is proposed. The proposed summing network is given in Figure 5.3, where the operational amplifiers are assumed to be ideal elements. That is, the amplifiers are assumed to have infinite open-loop gain, infinite input impedance, zero offset, zero output resistance, and infinite bandwidth. These assumptions are not unreasonable for the mechanical system being analyzed.

To cancel the complex pole pair produced by the spring-mass system a network that produces the equivalent complex zeroes is proposed. The desired compensator network can be obtained by parallel combination of simple order systems as shown in Figure 5.4 where K_1, K_2 and K_3 are gain constants and a and b are simple order poles.

Since the complex pole pair from equation (5-6) is $s^2 + 5.84s + 66.8$, the poles a and b in Figure 5.4 must be chosen to produce the form

$$\frac{s^2 + 5.84s + 66.8}{(s + a)(s + b)} = K_1 + \frac{K_2}{s + a} + \frac{K_3}{s + b} \quad . \tag{5-8}$$

Letting $a = 0$, $b = 10$ and $K_1 = 1$ simplifies equation (5-8) and results in $K_2 = 6.68$ and $K_3 = -10.84$. Rounding these values to the nearest whole number produces a transfer function for the compensator in Figure 5.4 of

$$G_1(s) = \frac{s^2 + 6s + 70}{s(s + 10)} \quad . \tag{5-9}$$

Insertion of a real pole at $s = -25$ insures a faster roll off at higher frequency and reduces the phase margin, thereby decreasing system response time.
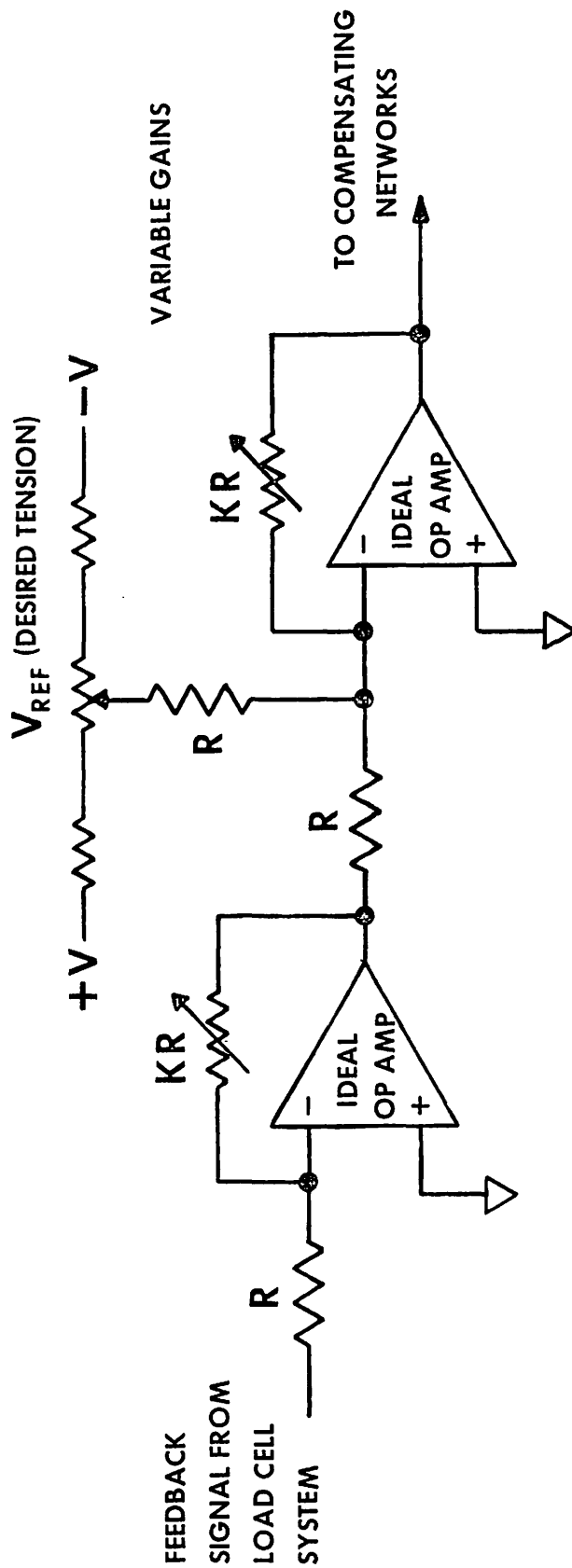
Figure 5.3. Proposed Summing Network to Replace the Retransmitting Slidewire Recorder.
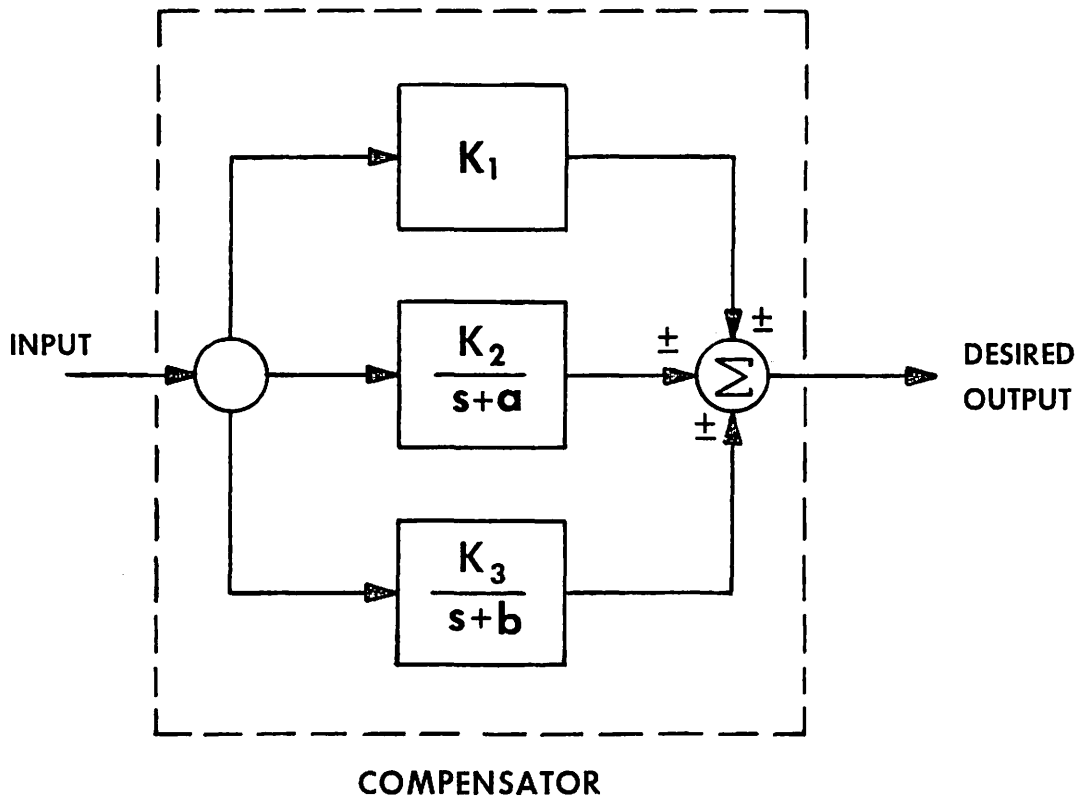
COMPENSATOR

Figure 5.4. Parallel Network Compensator.

An amplifier with variable gain will be required to position the roots within the bounded region of Figure 5.2, page 71. Combining equation (5-9) with the real pole at $s = -25$ and a variable gain K_{C1} produces an overall transfer function for the new compensator of

$$G_{C1}(s) = \frac{K_{C1}(s^2 + 6s + 70)}{s(s + 10)(s + 25)} \; . \tag{5-10}$$

The system block diagram with the compensator network described by equation (5-10) is shown in Figure 5.5.

The new open-loop transfer function for the system is given by

$$GH(s) = \frac{K_{C1}K_{GT}K_T K_{fb}(s^2 + 6s + 70)}{MRs(s + 10)(s + 25)(s^2 + 5.84s + 66.8)} \; , \tag{5-11}$$

which becomes upon substitution for K_{GT}, K_T, K_{fb}, M and R

$$GH(s) = \frac{0.5 \, K_{C1}(s^2 + 6s + 70)}{s(s + 10)(s + 25)(s^2 + 5.84s + 66.8)} \; . \tag{5-12}$$

In equation (5-12) the complex zeroes represented by $s^2 + 6s + 70$ could have been chosen to coincide exactly with the complex poles represented by $s^2 + 5.84s + 66.8$. This is considered to be unnecessary since the system's mathematical model is only an approximation. Therefore, cancellation of the complex pole pair in equation (5-12) with the complex zero pair will not greatly affect system analysis. This action reduces equation (5-12) to
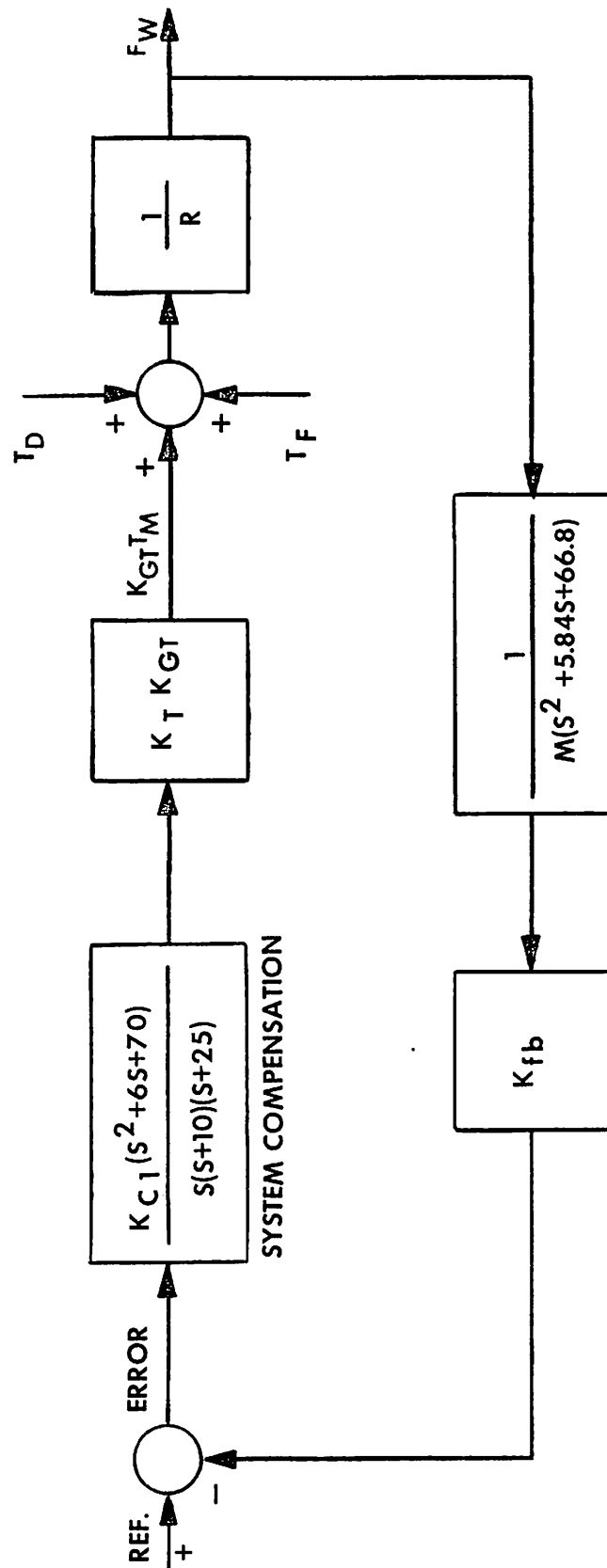
Figure 5.5. System Block Diagram Showing Compensation Network.

$$GH(s) = \frac{0.5K}{s(s + 10)(s + 25)} \quad , \qquad (5\text{-}13)$$

where K_{C1} has been replaced simply by K.

Root locus techniques can be used to determine a range for K that will cause the roots of the characteristic equation to be within the bounded region of Figure 5.2, page 71. After determining a range for K, a computer simulation using the CSMP program can be utilized to verify desired system response.

From equation (5-13) the characteristic equation 1 + GH(s) = 0 is

$$s(s + 10)(s + 25) + 0.5K = 0 \quad . \qquad (5\text{-}14)$$

The root locus of equation (5-14) is shown in Figure 5.6. Since the locus passes through the bounded region of acceptability, a value of K can easily be determined from the root locus by measuring the vector lengths from the poles to the desired root location.[15]

Choosing a point on the root locus in the region of acceptability that corresponds to a damping ratio of approximately 0.707 produces a gain of $K \simeq 894$, where the vector lengths from the three poles are given by

$$K = |5.8||7.2||21.4| = 893.66 \quad . \qquad (5\text{-}15)$$

The range of K satisfying the design requirements can be determined in a similar manner by measuring the vector lengths from the poles to the root locations corresponding to the intersection of the root locus with the maximum and minimum values for the damping ratio. Hence the range of the open-loop gain is

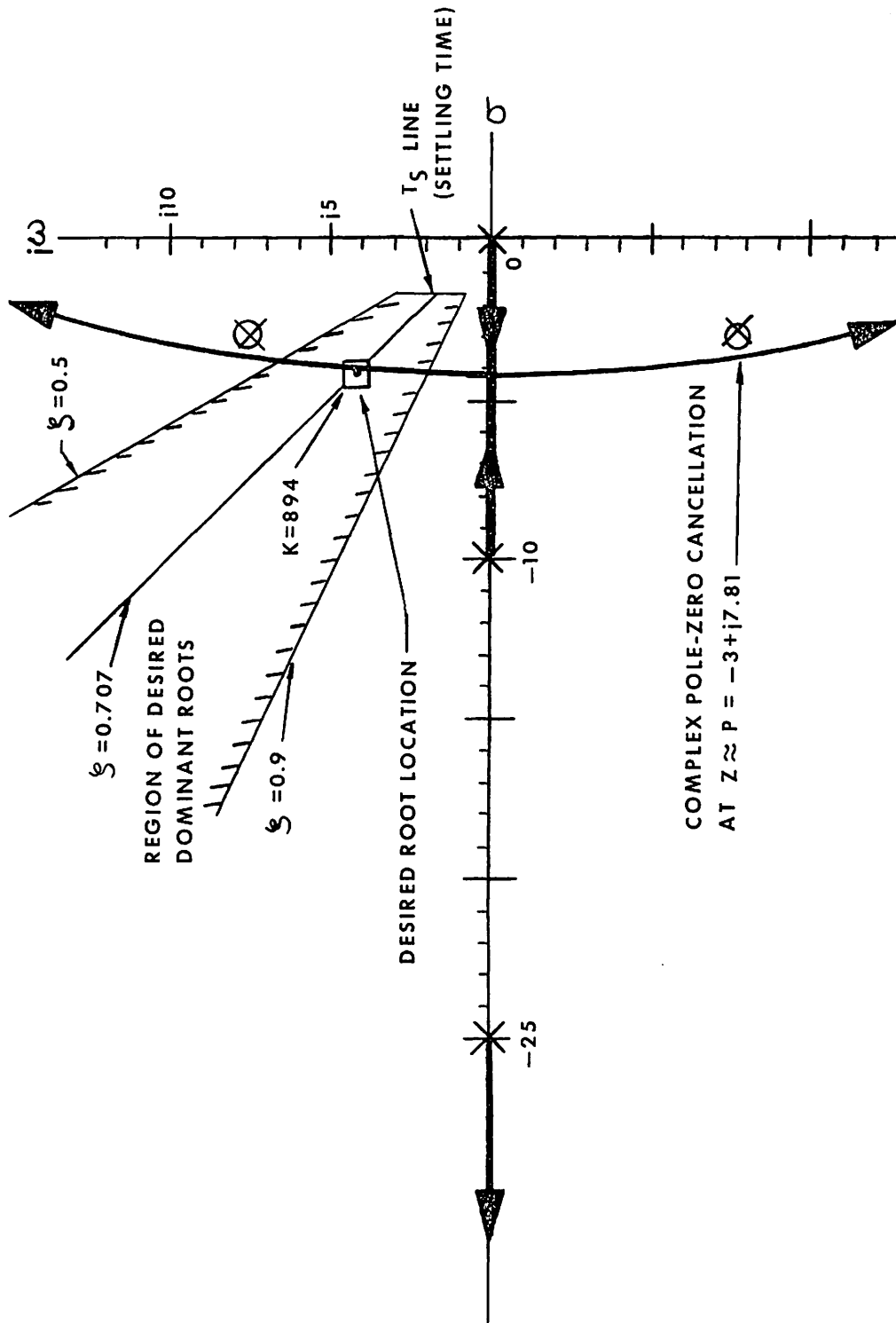Figure 5.6. Root Locus for the Compensated System Showing Desired Dominant Root Location.

$$590 \leq K \leq 1500 \quad . \qquad (5\text{-}16)$$

Inserting the value for K determined from the root locus into equation (5-12) yields an open-loop transfer function of

$$GH(s) = \frac{894(s^2 + 6s + 70)}{s(s + 10)(s + 25)(s^2 + 5.84s + 66.8)} \quad . \qquad (5\text{-}17)$$

The closed-loop system for the gain in equation (5-15) is given by

$$\frac{F_W(s)}{R(s)} = \frac{\dfrac{894(s^2 + 6s + 70)}{s(s + 10)(s + 25)(s^2 + 5.84s + 66.8)}}{1 + \dfrac{894(s^2 + 6s + 70)}{s(s + 10)(s + 25)(s^2 + 5.84s + 66.8)}} \quad , \text{ or}$$

$$\frac{F_W(s)}{R(s)} \simeq \frac{894(s^2 + 6s + 70)}{(s + 27)(s^2 + 8s + 33.6)(s^2 + 5.84s + 67.2)} \qquad (5\text{-}18)$$

where R(s) is a reference input. The simulated CSMP response of the closed-loop system to a step input representing a demand of 250 pounds tension in the superconductor is shown in Figure 5.7. From this figure it is seen that the overshoot is essentially zero, and the settling time is less than 1.5 seconds. Since the system is a type 1 system, the steady state error is zero. Hence all of the design specifications given in Table 5.1, page 70, have been met.

As a final check on the system's stability, the response to a disturbance pulse representing a momentary loss in conductor tension was simulated using the CSMP program. The results of this simulation are shown in Figure 5.8. A disturbance of this nature could occur if the
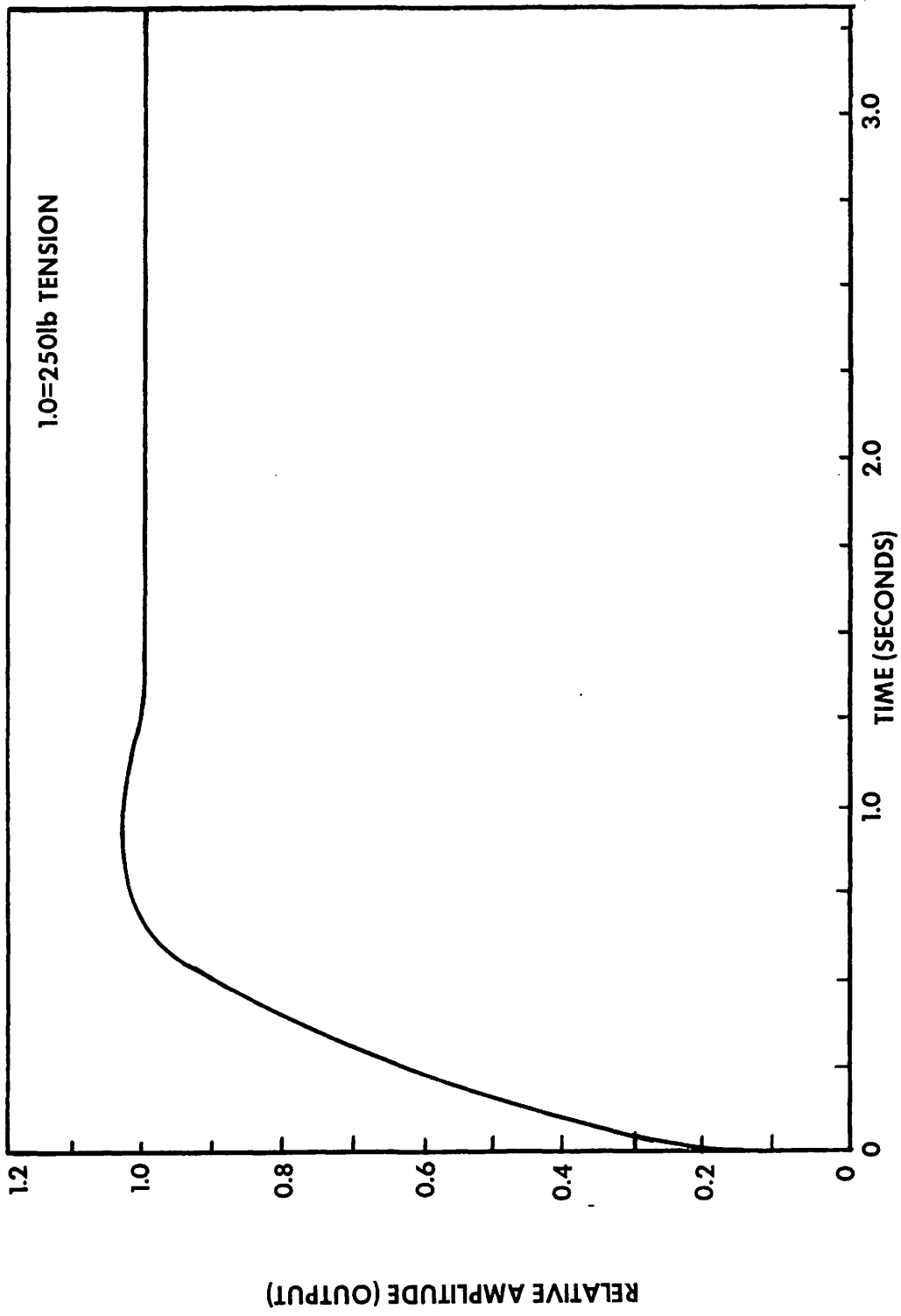
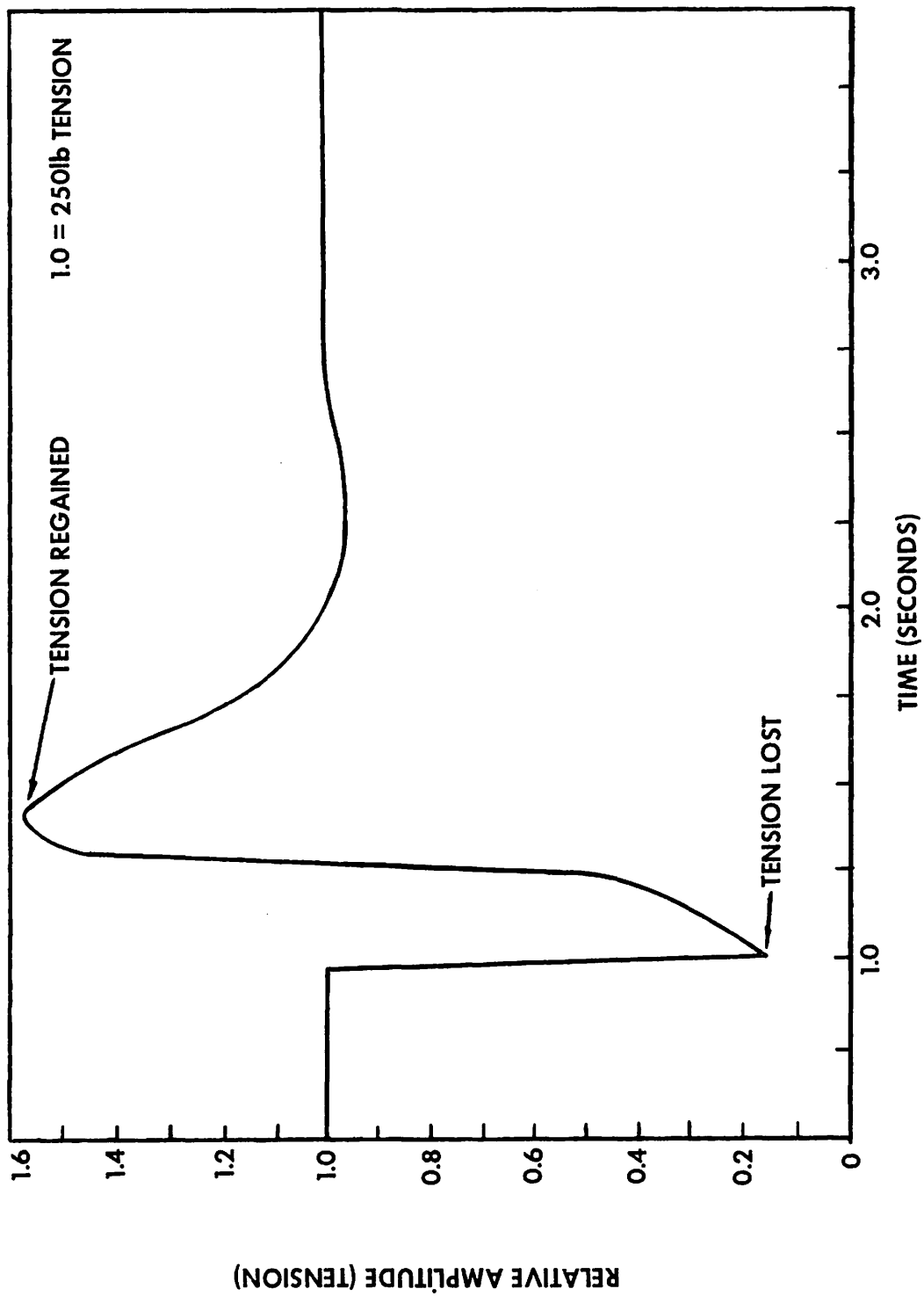Figure 5.7. Simulated Response to a Step Input for the Compensated System.

Figure 5.8. Simulated Response to a Pulse Disturbance for the Compensated System.

superconductor slipped between the tension machine's belts, thereby resulting in a loss in tension followed by a sudden jerk when it was regained. Figure 5.8 shows that the system recovers from such an upset in less than 2 seconds.

The computer programs for both the step input and the pulse disturbance are given in Appendix D.

Discussion

Although the results shown in this chapter are based to a great extent on theoretical calculations, it is the author's opinion that insertion of the spring and dashpot combination in series with the tension machine and replacement of the commercial PID controller and recorder with the compensation networks described in this chapter are definitely necessary requirements for stabilizing the system.

Operating experience with the original uncompensated system shown in Figure 2.3, page 11, confirmed the oscillatory response from a pulse disturbance shown in Figure 4.4, page 64. Results from replacing the recorder with the summing network shown in Figure 5.3, page 75, indicated the need for a faster controller since the "error" signal was no longer being filtered by the recorder.

The compensation networks given in Figure 5.4, page 76, combined with the amplifier with variable gain and simple order pole would not be difficult to build. The design of the amplifiers however must provide variable components since the complex pole pair representing the mass-spring system is only an approximation.

CHAPTER VI

CONCLUSION

The purpose of this thesis was to provide stabilization for an automatic tensioning device used to control the tension in a superconductor being wound to form large superconducting coils. Due to the nonelastic property of the superconducting fibers comprising the conductor, conventional winding techniques involving right angle bends in the conductor could not be used to control tension. Instead, a machine was designed to allow passage of the superconductor through a belt system connected to a torque motor which acted in opposition to the superconductor's forward motion through the belts.

At the outset of the tension machine's design it was desired to have the machine act as a free body (refer to Chapter II, pages 6, 7, 8 and 9) with only the load cell to restrict its motion. Prior to any investigation of the feedback system shown in Figure 2.3, page 11, compensation requirements were to be provided by a commercial PID controller and retransmitting slidewire recorder.

In Chapter III the mathematical model indicates a highly unstable system with complex roots very close to the $j\omega$-axis. These roots are caused by the mass-spring combination of the tension machine and load cell. Analysis of the system shows the commercial PID controller and recorder to be insufficient for system compensation requirements, even though the mechanical system's complex pole pair was moved considerably away from the $j\omega$-axis by the insertion of a spring and dashpot in series

85

with the tension machine. Complex zeroes to cancel the complex pole

pair is proposed along with deletion of the PID controller and recorder.

A summing network is used in place of the recorder to compare the

load cell feedback signal with the reference or demand input. An

additional amplifier with variable gain and simple order pole is

included in the compensation network.

System performance for a step input and to a disturbance input is

simulated on a digital computer using the Continuous System Modeling

Program (CSMP) developed by the IBM Corporation.

It was brought out in this thesis that the use of PID controllers

for system compensation requirements is limited. This limitation is

mainly due to the controller's fixed algorithm or transfer function and

low frequency response. Although faster controllers are available, PID

controllers lend themselves more readily to process systems involving

the control of temperature, proportional flow, pressure regulation and

similar parameters where the controlled variable cannot change rapidly.

The obvious misapplication of the PID controller in trying to

stabilize the control system analyzed in this thesis indicates the

importance of developing the analytical model prior to investigation

of system compensation requirements.

The model development and system analysis provided the author with

a better understanding of how physical components relate to the

analytical world. The unsuccessful application of the PID controller

was not a total waste, for it also afforded the author with a better

understanding of a device used extensively in process control. A brief

description of the PID controller is given in Appendix A.

LIST OF REFERENCES

LIST OF REFERENCES

1. Oak Ridge National Laboratory, "ORMAK, the Oak Ridge Tokomak Controlled Thermonuclear Research Experiment," Oak Ridge, Tennessee, July, 1975.

2. Steiner, Don, "Nuclear Fusion: Focus on Tokomak," IEEE Spectrum, July, 1977, pp. 32-38.

3. Kintner, Edwin, "Bringing Fusion Electric Power Closer," Special reprint from Grumman Aerospace Horizons, vol. 13, No. 2, 1977.

4. Skilling, Hugh H., Electrical Engineering Circuits, John Wiley and Sons, Inc., New York, 1965, p. 7.

5. Johnson, Neil E., "The Stress Analysis of Non-Homogeneous Superconducting Solenoids," Proceedings of the First International Cryogenic Materials Conference, Vol. 22, pp. 490-499, July, 1975.

6. Bedford, R. E. and Vilas D. Nene, "Voltage Control of the Three-Phase Induction Motor by Thyristor Switching: A Time-Domain Analysis Using the α-β-0 Transformation," IEEE Transactions on Industry and General Applications, vol. IGA-6, pp. 553-562, November/December, 1970.

7. Shepherd, William, "On the Analysis of the Three-Phase Induction Motor with Voltage Control by Thyristor Switching," IEEE Transactions on Industry and General Applications, vol. IGA-4, No. 3, pp. 304-311, May/June, 1968.

8. Gourishankar, Vembu, Electromechanical Energy Conversion, International Textbook Company, Scranton, Pennsylvania, 1965.

9. Knowlton, A. E., Standard Handbook for Electrical Engineers, McGraw-Hill Book Company Inc., New York, 1957, p. 712.

10. Shepherd, William, "Steady-State Analysis of the Series Resistance-Inductance Circuit Controlled by Silicon Controlled Rectifiers," IEEE Trans. on Industry and General Applications, vol. IGA-1, pp. 259-265, July/August, 1965.

11. Shepherd, William and Jack Stanway, "The Polyphase Induction Motor Controlled by Firing Angle Adjustment of Silicon Controlled Rectifiers," 1964 IEEE International Convention Record, vol. 12, pt. 4, pp. 135-154, March, 1964.

12. Dewar, S. B. and A. Straughen, Power Semiconductor Circuits, John Wiley & Sons, New York, 1975, p. 162.

13. Shepherd, William and Jack Stanway, "An Experimental Closed-Loop Variable Speed Drive Incorporating a Thyristor Driven Induction Motor," IEEE Transactions on Industry and General Applications, vol. IGA-3, pp. 559-565, November/December, 1967.

14. D'Azzo, John J. and Constantine H. Houpis, Feedback Control System Analysis and Synthesis, McGraw-Hill Book Company, Inc., New York, 1960, pp. 26-31.

15. Dorf, Richard C., Modern Control Systems, Addison-Wesley Publishing Company, Reading, Massachusetts, 1967.

16. Tyner, Mack and Frank P. May, Process Engineering Control, The Ronald Press Company, New York, 1968.

17. Hung, J. C., "Unpublished Lecture Notes," Electrical Engineering Department, The University of Tennessee, 1971.

18. Speckhart, Frank H. and Walter L. Green, A Guide to Using CSMP— The Continuous System Modeling Program, Prentice-Hall, Inc., Englewood Cliffs, New Jersey, 1976.

19. Luppold, D. S., "Automatic Control Lecture Notes," Leeds and Northrup Company, Technical Training Center, North Wales, Pennsylvania, 1975.

20. Series 80, 3-Action C.A.T. Controller, Leeds and Northrup, North Wales, Pennsylvania, 1974.

APPENDICES

APPENDIX A

DISCUSSION OF A PID CONTROLLER

This appendix contains a brief description of a PID controller.
Much of the information contained herein was taken from material
discussed in Process Engineering Control by Mack Tyner and Frank P. May.[16]

The term PID controller, used rather loosely in the industrial
world, is an abbreviation for a controller having proportional, integral
and derivative control actions. These control actions may be combined
in a single controller or used separately to produce a direct-current
signal for a final control device.

When the control actions are used separately, the controller must
be a noninteracting controller. That is, each control action must be
derived from its own amplifier network as shown in Figure A.1.

As depicted from Figure A.1, it takes a minimum of four amplifiers
to provide all three control actions in a noninteracting controller.
The output is simply the sum of all three amplifiers. An interacting
controller generally requires only one amplifier to provide the PID
control actions as shown in Figure A.2.[19]

The ideal proportional control action of a one, two or three action
controller produces an output that is proportional to the actuating
signal input. This input signal is most often an error signal that
represents the departure of the controlled variable from a reference
set point. If the negative feedback signal of the controlled variable
is represented by -c(t), and the reference set point is represented by
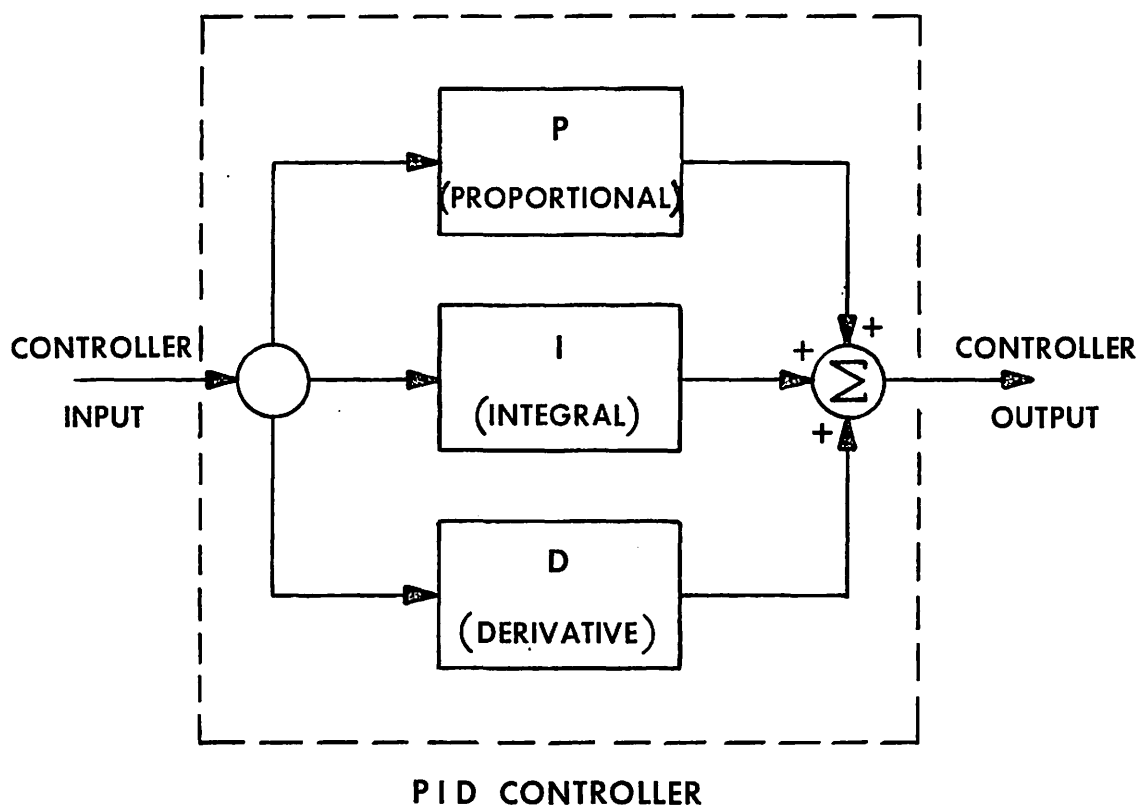
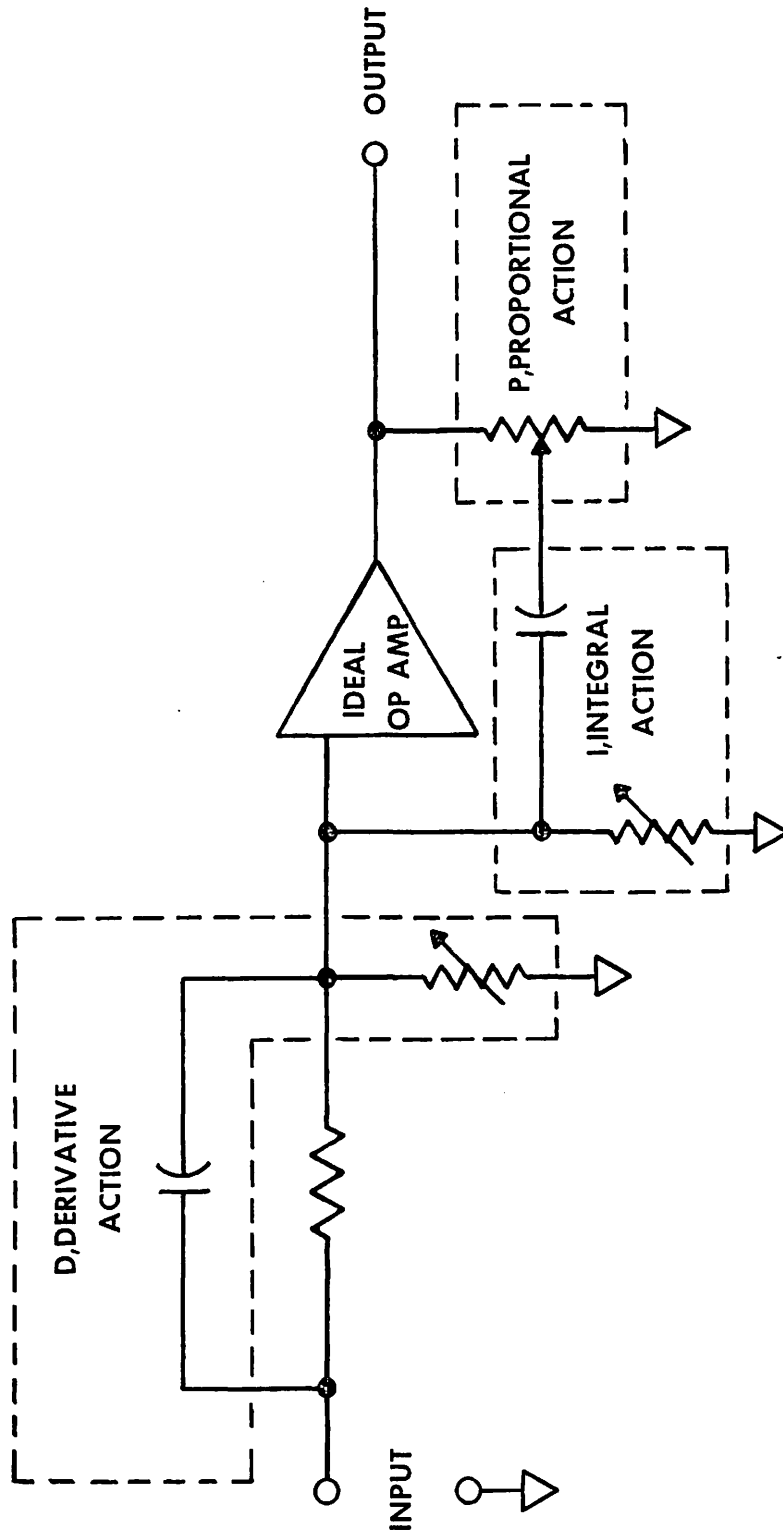PID CONTROLLER

Figure A.1. A Noninteracting PID Controller.

Figure A.2. An Interacting PID Controller.

Source: Luppold, D. S., "Automatic Control Lecture Notes," Leeds and Northrup Company, Technical Training Center, North Wales, Pennsylvania, 1975.

r(t), then the error signal, e(t), to the controller is equal to r(t) - c(t). Letting the output of the proportional controller be represented by m(t) results in the following expression for the controller network:

$$m(t) = [r(t) - c(t)]K_c \quad , \text{ or}$$

$$m(t) = e(t)K_c \tag{A-1}$$

or taking the Laplace transform of (A-1) produces

$$M(s) = E(s)K_c \tag{A-2}$$

where K_c is the controller proportionality or gain constant and s is the Laplace transform variable. Figure A.3(a) shows an ideal operational amplifier network representing equation (A-1) for a simplified proportional action controller. In this figure the closed-loop gain, $-R_f/R$, of the amplifier is the proportional action gain. The negative sign on the gain constant arises from the amplifier being used in Figure A.3(a) as an inverter.

When the controlled variable, c(t), deviates from the set point, r(t), the resulting error signal is amplified by the proportional gain constant, K_c, to produce a new controller output proportional to the deviation in the controlled variable. This new output tends to decrease the error to the controller indicating that the controlled variable is approaching the set point. However, since there is only a finite gain available in the system, there is generally an offset between the controlled variable and the desired output. To reduce the error to zero (at set point) a controller with reset action must be employed.[16]
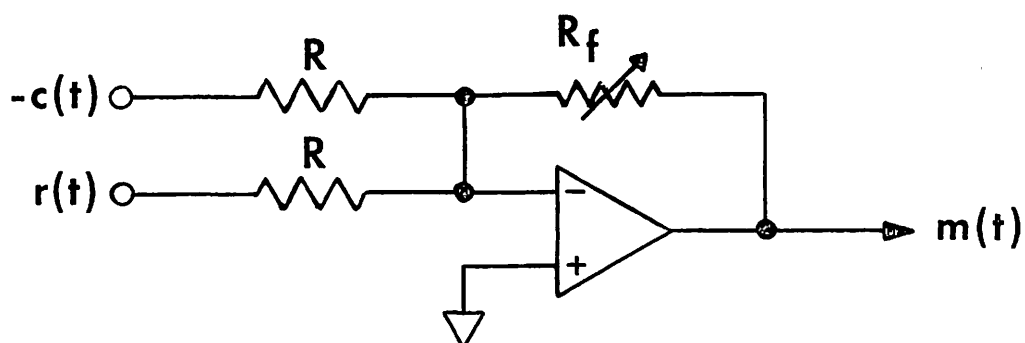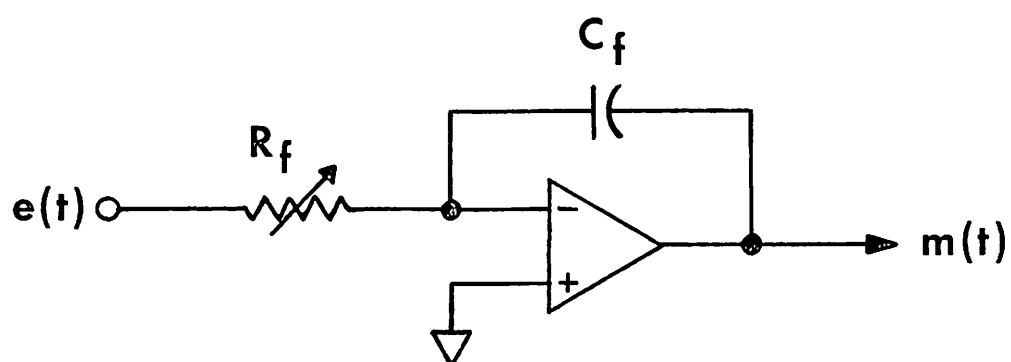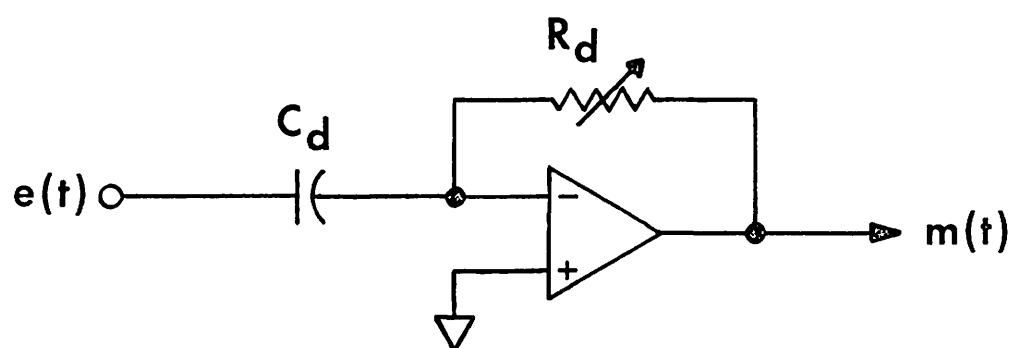
Figure A.3. Simplified Control Actions Based on the Ideal Operational
Amplifier. (a) Proportional. (b) Integral.
(c) Derivative.

In control systems where the controlled variable changes continuously due to continuing load changes, proportional action alone cannot return the controlled variable to the set point.[20] Introducing integral action into the control system will produce a corrective action proportional to the time integral of the error $[r(t) - c(t)]$ and hence eliminate the static error between output and set point. A simple integral action network is shown in Figure A.3(b) where the output $m(t)$ is proportional to the time integral of the actuating error $e(t)$, or

$$m(t) = - \frac{1}{\tau_i} \int_0^t e(t) \, dt \qquad \text{(A-3)}$$

where τ_i is the RC time constant associated with resistor R_f and capacitor C_f.

Combining integral action with proportional action produces a proportional-plus-integral (PI) controller. A PI controller produces an output proportional to the actuating error plus an output proportional to the time integral of the actuating error. The relationship between input error and controller output can be represented by

$$m(t) = e(t) K_c + \frac{1}{\tau_i} \int_0^t e(t) dt \quad \text{, or}$$

$$M(s) = E(s)K_c + \frac{E(s)}{\tau_i s} \qquad \text{(A-4)}$$

where s is the Laplace transform variable.

In commercial PI and PID controllers integral action is often referred to as reset. Calibrated in repeats per unit of time, reset is the reciprocal of τ_i, the integral time constant. The term repeats per unit of time refers to the number of times the integral response equals the proportional response per unit of time. The amount of time required for the integral action to "repeat" the proportional action is the integral time constant. Since units of reset is the reciprocal of τ_i, small values of τ_i correspond to large integral action, and large values correspond to small integral action. A desirable feature of reset action is that the controller output will continue to increase as long as an input error exists. This means that in a closed-loop system the steady-state error will eventually become zero. However, integral action does not contribute to the stability of the closed-loop system and can produce undesirable overshoot upon startup of the control system.[16]

The third control action to be discussed is rate or derivative action. This type of control action produces an output proportional to the rate of change or derivative of the actuating error. A simple derivative action network is shown in Figure A.3(c) where the output m(t) is proportional to the derivative of the actuating error e(t), or

$$m(t) = - \tau_d \frac{de(t)}{dt} \tag{A-5}$$

where τ_d is the derivative time constant associated with the elements R_d and C_d.

Derivative action is not used alone in a controller, but is combined with proportional or proportional-plus-integral control actions. A proportional-plus-derivative (PD) controller will produce an output proportional to the actuating error plus an output proportional to the derivative of the actuating error. This relationship is represented by

$$m(t) = e(t)K_c + \tau_d \frac{de(t)}{dt} \qquad (A-6)$$

where $m(t)$, $e(t)$, K_c and τ_d were defined previously. Taking the Laplace transform of equation (A-6) yields

$$M(s) = E(s)K_c + \tau_d sE(s) \quad . \qquad (A-7)$$

In a PD controller the derivative time constant, τ_d, in units of time, is the amount of time required for the proportional response to become equal to the derivative response when the actuating error signal to the controller is a ramp function. This can best be understood by referring to Figure A.4 where the output, $m(t)$, for a ramp actuating error signal $e(t)$ is the combined proportional and derivative actions. The time for the proportional action, shown as a dotted line, to equal the derivative action is τ_d, the derivative time constant. The parameters K_d and K_c shown in the figure are the gain constants associated with the derivative and proportional control actions. Derivative action is sometimes referred to as an anticipatory action since it advances the proportional gain. Since derivative action produces an output ahead of proportional action, it opposes all changes
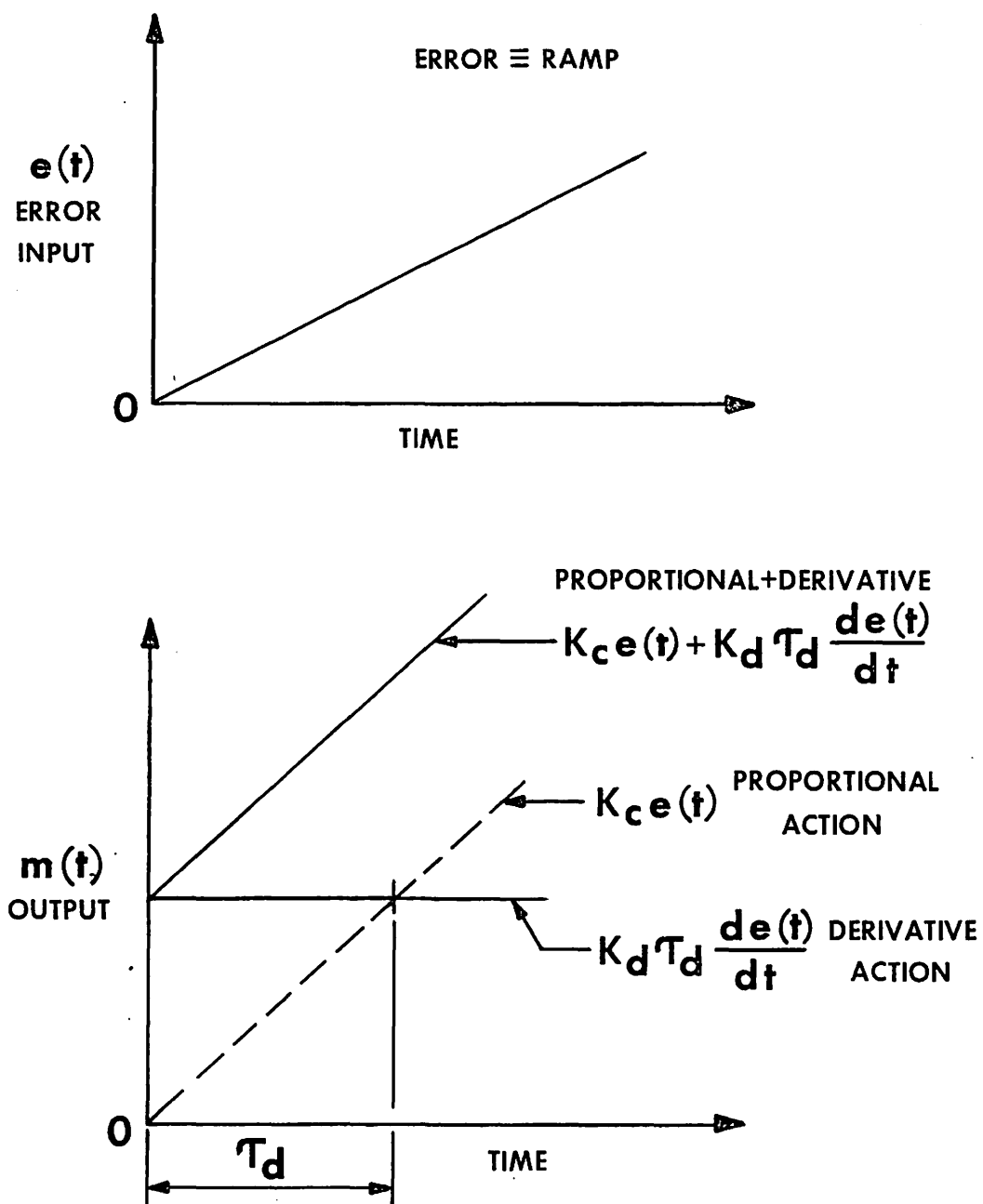
Figure A.4. Output Response for a PD Controller to a Ramp Actuating Error.

Source: Tyner, Mack and Frank P. May, Process Engineering Control, The Ronald Press Company, New York, 1968, p. 185.

in the system, thereby producing a stabilizing effect in closed-loop systems. However, derivative action tends to widen the system bandwidth and increases system noise.

Combination of the three control actions proportional, integral and derivative produces the PID controller. The controller output, $m(t)$, is represented by

$$m(t) = K_c e(t) + \frac{K_i}{\tau_i} \int_0^t e(t)dt + K_d \tau_d \frac{de(t)}{dt} \qquad \text{(A-8)}$$

where the variables were defined earlier. The Laplace transform of equation (A-8) produces

$$M(s) = K_c E(s) + \frac{K_i E(s)}{\tau_i s} + K_d \tau_d s E(s)$$

or

$$\frac{M(s)}{E(s)} = K_c + \frac{K_i}{\tau_i s} + K_d \tau_d s \quad . \qquad \text{(A-9)}$$

Simplifying equation (A-9) yields

$$\frac{M(s)}{E(s)} = K_c (1 + \frac{K_1}{s} + K_2 s) \qquad \text{(A-10)}$$

which represents the three mode controller's transfer function. K_1 and K_2 in equation (A-10) have replaced $K_i/K_c \tau_i$ and $K_d \tau_d/K_c$ respectively.

By varying the gains associated with each of the three control actions allows the controller to be tuned to match many types of control systems. One major disadvantage of the PID controller is its limited

transfer function which can produce, at most, two zeroes and a pole at
the origin.

APPENDIX B

TORQUE MOTOR EQUIVALENT CIRCUIT PARAMETERS

This appendix gives the equivalent circuit parameters (refer to the equivalent circuit Figure 3.4, page 19) for the induction motor used in the tension machine. Measurements made by the motor manufacturer provide the necessary information to determine the equivalent circuit parameters.

From the manufacturer's running light test on the motor, wattage per phase was 40 watts. The dc resistance per phase, R_1, of the stator winding was determined to be 4.06 ohms across the terminals, or 2.03 ohms per phase. Allowing for the skin effect, this value of resistance is multiplied by a factor of 1.1 to obtain the ac effective resistance per phase of the stator winding.[8] Thus, the ac effective resistance per phase is 2.23 ohms.

The losses in the induction machine during running light tests are due to copper loss in the stator windings due to the no load current, I_{nl}, core loss in the iron of the stator and rotor, and mechanical losses such as friction.[8] Input power per phase, W_{ph}, was determined by the manufacturer to be 40 watts. Hence, input power must equal the losses under running light conditions, or

$$W_{ph} = P_{nl} + I^2_{nl}R_1 \tag{B-1}$$

where P_{nl} is the core loss plus mechanical losses and $I^2_{nl}R_1$ is the copper loss in the stator windings. I_{nl} is 2.5 amps. Therefore, the copper loss in the stator due to the no load current is

$$I^2_{nl}R_1 = (2.5)^2(2.23) \; , \; \text{or}$$
$$= 13.94 \text{ watts} \quad . \tag{B-2}$$

Substitution of this value into equation (B-1) and solving for the core and mechanical losses gives

$$P_{nl} = 40 - 13.94 \quad , \text{or}$$
$$= 26.06 \text{ watts} \quad . \tag{B-3}$$

Wind and friction losses of the motor are approximately 6.5 watts. Hence, core loss can be determined by subtracting the mechanical losses from P_{nl}, or

$$P_c = P_{nl} - P_{wf} \quad , \text{or}$$
$$P_c = 26.06 - 6.5$$
$$P_c = 19.56 \text{ watts} \tag{B-4}$$

where P_c is the core loss and P_{wf} is the wind and friction losses.

The core loss component of current, I_c, and the magnetizing component of current, I_m, can be determined now that the core loss is known. Voltage to the motor under running light conditions was equal to 220 volts rms. Hence, the core loss component of current is

$$I_c = V_1 g_c \quad , \text{or}$$

$$I_c = \frac{V_1 P_c}{V_1^2} \qquad \text{(B-5)}$$

where V_1 is the input voltage per phase and g_c is the core loss component per phase. Substitution for P_c and V_1 into equation (B-5) yields

$$I_c = \frac{P_c}{V_1} = \frac{19.56}{220/\sqrt{3}}$$
$$= 0.15 \text{ amp} \qquad . \qquad \text{(B-6)}$$

Since the magnetizing component of current, I_m, is

$$I_m = [I_{nl}^2 - I_c^2]^{1/2} \qquad , \qquad \text{(B-7)}$$

substitution for I_{nl} and I_c into equation (B-7) yields

$$I_m \simeq I_{nl} = 2.5 \text{ amps} \qquad . \qquad \text{(B-8)}$$

Using I_m to calculate the susceptance, b_m, of the air gap gives

$$b_m = \frac{I_m}{V_1} \qquad , \text{ or}$$
$$= 0.019 \text{ mhos per phase} \qquad . \qquad \text{(B-9)}$$

The reciprocal of b_m is X_m, the reactance of the air gap. From equation (B-9), X_m is calculated to be

$$X_m = 50.8 \text{ ohms} \qquad . \qquad \text{(B-10)}$$

From the blocked rotor tests, input power per phase, P_{br}, was 693 watts. The blocked rotor current per phase, I_{br}, was measured to be 6.9 amperes at full rated voltage. The equivalent resistance referred to the stator, Req_1, can be determined as follows:

$$Req_1 = R_1 + a^2R_2 = \frac{P_{br}}{I_{br}^2} \quad . \tag{B-11}$$

Substitution for R_1 into equation (B-11) gives a value for a^2R_2 of

$$a^2R = Req_1 - R_1 = 12.32 \text{ ohms per phase} \quad . \tag{B-12}$$

The reactance referred to the stator, Xeq_1, is represented by

$$\begin{aligned} Xeq_1 &= X_1 + a^2X_2 \\ &= \omega_1L_1 + a^2\omega_1L_2 \\ &= \left[\left(\frac{V_{br}}{I_{br}} \right)^2 - Req_1^2 \right]^{1/2} \quad . \end{aligned} \tag{B-13}$$

Upon substitution for V_{br}, I_{br} and Req_1 into equation (B-13), Xeq_1 becomes

$$Xeq_1 = 11.2 \text{ ohms per phase} \quad , \tag{B-14}$$

and assuming $X_1 = a^2X_2$ assigns a value of 5.6 ohms to these reactances.

The equivalent circuit parameters per phase are listed below:

$$R_1 = 2.23 \text{ ohms}$$
$$a^2R_2 = R_2' = 12.32 \text{ ohms}$$

$$X_1 \quad = \quad 5.6 \text{ ohms}$$

$$a^2 X_2 \quad = \quad X_2' = 5.6 \text{ ohms}$$

$$X_m \quad = \quad 50.8 \text{ ohms} \quad .$$

APPENDIX C

CONVERSION OF UNITS

This appendix gives the conversion of units of $(volt)^2(ohm)/$
$(radians/second)(ohm)^2$ to inch pounds.

$$\frac{(volt)^2(ohm)}{(rad/sec)(ohm)^2} = (volt\text{-}second)\ \frac{volt}{ohm}\quad,\ or$$

$$= (volt\text{-}second) \times \left[\frac{\dfrac{joule}{coulomb}}{(volt)}\right] \times \left[\frac{volt}{ohm}\right]$$

$$\times\ \frac{(1\ ampere)}{\left[\dfrac{1\ volt}{ohm}\right]} \times \left[\frac{1\ coulomb}{second}\right]\quad,\ or$$

$$= (joule) \times \frac{(newton\text{-}metre)}{joule}\quad,\ or$$

$$= (newton\text{-}metre) \times \frac{\left[\dfrac{kg\ -\ m^2}{sec^2}\right]}{(newton\text{-}metre)} \times \frac{(1\ lbm)}{(454g)}$$

$$\times\ \frac{(39.37\ in)^2}{m^2} \times \left[\frac{lb_f}{32.2\ \dfrac{ft\text{-}lbm}{sec^2}}\right] \times \frac{1\ ft}{12\ in}\quad,\ or$$

$$= 8.84\ inch\text{-}pounds\ (in\text{-}lbs)\quad.$$

APPENDIX D

COMPUTER PROGRAMS

This appendix contains the computer programs used to determine the tension machine control system's simulated response to a step input and to a pulse disturbance. Programs for the simulated response for both the uncompensated and compensated systems are given. These programs are actually program statements for the Continuous System Modeling Program (CSMP) developed by the IBM Company. The programs are listed in Tables D.1 through D.4. Block diagrams of the control system for the uncompensated and compensated cases are included to correspond with the programs.

TABLE D.1

CSMP PROGRAM STATEMENTS TO DETERMINE
THE RESPONSE TO A STEP INPUT FOR
THE UNCOMPENSATED SYSTEM[a]

```
INPUT=0.005*STEP(0.0)
ERROR=INPUT-0.556*X6
X1=REALPL(0.0,0.4,ERROR)
X2=0.5*X1
X3=1.67*INTGRL(0.0,X1)
X4=X2+X3
X5=550,000*X4
OUTPUT=0.333*X5
X6=CMPXPL(0.0,0.0,0.005,166.79,OUTPUT)
TIMER DELT=.01,FINTIM=10,PRDEL=.05,OUTDEL=.05,DELMIN=1.E-12
PRTPLT OUTPUT (ERROR)
LABEL STEP RESPONSE TO UNCOMPENSATED SYSTEM 1 PID ONLY
END
STOP
```

[a]Reference Figures 4.3, page 63, and D.1, page 113.

TABLE D.2

CSMP PROGRAM STATEMENTS TO DETERMINE THE
RESPONSE TO A PULSE DISTURBANCE FOR
THE UNCOMPENSATED SYSTEM[a]

```
INPUT=0.005*STEP(0.0)
ERROR=INPUT-X8
X1=REALPL(0.0,0.4,ERROR)
X2=0.5*X1
X3=1.67*INTGRL(0.0,X1)
X4=X2+X3
X5=550,000*X4
TD=TD1+TD2
TD1=-600*STEP(2.00)
TD2=600*STEP(2.30)
X6=X5+TD
OUTPUT=0.333*X6
X7=CMPXPL(0.0,0.0,0.005,166.79,OUTPUT)
X8=0.556*LIMIT(0.0,0.018,X7)
TIMER DELT=.01,FINTIM=9,PRDEL=.05,OUTDEL=.05,DELMIN=1.E-12
PRTPLT OUTPUT (ERROR)
LABEL PULSE DISTURBANCE RESPONSE TO UNCOMPENSATED SYSTEM1 PID ONLY
END
STOP
```

[a]Reference Figures 4.4, page 64, and D.2, page 114.

TABLE D.3

CSMP PROGRAM STATEMENTS TO DETERMINE
THE RESPONSE TO A STEP INPUT FOR
THE COMPENSATED SYSTEM[a]

```
INPUT=0.005*STEP(0.0)
ERROR=INPUT-0.001335*X8
X1=1*ERROR
X2=6.68*INTGRL(0.0,ERROR)
X3=1.08*ERROR
X4=REALPL(0.0,0.10,X3)
X5=X1+X2-X4
X6=REALPL(0.0,0.04,X5)
X7=80329*X6
OUTPUT=0.33333*X7
X8=CMPXPL(0.0,0.0,0.3573,8.173,OUTPUT)
TIMER FINTIM=5.0,PRDEL=.01,OUTDEL=.05,DELMIN=1.E-8
PRTPLT OUTPUT (ERROR)
LABEL STEP RESPONSE FOR COMPENSATED SYSTEM
END
STOP
```

[a]Reference Figures 5.7, page 82, and D.3, page 115.

TABLE D.4

CSMP PROGRAM STATEMENTS TO DETERMINE THE
RESPONSE TO A PULSE DISTURBANCE FOR
THE COMPENSATED SYSTEM[a]

```
INPUT=0.005*STEP(0.0)
ERROR=INPUT-0.001335*X8
X1=1*ERROR
X2=6.68*INTGRL(0.0,ERROR)
X3=1.08*ERROR
X4=REALPL(0.0,0.10,X3)
X5=X1+X2-X4
X6=REALPL(0.0,0.04,X5)
X7=80329*X6
X9=X7+TD
TD=TD1+TD2
TD1=-600*STEP(1.00)
TD2=600*STEP(1.30)
OUTPUT=0.33333*X9
X8=CMPXPL(0.0,0.0,0.3573,8.173, OUTPUT)
TIMER FINTIM=5.0,PRDEL=.01,OUTDEL=.05,DELMIN=1.E-8
PRTPLT OUTPUT (ERROR)
LABEL PULSE DISTURBANCE RESPONSE FOR COMP SYS
END
STOP
```

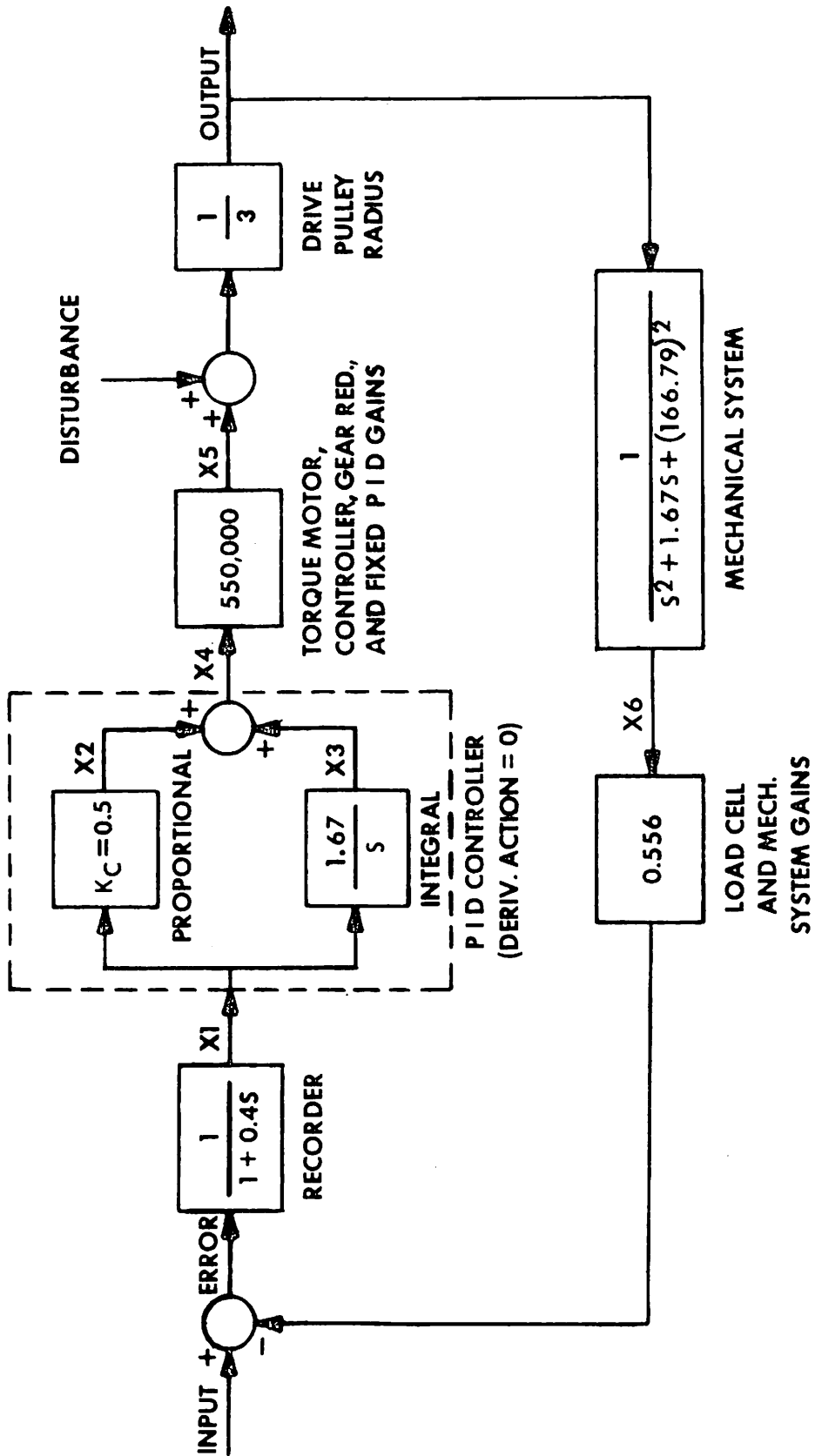[a]Reference Figures 5.8, page 83, and D.4, page 116.

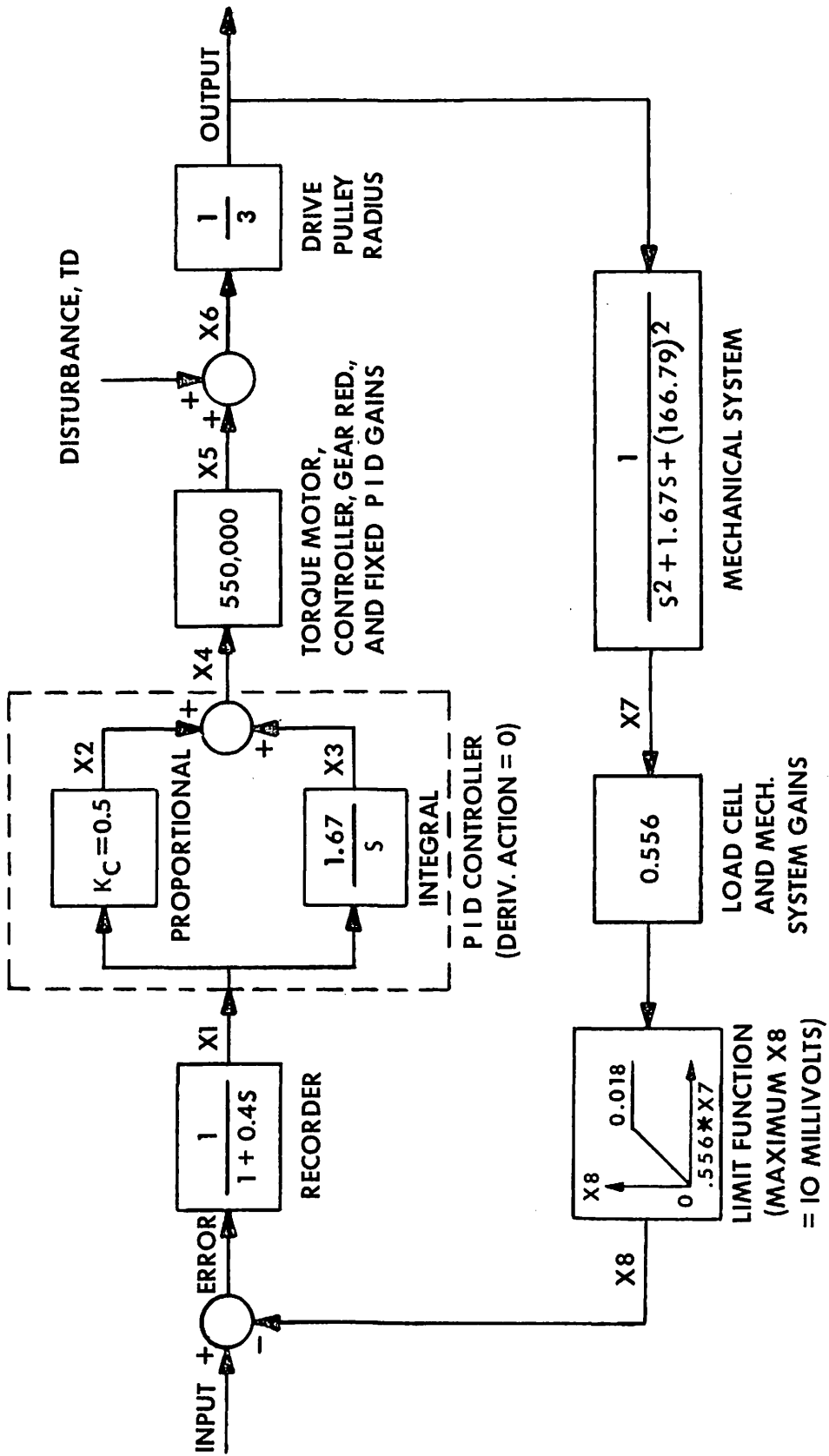Figure D.1. System Block Diagram for Computer Program in Table D.1.

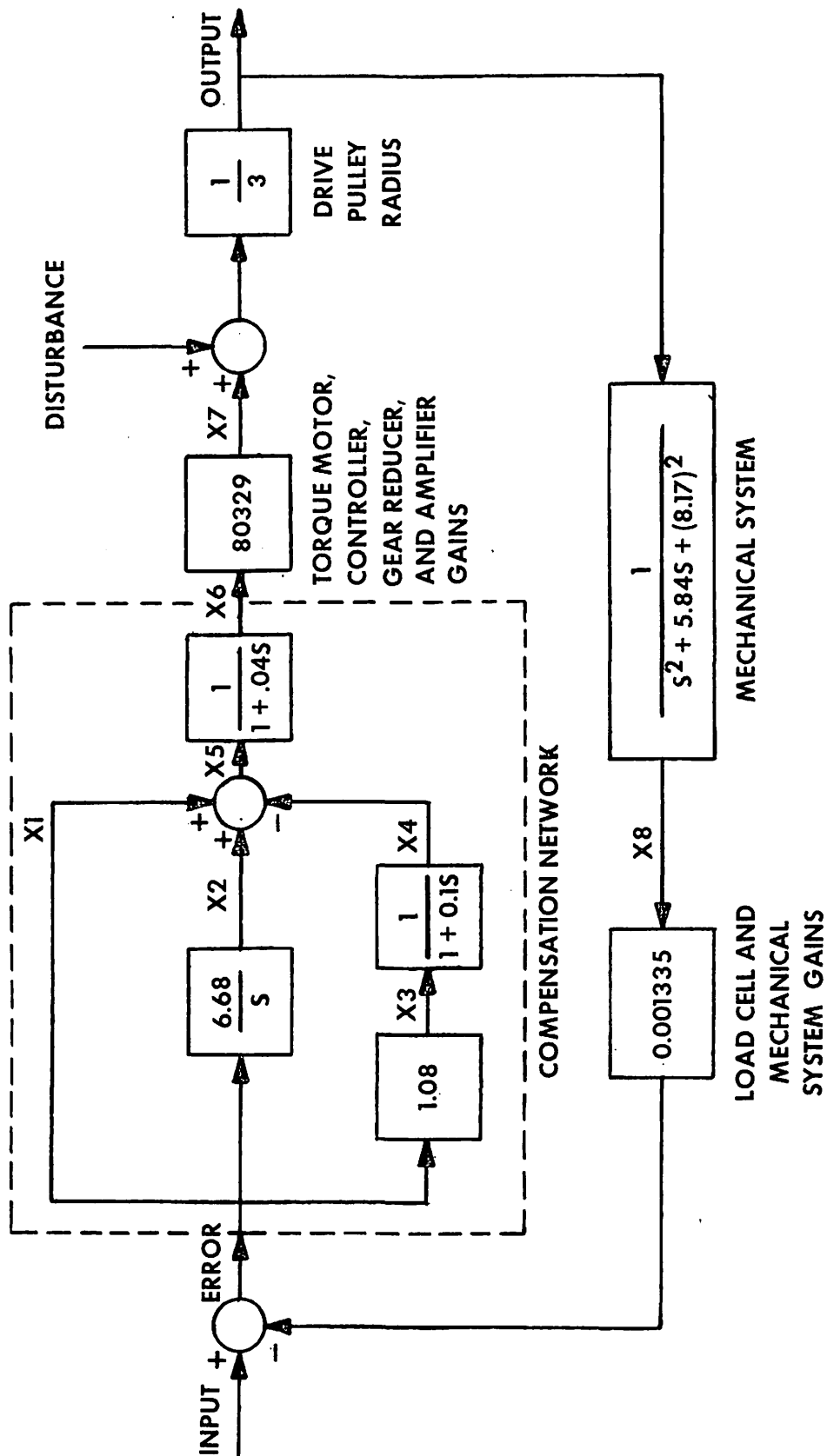Figure D.2. System Block Diagram for Computer Program in Table D.2.

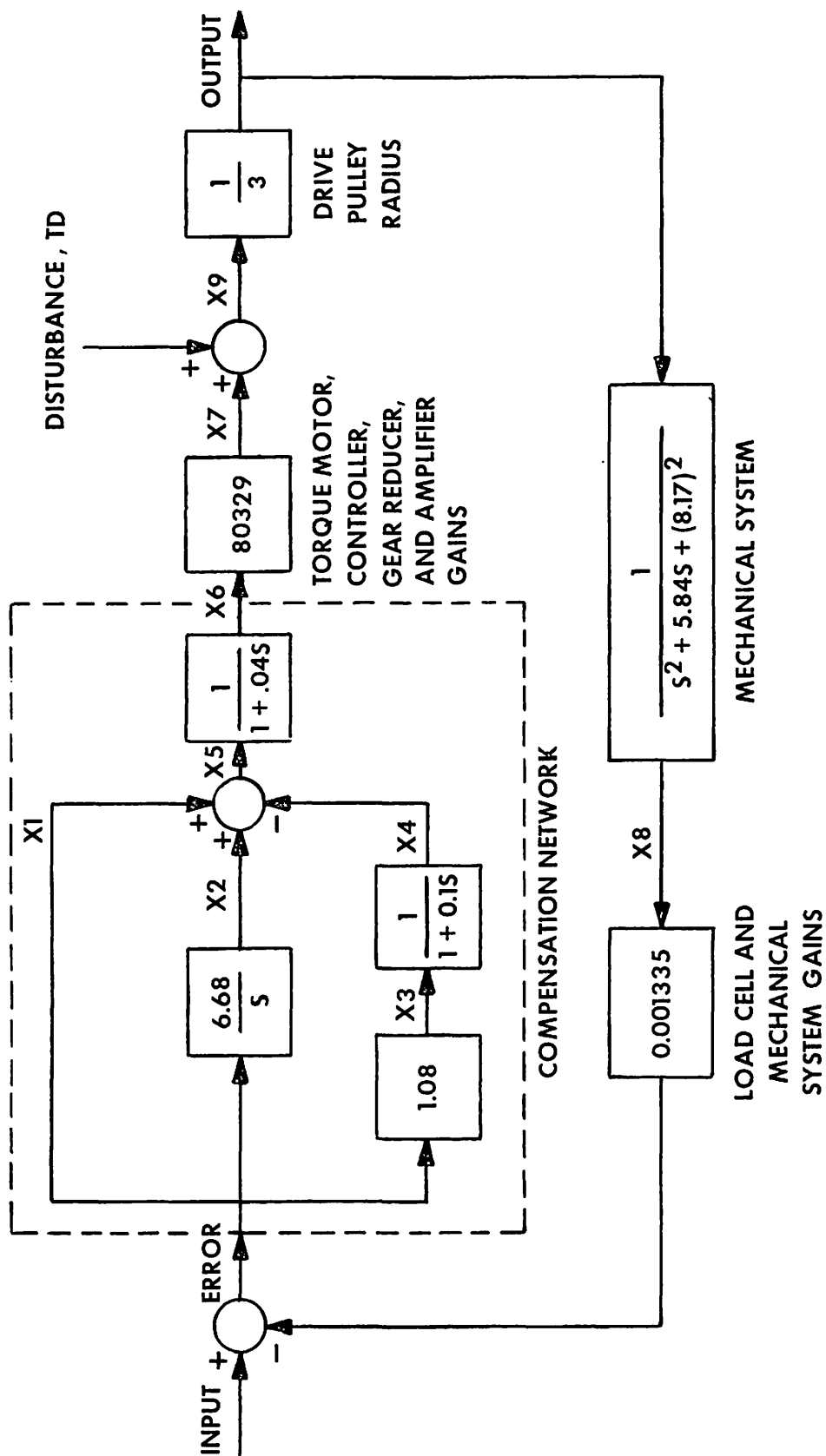Figure D.3. System Block Diagram for Computer Program in Table D.3.

116

Figure D.4. System Block Diagram for Computer Program in Table D.4.

VITA

Gary Melvin Henderson was born in Atlanta, Georgia, on January 23, 1947. He attended public schools in Clarkston, Georgia, and graduated from Clarkston High School in 1965. After high school graduation he worked for Southern Bell Telephone Company in Decatur, Georgia, and attended the DeKalb Junior College in Clarkston, Georgia, during the evenings. In the winter of 1966 he transferred to the University of North Carolina at Charlotte where he was graduated with a Bachelor of Science degree in Electrical Engineering in June 1969. Since June 1969 he has been employed by Union Carbide Corporation, at Oak Ridge, Tennessee. He is currently a design engineer in the Instrument Engineering Department for the Y-12 Plant.

In September 1969 he entered the Graduate School at the University of Tennessee to begin study towards a Master of Science degree in Electrical Engineering.

He was listed in Who's Who among Students in American Universities and Colleges for 1969, and is currently a member of the Instrument Society of America and is a registered professional engineer in the state of Tennessee.

He is married to the former Susan Elenore Allen of Charlotte, North Carolina. He and his wife have two sons, Gary Brock and Michael Allen.